THE EFFECT OF MAGNETIC FIELDS IN CHEMISTRY AND BIOLOGY

by

J.R. Woodward

A thesis submitted for the degree of

Doctor of Philosophy

Merton College

Michaelmas Term, 1997

THE EFFECT OF MAGNETIC FIELDS IN CHEMISTRY AND BIOLOGY

A thesis submitted for the degree of Doctor of Philosophy

by J. R. Woodward

Merton College Michaelmas Term, 1997

ABSTRACT

This thesis is concerned with the effect of static and oscillatory magnetic fields on the yield of radical recombination reactions and the proposal that such effects may constitute a possible mechanism for the interaction of environmental electromagnetic fields with biological systems.

A brief overview of research pertaining to the biological effects of environmental electromagnetic fields is presented. Next, the concept of the radical pair is introduced and the theory of its behaviour in solution is examined in order to illustrate the mechanism by which magnetic fields can affect its probability of separation.

Three different experimental systems involving the attack of free-radicals on DNA are presented. The extent of DNA damage is assayed in the presence and absence of a static magnetic field. These systems involve the killing of yeast cells as observed by the growth of subsequent colonies, direct observation of strand breaks to DNA, *in vitro,* by gel electrophoresis and the direct observation of intra-nuclear DNA damage by microgel analysis. In all systems, magnetic field effects are observed but are difficult to reproduce consistently.

The design of novel apparatus for the observation of resonant radiofrequency effects is described. The application of a 30-40 MHz oscillating magnetic field is found to alter the yield of exciplex fluorescence in the photoreaction of anthracene-d_{10} and 1,3-dicyanobenzene. The effect is interpreted in terms of a change in the efficiency of singlet $\leftrightarrow$ triplet interconversion in the {anthracene cation - DCB anion} radical pair when the oscillating field is in resonance with hyperfine splittings in the DCB anion radical.

Acknowledgments

In and around the science area

First and foremost, much love and thanks go to Keith for his unfailing support, advice, friendship and kindness over the years I have worked with him. He has helped me in many aspects of my life besides chemistry and was always ready for a pint and a chat on Tuesday evenings! Thanks also go to Joan for her friendship, help and fantastic group dinners.

Dr John Knowland for providing me with the knowledge and means to perform the biological experiments, and for instilling in me a sense of scientific rigour.

Everyone in Biochemistry who helped me with my experiments - Pete, Melanie Gunilla and Shirley, but particularly to Rosie for the amount of her own time she spent teaching me gel and tissue culture techniques and generally for being good company.

The National Radiological Protection Board for their financial support.

Rich for being the perfect friend and colleague throughout the time we have worked together.

May for teaching me the advantages of being organised, for her fantastic cooking and for always being in the lab before me to smirk when I arrived!

Rob and Tariq for carrying on where Rich and I left off, for their great help with reading this thesis and for making the lab a very pleasant place to write up.

For all the Part IIs who have shared the lab with me over the years - Marie, Justine, Nick, Alex, Neil, Oscar, Tom and Ed - it's been a blast.

To all of the staff of the Physical and Theoretical Chemistry Laboratory for their help, friendship and support. Particular thanks to Nev and John from Electronics who spent so many hours fixing things that I couldn't, and to Tony and Mervin for making a trip to stores a treat.

To everyone in PTCL tea for distracting and amusing me.

Pete for keeping the computers under control.

Dr. Elena Bagryanskaya for her help with RF circuits.

To Christiane and Peter for much useful discussion regarding the RF experiment.

Finally to Chris Kay for science and friendship shared over many curries.

Outside the science area

Dave for being a part of my life I love and rely on and always will.

Freddy for our many walks and talks, drunken and sober and for your friendship - just as strong after all these years.

All my friends with whom I have played over the last few years, especially to Steve for excellent movie chats and to Mick and Sarah for beers, footy and fun.

Horlicks, for cars and kicks and for still making me feel like we're at school.

Doug and Sid for weekend joy. 'Nothing's forgotten, Nothing is ever forgotten.'

Vickers for Street Theatre, 'Waterloo Bahnhof', 'Vickers Skiing', spying and the uncountable other antics we had.

All the members of Lazyfield, the Rock Gods - being on stage with you was just the best thing ever.

Pauline for many precious times now gone but never forgotten.

Emma, Robin and Andy, my housemates over the last year, for friendship, parties, nights in, nights out and for allowing me to obtain my professional qualification as a maid!

Danny and Ness for love, friendship and remarkable inventions!

Pops for helping me try out most of Oxford's restaurants, for lengthy discussions on life, and for love and support.

Mum. I cannot possibly try to thank you here for all that you've given me and all that you've made me but I can say that this thesis wouldn't exist, but for your love.

Table of Contents

Chapter 1

Introduction

Throughout history, technological advancements have changed, and arguably improved, the quality of life and nature of society. Perhaps the single most influential of all these advancements was the discovery and harnessing of electricity. The importance of electricity in the world as we know it is paramount - it is perhaps not an exaggeration to suggest that modern society in developed countries would collapse if we were left without electricity.

As with almost all impacting technologies, it is often not until we have enjoyed the benefits of our discoveries that we start to question any potential hazards that may be introduced by our newest idol. With electricity, there are many aspects of its use that we need to investigate. Clearly, direct exposure to electricity itself is potentially fatal. Indirectly, the production of electricity has a number of associated problems, notably the significant depletion of the worlds resources and the pollution of the atmosphere, not to mention our absolute dependency upon it.

But are there perhaps further consequences of the use of electricity? Transport of electricity invokes exceedingly high potentials to reduce heat loss and gives rise to AC and DC electric and magnetic fields - these will be regarded collectively as environmental electromagnetic fields (EMFs). Most electrical equipment also gives rise to EMFs and the magnitude and nature of such fields will be discussed later. In the last few years, there has been great concern about the potential influence of EMFs on the health of individuals exposed to them. The initial concern over such effects was raised in an epidemiological study conducted in Denver in 1979 by Wertheimer and Leeper [1] who found that children living close to overhead electric cables had an almost 3-fold likelihood of acquiring leukemia.

Although the study was much criticised, it brought the issue to the attention of the scientific community and spawned many further studies. Some of these are discussed below.

1.1 Epidemiological studies of the carcinogenic effects of power lines.

The Wertheimer and Leeper study led to a repeat study performed in Denver by the New York State Power Commission [2] and also a study in Los Angeles [3]. The first long term study was published in Sweden and utilised detailed records on power usage. Average magnetic field levels were calculated over a 12 month period and the study found that those houses with an average level above 2mG showed a relative risk of pediatric leukemia of 2.7. An increased risk of 3.8 was found in those houses with a magnetic field above 3mG.

There have been many epidemiological studies in this field since the initial report and such studies will no doubt continue to be made. Many studies invoke distinct subsets of the population in order to focus upon particular factors. In general, such studies involving high exposure groups, such as power line workers, have found no elevated health risk in adult populations. Exceptions include a study by Floderus et al. [4], who found that incidences of chronic lymphocytic leukemia were increased for adults in electrical occupations, and studies of male breast cancer by Tynes and Anderson [5] and Matanoski et al [6] who found increased likelihood of contracting such cancers in telephone-line workers.

Epidemiological studies are clearly of great importance in studying the effect of environmental fields in biology. Indeed, without such investigations it is questionable as to whether we would be aware of any potential risks of our modern environment. However, in order to establish a direct link between EMFs and

disease, it is imperative to demonstrate a biological effect within the confines of a tightly controlled scientific experiment. Even the most rigorous of epidemiological studies can never establish a cause-effect relationship with complete certainty due to the variation present within any population sample, biologically, sociologically and geographically. In this respect, epidemiological studies appear vague and unconvincing. However, in one respect, epidemiological studies are far more specific than experiments designed to prove mechanisms of direct interaction between EMFs and clearly defined biochemical processes, in that they refer to specific diseases of which global and national occurrences are well documented. Thus they are the most important studies in identifying the significance of any EMF interactions in real terms. Even the best biochemical investigations give us no information on the overall biological effect of the field even though its mechanism of interaction may be completely elucidated. This highlights a problem for the laboratory scientist in that, regardless of whether a conclusive mechanism of interaction between EMF and biochemical / biological behaviour can be established, a whole new field lies ahead in trying to describe and measure the significance of this interaction.

These problems aside, it is the aim of this thesis to take a scientific approach to the problem and try to measure the validity of one possible form of interaction whilst learning as much about the associated fundamental chemical processes as possible.

1.2 Environmental electric and magnetic fields

Before attempting to examine the way in which chemical and biological systems are influenced by electromagnetic fields, we must first understand the nature of the electromagnetic fields present in our environment. Within the natural environment, there are both alternating current (AC) and direct current (DC) fields

i.e. oscillatory and non-oscillatory fields. Such fields also consist of two components - an electric field and a magnetic field. DC magnetic and electric fields are usually greater in magnitude than AC ones. The static electric field at the surface of the earth is about 130 Vm^{-1}. The magnetic field varies with latitude (as the Earth behaves essentially as a giant bar magnet) but, in the United States for instance, has a value of about 500mG (field conversions appear in appendix A). These DC fields are not detected by humans, but are used by birds, migratory animals and bacteria for navigation. DC magnetic fields in a domestic environment usually have a magnitude of around 10mG. AC magnetic fields are usually of about 0-2mG.

Electric and magnetic fields influence the human body in very different ways. Electric fields are strongly attenuated as they penetrate the body. This is due to the membrane potential of cells effectively screening the field. Magnetic fields, however, enter the body effectively unchanged. If we consider a static electric field of 130 Vm^{-1}, the actual field experienced under the skin would have a value of only 1.3×10^{-5} Vm^{-1}. It would thus appear unlikely that it is the electric field which is influencing biological processes, unless it is affecting the cell membrane potential. Magnetic fields, both static and electric, can be much larger than the average values near electrical equipment and power lines. Standing directly under a power transmission line would cause a person to experience a magnetic field (AC) of about 1G (0.1mT). Such fields can extend for distances of about 500m. Even larger fields can be experienced close to electrical appliances, although in such cases the field falls off rapidly with distance. However, many appliances are used close to the body (e.g. visual display units, hairdryers, electric razors etc) and clearly can expose the body to significant magnetic fields. A thorough account of electric and magnetic field exposures is given by Barnes [7].

1.3 The possible nature of the interaction

There are a number of different possible mechanisms by which external electric and magnetic fields can interact with the processes and structures present in biological systems. A brief overview is given below.

1.3.1 Interaction of electric fields

There are two main biological subsystems with which electrical fields can interact: biological fluids and cell membranes [8]. Biological fluids are complex mixtures of many species including polar molecules, ions, proteins and small particles. Electric fields can affect the mobility of these species although the fields must be strong enough to overcome other forces controlling their movement, for example osmotic forces. Chemical reactions within the body whose rate is limited by the concentration of a particular species can thus be affected by the drift velocity of the species required. Electric fields both AC and DC can serve to reduce or increase the drift velocity and thus affect the rate of chemical processes.

Electric fields are highly significant in the regular function of membranes. As mentioned previously, cell membranes shield the interior of the cell very effectively due to the very high effective membrane resistivity [9]. However, external fields can affect the rate of passage of ions through the membrane and many models have been proposed to explain the details of such processes [10 - 12]. Electric fields applied parallel to the plane of the membrane can also affect the binding of ions and molecules onto the surface of cells due to an electrophoretic effect causing opposite sides of the membrane to become polarised [13, 14].

1.3.2 Interaction of magnetic fields

Cell membranes are also implicated in effects of magnetic fields [15, 16]. Membranes are close to phase transitions at physiological temperatures and possess liquid-crystal type properties. It is proposed that static magnetic fields could affect membrane fluidity [17, 18]

AC magnetic fields can interact either directly on magnetic particles or by induction of electric fields.

Direct interaction of magnetic fields with magnetic particles has been proposed as a mechanism of direct interaction of AC magnetic fields due to the presence of magnetite particles in the tissues of many organisms, including some mammals [19, 20]. The presence of magnetite particles in the human brain has been demonstrated [21]. A suggested mechanism implicates the oscillating field and magnetite particles in the opening and closing of pressure sensitive membrane ion channels [22]. The number of magnetite particles present in the brain is so small compared with the number of brain cells, that the significance of such an interaction is doubtful.

Magnetic fields can cause the induction of electric current loops in tissues orthogonal to the applied magnetic field. Transduction of these currents into biological events are chiefly thought to take place via the cell membrane as discussed earlier.

As for any oscillating field, a resonance interaction is possible. Liboff [23] has proposed an ion cyclotron resonance (ICR) model that suggests an increase in ease of movement of some ions through cell membranes due to a resonance corresponding to environmental magnetic field magnitudes and frequencies. Belief

in such a mechanism has been hampered by some negative experimental findings [24-30] and the expected damping of resonant ion motion in a condensed phase.

The final mechanism is the focus of this thesis. Static magnetic fields can affect the yield of some radical combination reactions, and thus the concentration of free radicals present in a system, by affecting the interconversion of the overall radical spin-states and thus the ability of the radicals to react with one another. Free radicals are highly reactive species present in many biological processes and are implied in many diseases including cancers and notably in the aging process.

The next chapter introduces free-radicals and the concept that they are born in pairs. A discussion is included of the mechanisms by which radical yields may be affected by magnetic fields and the effects exhibited by magnetic fields of various magnitudes.

References

[1] **Wertheimer, N. & Leeper, E.**
Am. J. Epidemiol. **109** (1979) 273

[2] **Savitz, D.A., Wachtel, H., Barnes, F.A., John, E.M. & Turdik, J.G.**
Am . J. Epidemiol. **128** (1988) 21

[3] **London, S.J., Thomas, D.C., Bowman, J.D., Sobel, E., Cheng, T.C. & Peters, J.M.**
Am. J. Epidemiol. **134** (1991) 923

[4] **Floderus, B., Persson, T., Stenlund, C., Linder, G., Johansson, C., Kiviranta, J., Parsman, H., Lindblom, M., Knave, B., Wennburg, A. & Ost, A.**
'Occupational Exposure to Electromagnetic Fields in Relation to Leukemia and Brain Tumours. A Case-Control Study', National Institute of Occupational Health; Solna, Sweden 1992

[5] **Tynes, T. & Anderson, A.**
Lancet **336** (1990) 1596

[6] **Matanoski, G., Breysse, P.N. & Elliot, E.A.**
Lancet **337** (1991) 737

[7] **Barnes, F.S. Article in 'Electromagnetic Fields - Biological Interactions and Mechanisms'**
Advances in Chemistry series 250

[8] **Barnes, F.S. Article in 'Non-linear Electromagnetics'**
Uslenghi, P.L.L. Ed. Academic Press, New York, 1980. 391

[9] **Cooper M.S., Miller, J.P. & Fraser, S.E.**
Dev. Biol. **132** (1989) 170

[10] **Tsong, T.Y., Liu, D.S. & Chauvin, R.**
Bioelectrochemistry and Bioenergetics **21** (1989) 319

[11] **Liu, D.S., Astumian, R.D. & Tsong, T.Y.**
J. Biol. Chem. **265** (1990) 7260

[12] **Horn, L.W.**
Biophys. J. **64** (1993) 281

[13] **Poo, M.**
Nature **295** (1982) 332

[14] **Poo, M.M., Poo, W.J., Lam, J.W.**
J. Cell. Biol. **76** (1978) 483

[15] **Adey, W.R.**
Physiol. Rev. **61** (1981) 435

[16] **Tenforde, T.S. Article in 'Electricity and Magnetism in Biology and Medicine'**
San Francisco Press, San Francisco, CA. 1993.

[17] **Labes, M.M.**
Nature **211** (1966) 968

[18] **Aceto, H.Jr., Tobias, C.A. & Silver, I.L.**
IEEE Trans. Magn. **6** (1970) 368

[19] **Kirschvink, J.L., Jones, D.S. & MacFadden, B.J., Eds - 'Magnetite Biomineralization and Magnetoreception in Animals : A New Biomagnetism'**
Plenum, New York. 1985.

[20] **Kirschvink, J.L.**
Bioelectromagnetics **10** (1989) 239

[21] **Kirschvink, J.L., Kobayashi-Kirschvink, A. & Woodford, F.B.**
Proc. Natl. Acad. Sci. (USA) **89** (1992) 7683

[22] **Kirschvink, J.L., Kobayashi-Kirschvink, A., Diaz-Ricci, J. & Kirschvink, S.J.**
Bioelectromagnetics. Suppl. **1** (1992) 101

[23] **Liboff, A.R.**
J. Biol. Phys. **13** (1985) 99

[24] **Parkinson, W.C. & Hanks, C.T.,**
Bioelectromagnetics. **10** (1989) 129

[25] **Liboff, A.R. and Parkinson, W.C.**
Bioelectromagnetics. **12** (1991) 77

[26] **Prasad, A.V., Miller, M.W., Carstensen, E.L., Cox, Ch., Azadniv, M. & Brayman, A.A.**
Radiat. Environ. Biophys. **30** (1991) 305

[27] **Parkinson, W.C. & Sulik, G.L.**
Radiat. Res. **130** (1992) 319

[28] **Durney, C.H., Kaminski, M., Anderson, A.A., Bruckner-Lea, C., Janata, J. & Rappaport, C.**
Bioelectromagnetics **13** (1992) 19

[29] **Galst, S., Sandholm, J., Mamnerius, Y., Hojevik, P., Saalman, E. & Norden, B.**
Bioelectromagnetics **14** (1993) 315

[30] **Coulton, L.A. & Barker, A.T.**
Phys. Med. Biol. **38** (1993) 347

Chapter 2

Introduction to radicals and radical pairs

2.1 Basic theory of the radical pair

2.1.1 The nature of the chemical bond

Throughout this work, the formation and cleavage of covalent bonds is of utmost significance. It is, then, important that the nature of the covalent bond and the consequences of its fission are well understood. The formation of a bond between two hydrogen atoms is discussed as it is an excellent model for more complex systems.

The Schrödinger equation provides a complete solution for the electronic structure of the hydrogen atom. The single electron on the hydrogen atom resides in the 1s valence orbital. In order to model a system containing more than 2 particles we use the Born-Oppenheimer approximation (which states that the electron and nuclear wavefunctions can be considered independently). When a covalent bond is formed between 2 hydrogen atoms, the total wavefunction, ψ, can be approximated from a linear combination of the atomic valence orbitals.

$$\Psi = 1s_A \pm 1s_B \qquad \textbf{2.1}$$

The atomic orbitals interfere constructively to give rise to an orbital of lower energy than the parent atomic orbitals. This is the bonding orbital 1Sσ . Destructive interference leads to the formation of a higher energy orbital, the antibonding orbital

$1S\sigma^*$ (Note that here an asterisk denotes antibonding and not complex conjugate). These are shown in figure 2.1.1.

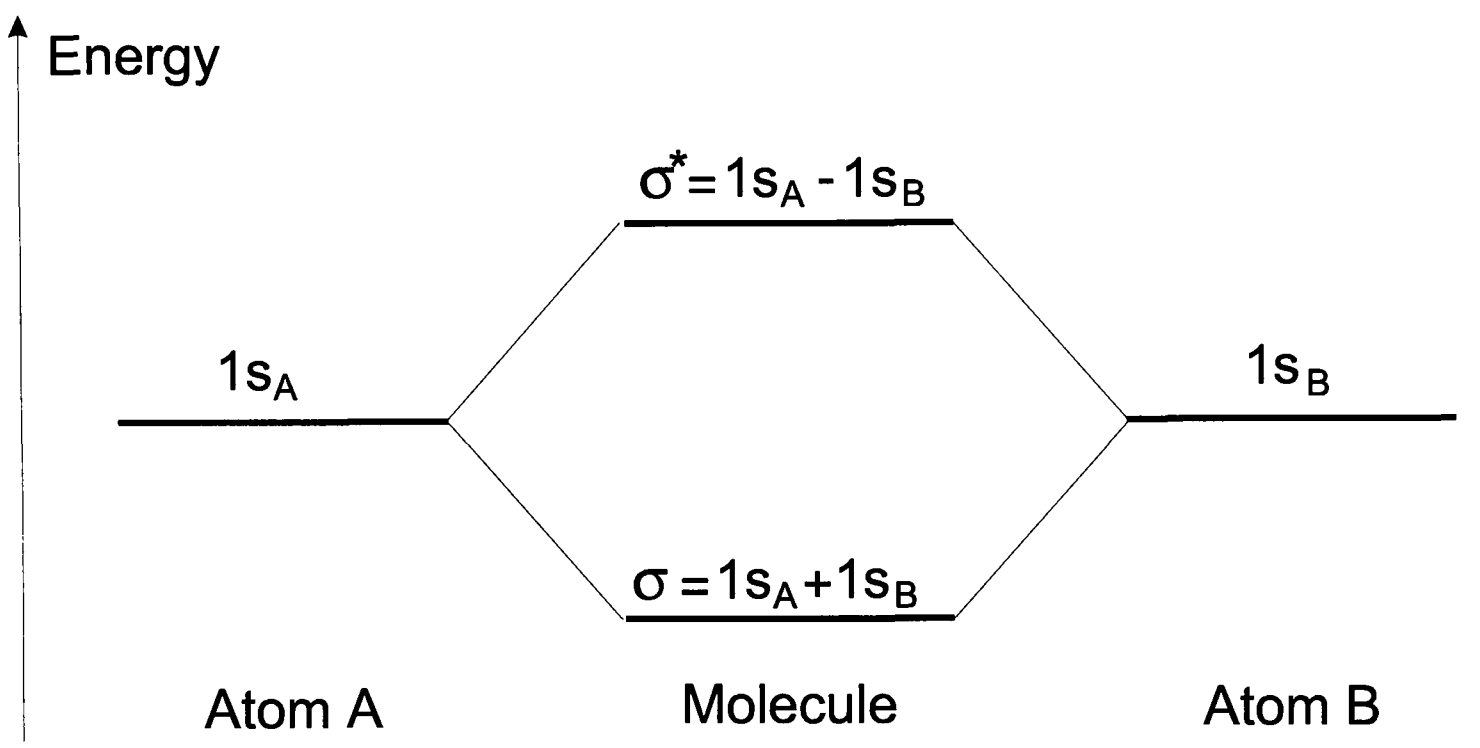

Fig 2.1.1. Energy diagram of bonding and antibonding orbitals.

The electron probability density is given by the square of the wavefunction ($\sigma^*\sigma$). Denoting the probability density functions of the orbitals with σ and σ^*,

$$(\sigma)^2 = (1s_A + 1s_B)^2 = 1s_A^2 + 1s_B^2 + 2(1s_A)(1s_B) \qquad \textbf{2.2}$$

$$(\sigma^*)^2 = (1s_A - 1s_B)^2 = 1s_A^2 + 1s_B^2 - 2(1s_A)(1s_B) \qquad \textbf{2.3}$$

The bonding orbital, σ, possesses electron density in the region between the two nuclei. For electrons (and indeed any fermions) the total wavefunction (the product of the spin and orbital wavefunctions) must be antisymmetric with respect to particle exchange. This means that the bonding orbital corresponds to the singlet state of the molecule. The antibonding σ^* orbital corresponds to the triplet state and

possesses zero probability of finding the electron at the mid-point between the nuclei. This leads to the molecule being destabilised relative to the unbonded system.

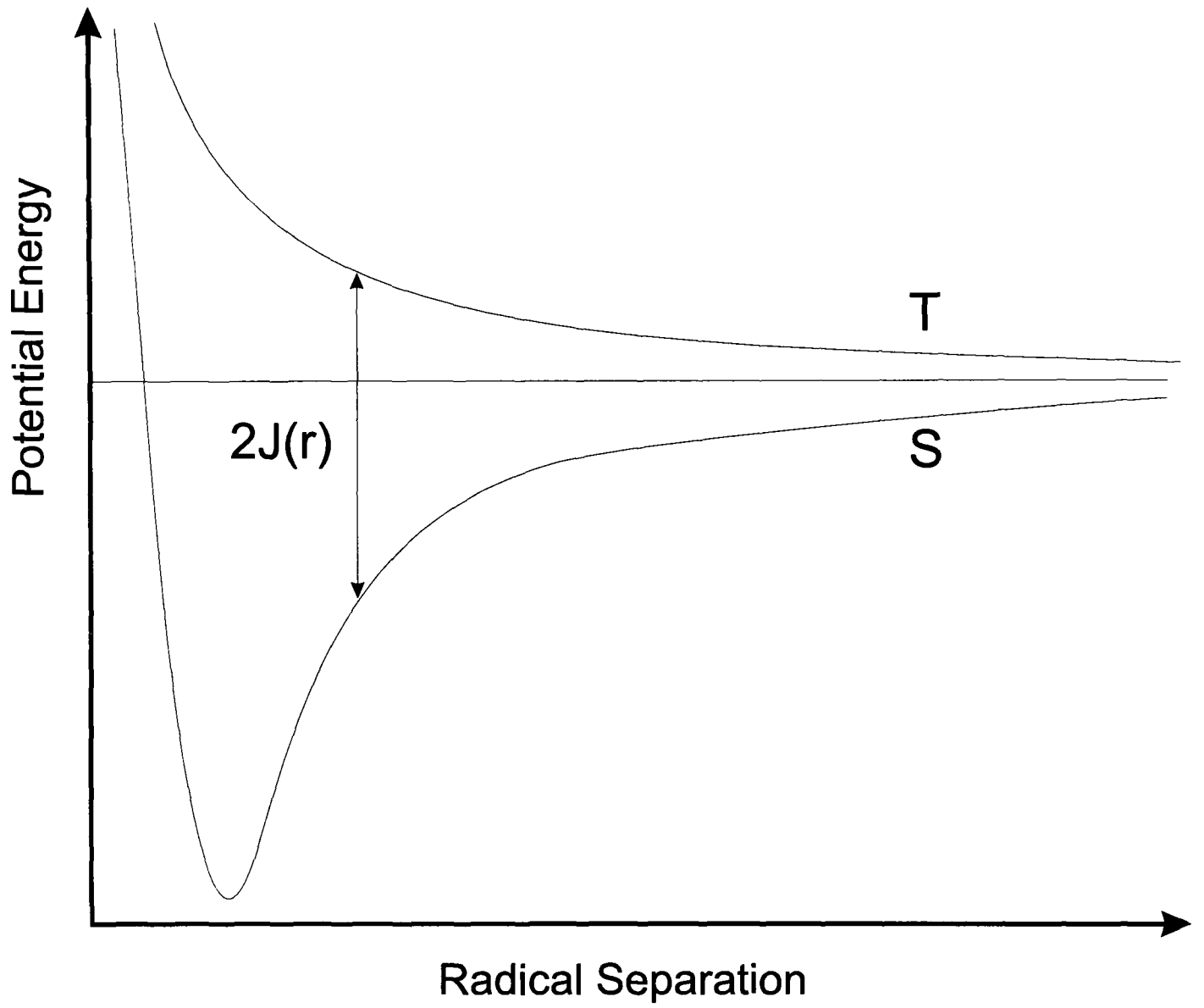

Figure 2.1.2. Energy dependence of singlet and triplet states with radical separation. The depth of the potential well is disproportionately small for ease of representation.

The wavefunctions of the singlet and triplet states of any molecule are similar in form to those described above. Bond fission involves separation of the constituent atoms of a covalent bond and thus figure 2.1.2 shows the variation in energy of the singlet and triplet states with internuclear distance.

If two hydrogen atoms approach closely from a distance, then their probability of reaction is dependent upon their relative spin states. Only when the atoms come together with antiparallel spins can bond formation take place. This simple situation indicates that the encounter of hydrogen atoms, and therefore any free radicals, is not the only criterion for their reaction. They must also possess unpaired electrons with spins antiparallel to one another. It is useful, therefore, when discussing the reaction of pairs of radicals, to define the overall spin multiplicity of the pair as singlet or triplet.

2.1.2 Excitation and radical pair formation

Now consider an organic molecule. Homolytic fission of any covalent bond gives rise to two species with single unpaired electrons. Such species are free radicals and clearly their formation must always occur in pairs. Bond fission is not the only process in which radical formation occurs; electron transfer and hydrogen abstraction reactions can also give rise to their formation. For a ground state organic molecule in solution, photoexcitation involves absorption of a photon of light promoting the molecule to an excited singlet state. Such a state undergoes fast internal conversion to a lower vibrational level and this excited singlet state has various fates dependent upon its lifetime. Intersystem crossing can occur to give a triplet state molecule. Some fates of the excited singlet or triplet molecule are described in figure 2.1.3.

All the non-radiative processes illustrated in figure 2.1.3 give rise to the formation of a pair of radical species. The fact that radicals are always generated in pairs is of critical significance - so much so that the term 'radical pair' is used to refer to this reaction intermediate at the stage of reaction prior to the existence of 'free' radicals. It must also be noted that, in all three reaction cases, the spin

multiplicity of the radical pair is indicated. The significance of the radical pair and of its spin state are discussed below.

Process	Description	
Radiative decay	Singlet state undergoes fluorescence $^1M^* \longrightarrow {}^1M + h\upsilon$	Triplet state undergoes phosphorescence $^3M^* \longrightarrow {}^1M + h\upsilon$
Hydrogen abstraction	Hydrogen atom is abstracted from solvent or other molecule in a Norrish Type II reaction $^{3/1}M^* + SH \longrightarrow {}^{3/1}\{MH^\bullet + S^\bullet\}$ A pair of radicals is produced	
Bond cleavage	Sigma bond cleavage occurs in a Norrish Type I reaction $^{3/1}M^* \longrightarrow {}^{3/1}\{R_1^\bullet + R_2^\bullet\}$ A pair of radicals is produced	
Electron transfer	Electron transferred to electron acceptor or from electron donor $^{3/1}M^* + A \xrightarrow[3/1]{} {}^{3/1}\{M^{\bullet+} + A^{\bullet-}\}$ $^{3/1}M^* + D \longrightarrow \{M^{\bullet-} + D^{\bullet+}\}$ A pair of radical ions is produced	

Figure 2.1.3. Some fates of an excited molecule in solution.

2.1.3 Geminate and freely-diffusing radical pairs

Consider now the fate of a radical pair formed by one of the processes described above. It was originally thought that the fastest reaction such species could undergo was diffusion controlled recombination on the microsecond and longer timescale. However, it was demonstrated in 1974 [1], by direct observation of iodine atoms, that a much faster recombination process occurs - 90% of the atoms recombining in the first five hundred picoseconds after creation in this particular case. This phase of the reaction is known as the geminate phase and involves the recombination of the pair of radicals initially formed together. The term 'geminate' applies to the radicals from the instant that they are created until the pair ceases to exist either by recombination or by the pair members drifting apart. The escaping radicals can then encounter radicals born in a separate geminate process on a much longer time-scale, this is the classical 'diffusion-controlled' reaction. The pair of radicals is said to be formed from 'freely-diffusing' radicals and are referred to as F-pairs.

2.1.4 The story of a radical pair

After formation, a radical pair has two fates: recombination or diffusion. For a singlet radical pair, the electron spins are antiparallel and the Pauli principle allows bond formation to take place. Therefore, the most likely fate of a singlet radical pair is recombination. For a triplet radical pair, however, bond formation is forbidden by the Pauli principle and thus the radicals will tend to diffuse apart. The spin-state of the radical pair must remain triplet until some process occurs to invert the electron spin on one of the radicals. For such an intersystem crossing process to occur, the radicals must diffuse apart to a distance where the interactions that can cause spin interconversion are large enough to overcome the difference in singlet and triplet energy. Figure 2.1.2 shows the way in which the singlet and triplet energies vary

with inter-radical separation. The singlet-triplet energy difference is conventionally given by 2J(r) - the electron exchange interaction. If the simple model of hydrogen atoms is used, then J(r) can be written

$$J(r) = J_0 e^{-(r/r_J)} \qquad \textbf{2.4}$$

J(r) falls off rapidly with distance. At equilibrium bond lengths, its value corresponds to a magnetic field strength of approximately 10^6T and thus dominates any local magnetic field. However, at radical separations of about 1nm, its magnitude has dropped to the sub-millitesla range, and now the spin mixing interactions can overcome the exchange interaction and intersystem crossing can occur. When the radicals have diffused to such a distance, their possible fates are as follows:

1. Intersystem crossing occurs and the radicals can diffuse back together and recombine.

2. Intersystem crossing does not occur and the radicals diffuse back together.

3. The radicals can diffuse apart completely, in which case their relative spin states are irrelevant.

(On re-encounter, the radical pair is not strictly in a singlet or triplet state, but a mixed state - this is discussed in chapter 3)

Situation 2 leaves the radical pair effectively unchanged and situation 3 leads to the creation of both F-pairs and free radicals that can subsequently undergo other reactions.. These processes are illustrated in figure 2.1.4.

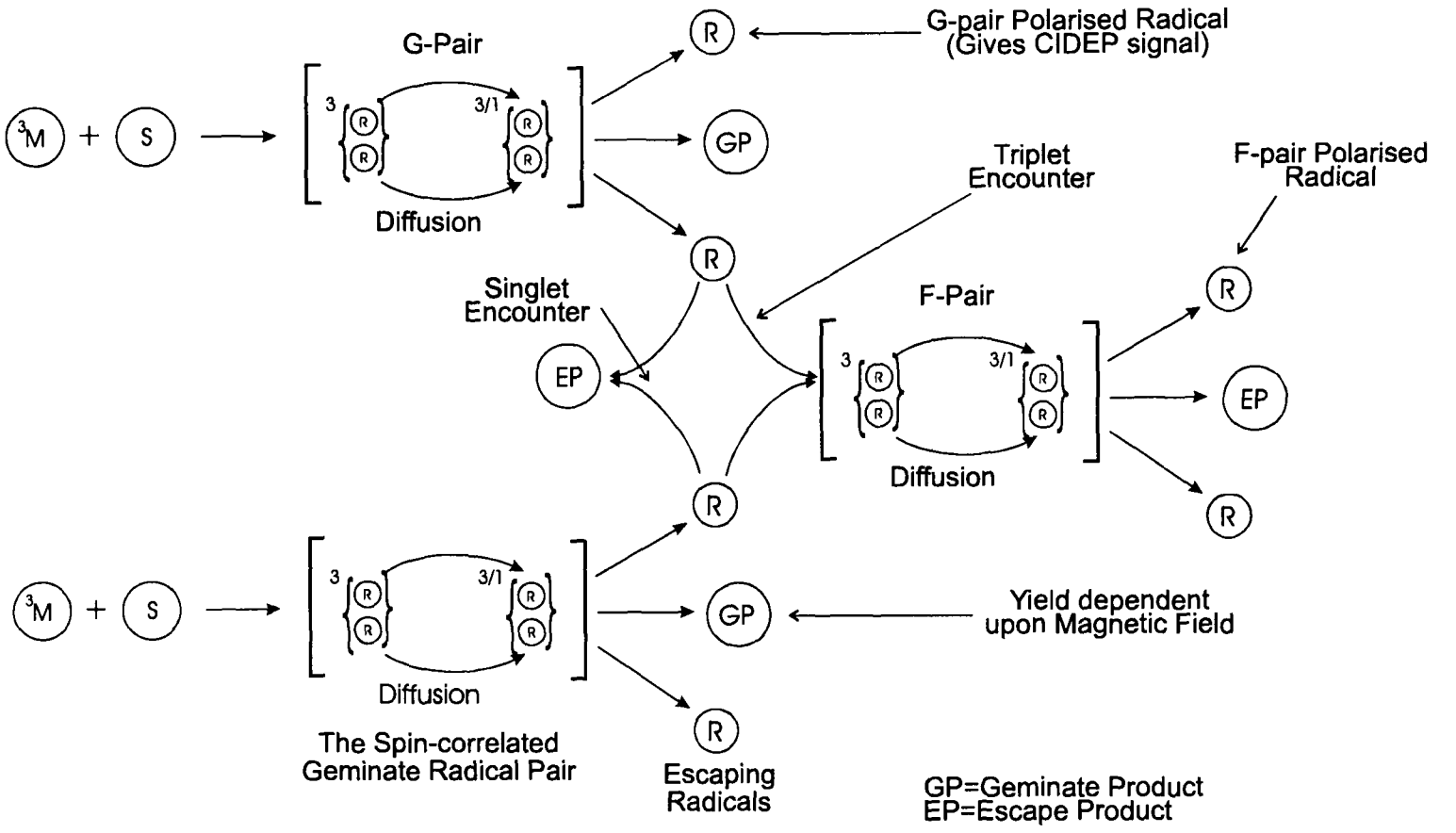

Figure 2.1.4. Radical pairs in solution.

2.1.5 Consequences of the radical pair

The behaviour of the radical pair described above gives rise to a number of physical phenomena which can be exploited to both investigate and control the kinetics in radical reactions.

1. The radicals produced from these processes give ESR spectra with anomalous line intensities. Products formed from these radicals exhibit NMR spectra with anomalous line intensities. Indeed it was due to the observation of such spectra that radical pair theory was developed. The observed effects are known as CIDEP and CIDNP (Chemically Induced Dynamic Electron / Nuclear Polarisation) [2,3].

2. The radical pair is a true reaction intermediate and has been observed most widely using flash-photolysis ESR [4,5] and also with RYDMR (Radical Yield Detected Magnetic Resonance) [6,7] , and TRSNP (Time Resolved Stimulated Nuclear Polarisation) [8]. These latter techniques involve the use of a static and high frequency resonant magnetic field in a technique loosely analogous to ESR. RYDMR employs optical detection methods and TRSNP detects the NMR of the reaction products.

3. The extent of intersystem crossing in the geminate radical pair can be influenced by the application of an external magnetic field. The objective of this work is to examine the conditions under which such effects may be optimised and to question their significance in a biological environment. Thus the details of how a magnetic field can affect this process is crucial to the work performed in this thesis. The next section discusses basic ESR theory and illustrates how the kinetics of radical reactions may be influenced by magnetic fields.

2.2 Basic theory of free radicals

2.2.1 An electron in a magnetic field

In order to understand and predict the behaviour of radical-pairs, it is first necessary to understand the nature of radicals themselves and their magnetic behaviour. Such ideas lie at the heart of (ESR) experiments and are included here to provide a basis of explanation for spin mixing processes.

A radical is a species possessing an unpaired electron. As electrons have the properties of charge and spin angular momentum, they possess a magnetic moment, μ_s, given by

$$\mu_s = -g_e \mu_B m_s \qquad \textbf{2.5}$$

where μ_B is the Bohr magneton (see appendix A). The magnetic moment is antiparallel to the spin angular momentum vector which has measurable components m_s. g_e is known as the g-value and has a value of 2.0023 for a free electron. The g-value of a radical depends on the electron environment and although little deviation from the free electron value is seen in carbon-centred radicals, considerably different g-values can be exhibited by transition-metal radicals.

Application of a magnetic field, B, necessitates two possible orientations of the magnetic moment, parallel or antiparallel to the applied field, and these orientations will differ in energy (the electron Zeeman splitting). The energy of a magnetic moment in the field is given by

$$E = -\mu \cdot B \qquad \textbf{2.6}$$

These two states are labeled by the spin-quantum number m_s, which can take values +1/2 (referred to as the α state) and -1/2 (referred to as the β state). Figure 2.2.1 shows the splitting of these states in a magnetic field. A static field is referred to as B_0 and is traditionally defined in the z direction.

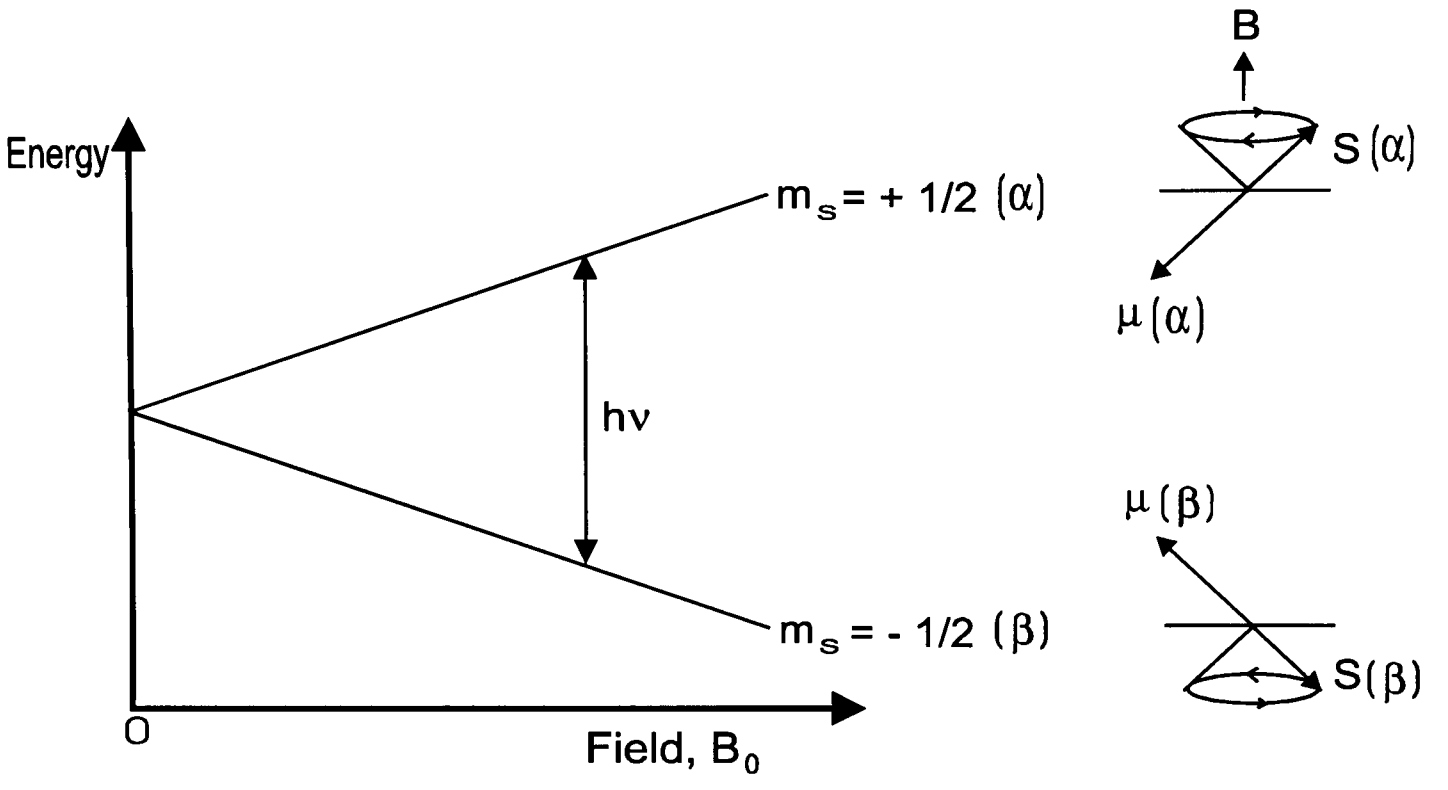

Figure 2.2.1. Electron Zeeman splitting in an external magnetic field.

From the Planck-Einstein relationship, for a transition

$$\Delta E = E_\alpha - E_\beta = h\nu = g_e \mu_B B_z \qquad \textbf{2.7}$$

Thus a radical can be made to undergo transition to the opposite spin state by absorption of radiation of the correct frequency. Most ESR experiments use a magnetic field of approximately 0.35T (3500G) corresponding to a microwave absorption frequency of 9.8 GHz.

2.2.2 Factors affecting ESR spectra

There are two main factors that give free radicals distinct ESR spectra. First is the g-value of the radical which has a characteristic value dependent upon the orbital angular momentum induced in the radical by the external magnetic field. Its magnitude is determined by the extent of the spin-orbit coupling which depends

upon the element at the radical centre its oxidation state and its chemical environment. As mentioned previously the g-value varies little between carbon-centred radicals, but is characteristic of them.

There is also an interaction of the electron magnetic moment with magnetic nuclei within the radical i.e. those nuclei possessing non-zero spin angular momentum. The nuclear spin number, I, can take many different integral or half integral values, usually ranging between zero and seven. Each nucleus has spin angular momentum with measurable components m_I, and associated magnetic moments given by

$$\mu_I = g_N \mu_N m_{Is} \qquad \textbf{2.8}$$

For proton nuclear spin, the magnetic moment is parallel to the angular momentum and thus the lower energy state for the proton is the α state.

In the presence of an external magnetic field, both electron and nuclear spins orient with respect to it. They interact via Fermi-contact and through-bond couplings. This interaction is of great significance and is known as the hyperfine interaction. It results in a splitting of the electron energy levels and thus ESR spectra consist of a series of lines corresponding to the various possible transitions. Figure 2.2.2 illustrates the coupling of an electron to a single hydrogen nucleus with a positive hyperfine coupling constant, a.

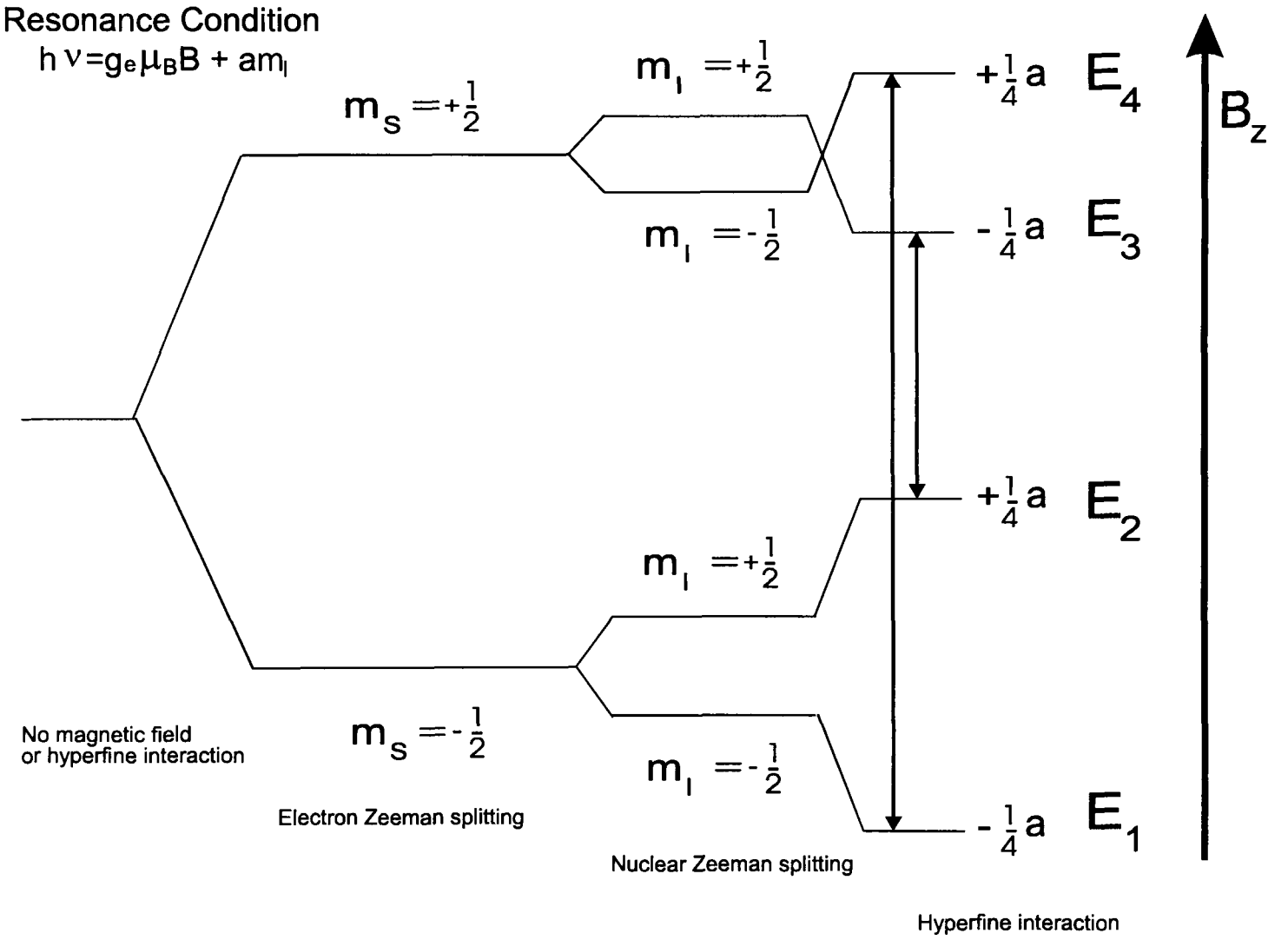

Figure 2.2.2. Zeeman and Hyperfine splittings. The allowed transitions, corresponding to the selection rules $\Delta m_s=\pm 1$ and $\Delta m_I=0$, are illustrated.

The selection rules that apply to transitions between these levels are $\Delta m_s=\pm 1$ and $\Delta m_I=0$. In more complicated systems, there are a number of possible transitions, many with the same transition frequency. Such degenerate transitions contribute to the same spectral line in the ESR spectrum and thus the probability of a certain transition frequency occurring is responsible for the relative intensity of the line. This is, however, only one factor governing the intensity of ESR transitions. For a system in thermal equilibrium with its surroundings, the absolute intensities of the spectrum are given by the Maxwell-Boltzmann distribution. For a first order spectrum with magnetically equivalent nuclei, the relative line intensities are given by the Binomial Coefficients. Time resolved ESR spectra obtained shortly after

radical creation often show line intensities that differ considerably from this. Such anomalous line intensities have origins in the spin-evolution of the radical pair.

2.2.3 Saturation and relaxation

At thermal equilibrium (i.e. Boltzmann) population of electron spin states, the lower spin state is more heavily populated than the upper state and thus when the resonance condition is met, there are more upward transitions than downwards and an absorption of microwaves occurs. As transitions take place, however, the population of the upper state will increase until the two states have equal populations and the upward transitions are equal in number to the downward ones. Thus although transitions still occur, they are not observed - no microwaves are absorbed or emitted. This phenomenon is known as saturation.

ESR spectra are readily observed in practice, however, and therefore there must be other processes at work trying to restore the Boltzmann population of levels. Such processes are radiationless transitions and are referred to as relaxation processes. These processes are significant not only in the observation of magnetic resonance transitions, but also because they may be one of those responsible for spin-mixing events in radical pairs, causing random spin flips.

2.2.4 Mechanisms of relaxation and spin-mixing

Relaxation is one of three processes that can cause spin-mixing.

1. Coherent mixing processes - driven by a local magnetic field and of two sorts - the Δg mechanism and the hyperfine mechanism.

2. Incoherent mixing due to the random processes of spin relaxation.

3. Chemical relaxation, where radicals undergo further reaction leading sometimes to new radicals and sometimes to repopulation of nuclear energy levels in identical radicals.

2.3 Coherent spin mixing

2.3.1 Singlet and triplet states in a magnetic field

It was established earlier that a radical pair is 'spin-correlated' when it is created i.e. the electron spins have different orientations relative to one another. Free radicals have been seen to possess magnetic moments that give rise to two different Zeeman energy levels when placed in an external magnetic field. Similarly, the magnetic properties of the radical pair itself must also be considered. For a singlet radical pair, the overall spin angular momentum is zero (S=0). Thus a singlet radical pair possesses no magnetic moment and is unaffected by the application of an external magnetic field.

A triplet radical pair, however, has a spin quantum number, S=1. There are three triplet states that are degenerate in the absence of a magnetic field. A magnetic field causes the degeneracy of these states to be removed giving rise to the Zeeman states T_0 , T_{+1} and T_{-1}. All these states are magnetic, but only the T_{+1} and T_{-1} states have magnetic moments in the external field direction, conventionally the z-axis. The T_0 state only has a net magnetic vector in the xy-plane. Figure 2.3.1 illustrates the variation of the energy of singlet and triplet states with magnetic field in a radical pair where the radicals are sufficiently far apart that the exchange interaction is small.

The S and T_0 states remain similar in energy as the field is increased. The T_{+1} and T_{-1} states, however, are sufficiently removed in energy to be effectively

decoupled, and are unable to interconvert with the S and T_0 states at high field values.

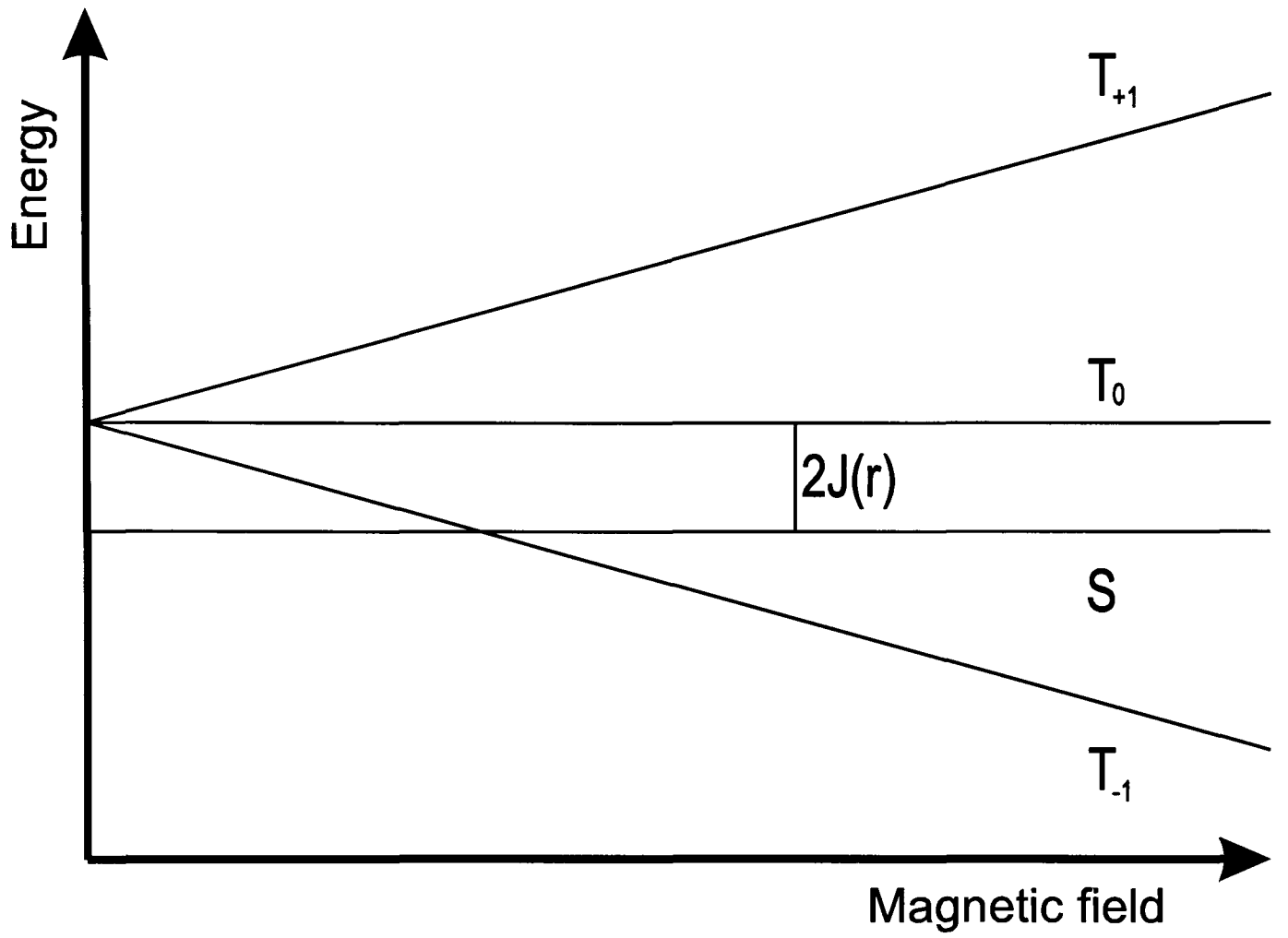

Figure 2.3.1. Singlet and triplet energy variation with magnetic field strength.

2.3.2 Vector representation of singlet and triplet states

The S and $T_{0,\pm1}$ states may be represented using a vector model which allows visualisation of the motion of the magnetic moments relative to the magnetic field. The unpaired electrons on the radicals are represented as precessing about the magnetic field direction at the Larmor frequency.

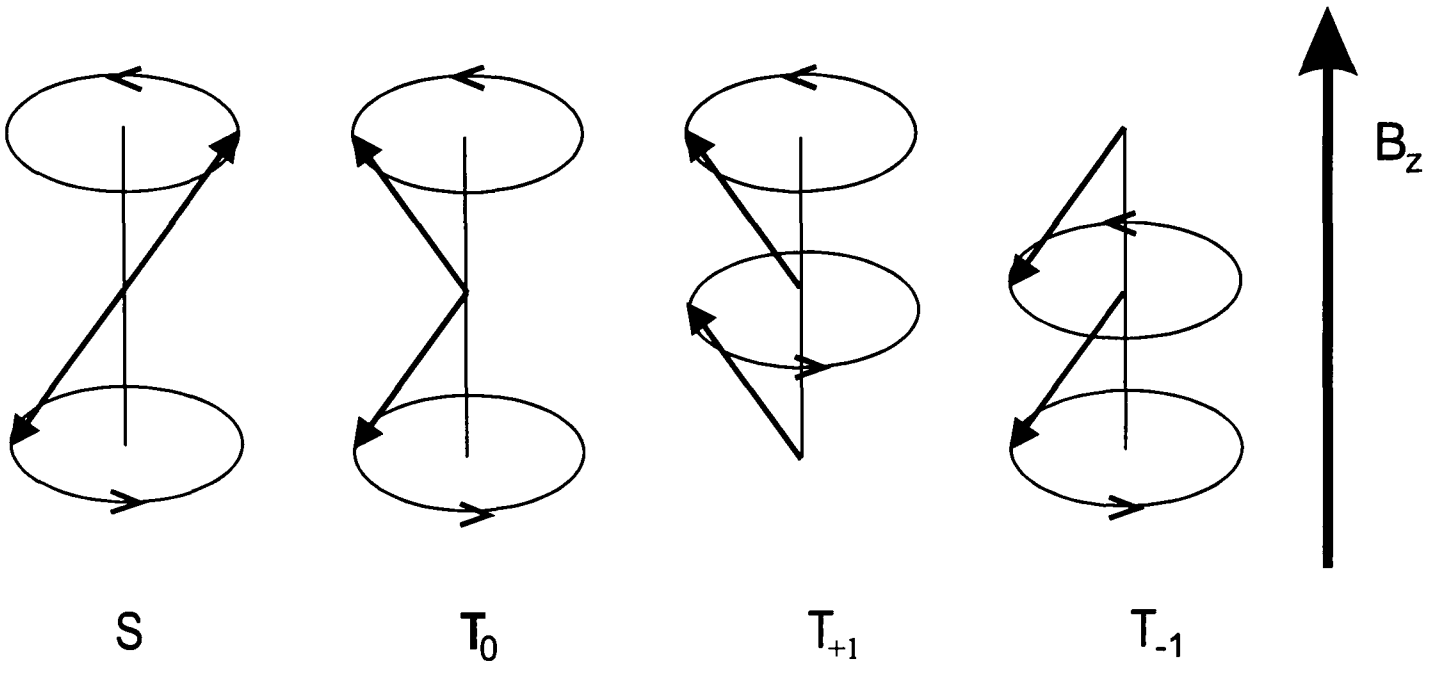

Figure 2.3.2. Vector representation of singlet and triplet states in an external magnetic field.

The Larmor frequency at which the electron spins precess is dependent upon the g-value of the radical (not necessarily g_e) and the local magnetic field, B_L, i.e. the field created by the external magnetic field, plus the field from hyperfine coupling to magnetic nuclei.

$$\omega = \frac{g\mu_B B_L}{\hbar} \qquad \textbf{2.9}$$

The S and T_0 states can be interconverted if the electron spins precess at different frequencies. In a frame rotating at the Larmor frequency of one of the electron spins which therefore appears stationary, figure 2.3.3 illustrates how the S state can evolve in time, rephasing its spins to generate a T_0 state.

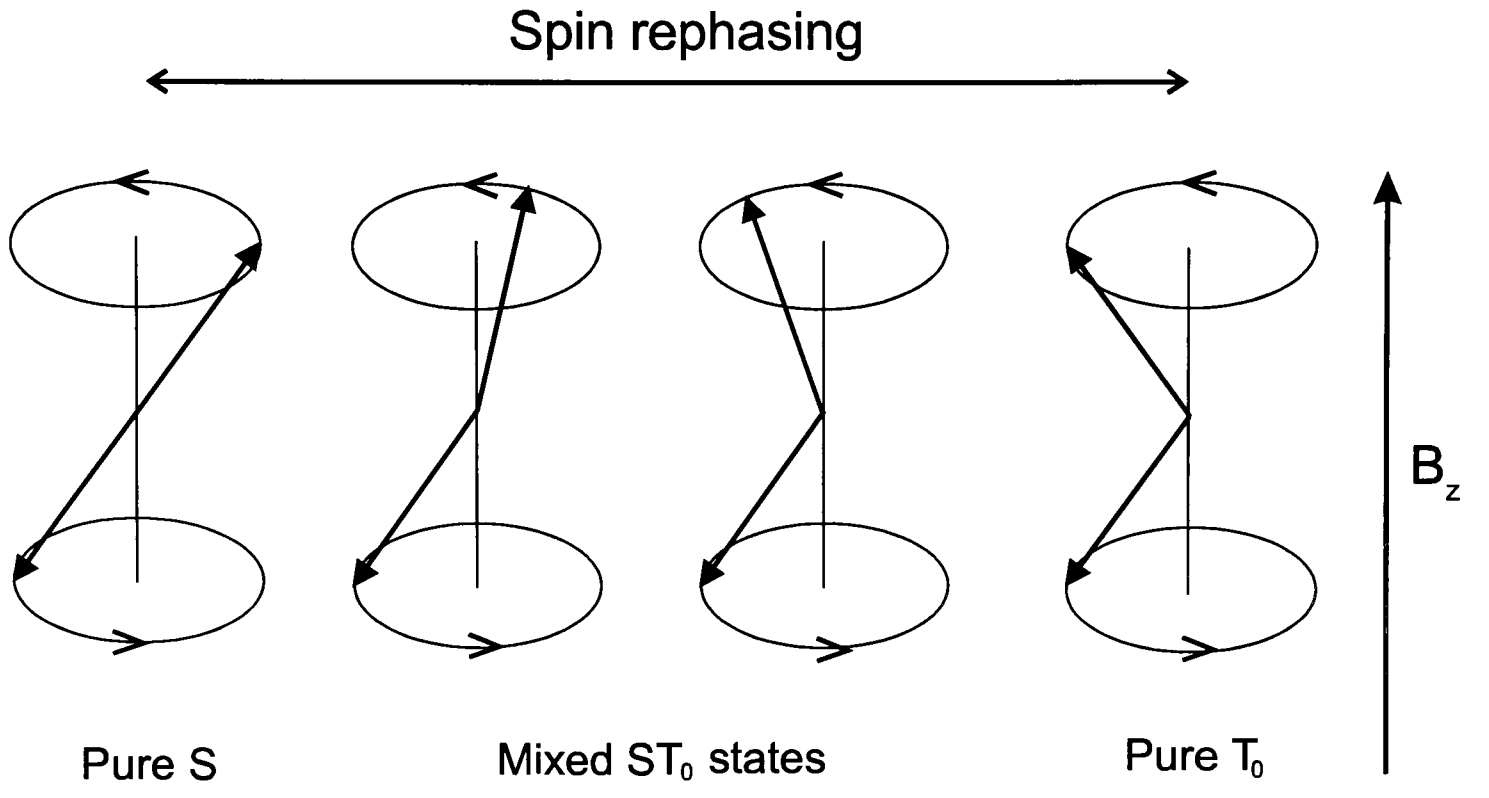

Figure 2.3.3. Spin mixing of the S and T_0 states in a radical pair. The reference frame is rotating at the Larmor frequecy of the lower electron spin

The equation shows that if the two radicals possess different g-values or different local magnetic fields, this difference in Larmor frequencies can be attained. This gives rise to two mechanisms of coherent spin-mixing known as the Δg mechanism and hyperfine mixing respectively.

2.3.3 The Δg mechanism

For carbon centred radicals, it has been stated that there is very little variation in g-value. Typical extremes are shown in figure 2.3.6.

Radical	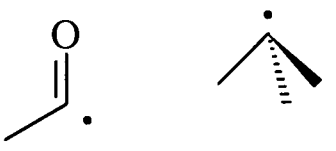		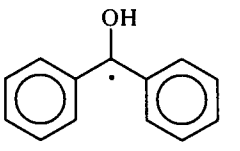	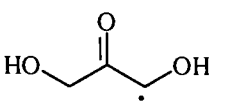
g-value	2.0005	2.0026	2.0030	2.0045

Figure 2.3.6. g-values of some typical organic radicals

For the examples shown, the maximum difference in g-values is $\Delta g=0.004$. This corresponds to spin-mixing time of 18ns at a magnetic field of 0.5T. This is too long to be significant for radical pairs in isotropic solution since the geminate pair lifetime is of the same order, although it may start to be influential in viscous or micellar solutions. The direct dependence of the Δg mechanism on local magnetic field strength means that it becomes much more significant at higher fields. Figure 2.3.7 shows the variation in spin-mixing time with Δg and local magnetic field.

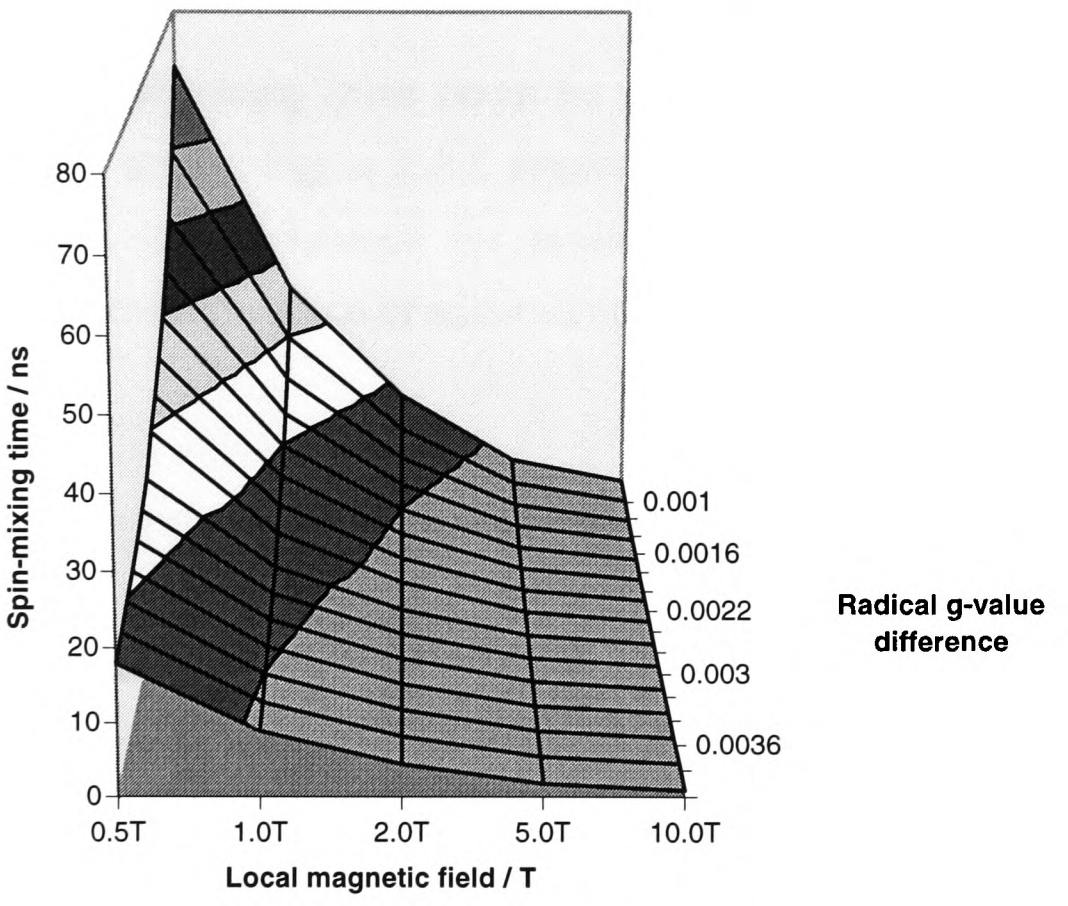

Figure 2.3.7. Variation of spin-mixing time with magnetic field and Δg value.

2.3.4 The hyperfine mechanism

The Larmor frequency of a radical is dependent on the magnetic field it experiences, which involves contributions from the external field and also from hyperfine coupling of the electron spin to the magnetic nuclei. Even a radical pair

consisting of identical radicals can undergo coherent spin-mixing as radicals present in different hyperfine states experience different local magnetic fields and thus the phase of the electron spins can alter and $S\text{-}T_0$ interconversion can occur.

If the members of a radical pair experience local magnetic fields differing by an amount ΔB_L, then complete spin-mixing occurs in a time Δt given by;

$$\Delta\omega\Delta t = \frac{g\mu_B \Delta B_L \Delta t}{\hbar} = \pi \qquad \textbf{2.10}$$

Thus the shortest mixing times occur for radicals in the most energetically separated hyperfine states. Figure 2.3.8 shows the variation of spin-mixing time with local magnetic field difference for radicals with identical g-values. This mechanism is the dominant source of spin-mixing for radical pairs in magnetic fields up to 1T.

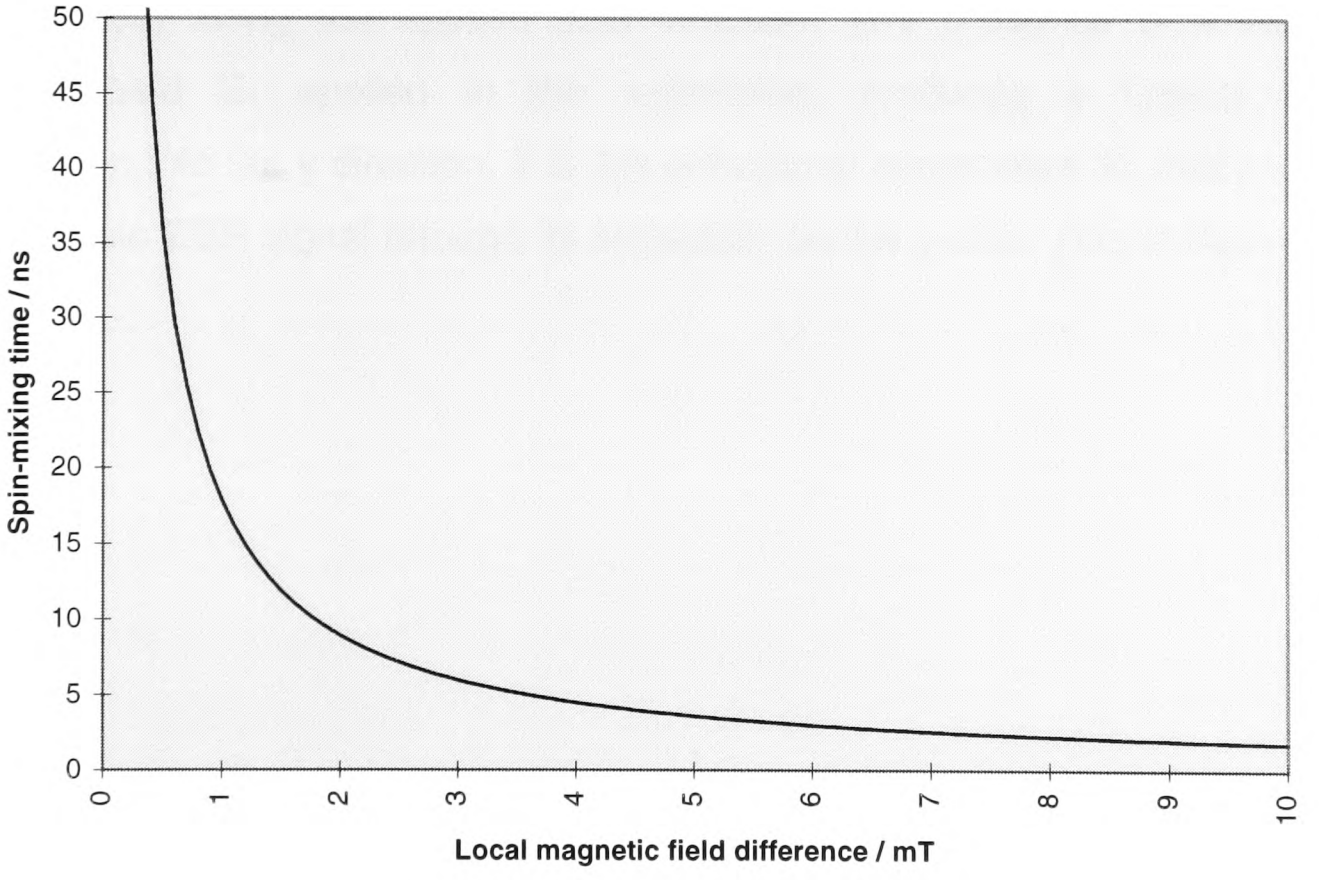

Figure 2.3.8. Variation of spin-mixing time with ΔB_L for radical pairs with Δg=0.

2.4 Incoherent spin mixing - relaxation processes

Relaxation processes occur due to random variations in the local magnetic field experienced by radicals in the liquid phase. They are discussed only briefly here as they are responsible for only minor contributions to the spin-evolution of the radical pair. A more complete coverage can be found in [9]. Relaxation processes are of great significance in ESR as they are responsible for the length of time over which an ESR signal from a transient radical can be observed, and the linewidth of the transition.

Section 2.2.3 explained how in any sample of free-radicals, there is a bulk magnetisation in the z-direction arising from a population difference between α and β spin states. There is no net magnetisation in the xy-plane, however, as the electron magnetic moments are randomly disposed about this axis. If free-radicals are generated by flash photolysis, they are created with an initial magnetisation $M_z(0) \neq M_z(eq)$ along the applied field direction. The presence of a resonant microwave field B_1 applied in the x-direction, produces a tipping of the magnetisation into the y direction. It is this orthogonal component M_y that produces the observable ESR signal through its projection on the y-axis. This is illustrated in figure 2.4.1.

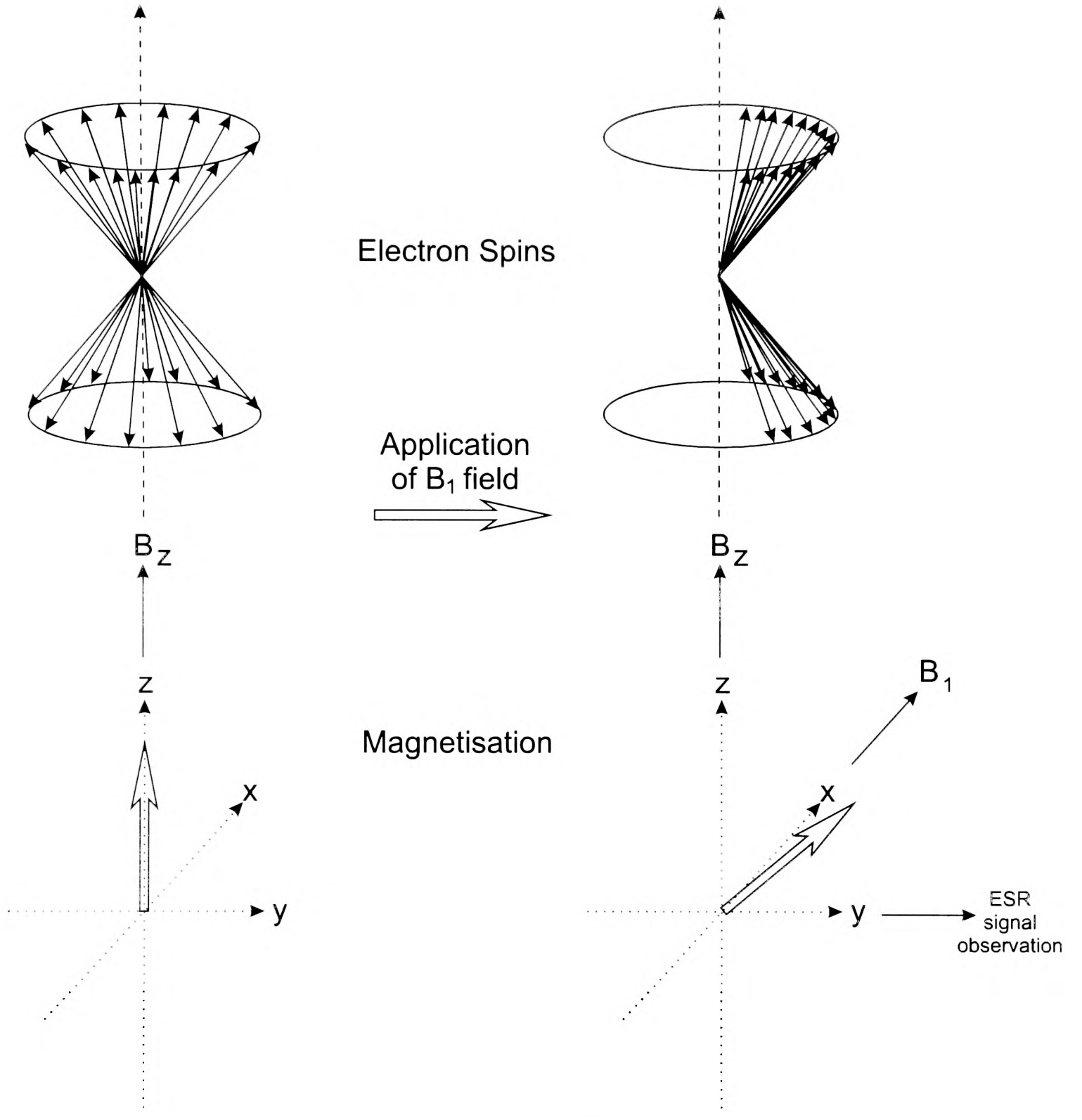

Figure 2.4.1. A bulk magnetisation in the z direction, represented as an ensemble of vectors with random phase in the xy-plane, is observed to obtain a magnetisation in the xy-plane on the application of a resonant magnetic field (B_1) in the x direction. The top half of the diagram illustrates the electron spins in the laboratory frame and the bottom half illustrates the bulk magnetisation with B_1 represented in the rotating frame.

2.4.1 Spin-Lattice relaxation

The relaxation of M_Z back to its equilibrium value in the absence of a B_1 field is referred to as spin-lattice or longitudinal relaxation. Its origin lies in the electron spin of a radical being subjected to varying local magnetic fields as a result of its motion. As a free-radical tumbles through a solution, it experiences a constantly fluctuating magnetic field. This field contains a component at the resonance frequency causing radiationless transitions and restoring the Boltzmann distribution of spin states. As it is the bulk magnetisation in the z-direction that is restored, the term longitudinal relaxation is employed. The return to equilibrium occurs exponentially with a characteristic relaxation time T_1.

$$M_z(t) - M_z(eq) = \{M_z(0) - M_z(eq)\}e^{-\frac{t}{T_1}} \qquad \textbf{2.11}$$

In the presence of a resonant B_1 field, the time evolution is not mono-exponential, but varies as a complex function given by the Bloch equations [10]. T_1 is responsible for the overall difference in spin state populations and thus determines the length of time for which ESR transitions can be observed in a transient experiment. As T_1 depends on the interaction of electron spin with motion within the surroundings, T_1 tends to be short in liquids (with a relevant viscosity dependence) and much longer in solids and at low temperatures.

2.4.2 Spin-spin relaxation

The tipping of the bulk magnetisation into the y direction either by the creation of radicals within a B_1 field (in the x direction) or by the application of a pulse of microwave radiation (as in a fourier transform ESR experiment) lends significance to the xy plane as regards relaxation. Within this plane, relaxation is referred to as spin-spin or transverse. It is also an exponential process with time constant T_2.

$$M_y(t) = M_y(0)e^{-\frac{t}{T_2}} \qquad 2.12$$

The definition of T_2 is as a parameter governing the linewidth of ESR transitions. There are two contributions to T_2. The first is a spin-dephasing process, the origin of which involves different spins experiencing slightly different local magnetic fields due to molecular tumbling giving a variety of precession frequencies and thus a gradual dephasing until there is no net magnetisation in the xy plane. The second represents the lifetime broadening caused by spin-lattice relaxation.

2.4.3 Consequences of relaxation for the radical pair

Relaxation has an effect on the spin-state of the radical pair since any process which flips an electron spin causes S - $T_{\pm1}$ transitions. Spin-spin relaxation processes affect spin-rephasing and therefore S - T_0 mixing.

Spin-relaxation induced in the radical pair generally occurs in a few microseconds for organic radicals in isotropic solution. This means that relaxation is effectively negligible in its effect on singlet-triplet interconversion as the radical pair lifetime is too short. However, in viscous or confined systems, the lifetime of the pair can be significantly increased and relaxation may become significant.

2.5 Relaxation by chemical reaction

Radicals are primarily known for their reactivity. There are two types of reaction that a radical can undergo that do not lead to a reduction in the number of radicals in a system - those that produce new radicals and those that do not. The former of these cases are easily spotted as the change in radicals gives a corresponding change in hyperfine couplings and produces distinctly evolving time resolved ESR spectra. Examples of such processes include radical rearrangements, dimerisations and additions.

Some chemical reactions take place, however, with no change in the nature of the radicals present but are important as they are responsible for relaxation processes. These are highlighted below.

1. Degenerate Electron Exchange (DEE) also referred to as diamagnetic-paramagnetic electron transfer. This involves the transfer of an electron from radical to parent molecule (so called 'electron-hopping') and results in a randomisation of nuclear spin-states. This process occurs commonly in radical-ion pairs, for example between the dicyanobenzene (DCB) radical anion and the DCB molecule;

$$DCB^{\bullet -} + DCB \rightarrow DCB + DCB^{\bullet -} \qquad \textbf{2.13}$$

2. Hydrogen atom transfer between radical and parent molecule. This also causes nuclear spin-state randomisation. For example in propan-2-ol.

$$CH_3C^{\bullet}OHCH_3 + CH_3CHOHCH_3 \rightarrow \qquad \textbf{2.14}$$
$$CH_3CHOHCH_3 + CH_3C^{\bullet}OHCH_3$$

3. A radical anion can accept a hydrogen atom from its protonated form. Although the hyperfine couplings are different in radical and molecule, the process can occur quickly enough that coalescence of related lines in the ESR spectrum can occur.

$$PhCO_2^{\bullet -} + PhCO_2H \rightarrow PhCO_2^{\bullet}H + PhCO_2^{-} \qquad \textbf{2.15}$$

4. Two radicals with opposite electron spin states can undergo a simultaneous 'spin-flip'. Such a process is known as Heisenberg exchange and has the same effect as spin-spin relaxation. A good example is that between two pyrene cations.

$$Py^{\uparrow +} + Py^{\downarrow +} \rightarrow Py^{\downarrow +} + Py^{\uparrow +} \qquad \textbf{2.16}$$

All these chemical processes can affect the spin evolution of the radical pair and may have to be taken into account in the interpretation of magnetic field effects.

References

[1] **Chuang, T.J., Hoffman, G.W. & Eisenthal, K.B.**
Chem. Phys. Lett. 25 (1974) 201

[2] **Muus, L.T., Atkins, P.W., McLauchlan, K.A., & Pedersen, J.B. (Eds.)**
Chemically Induced Magnetic Polarization, Reidel, Dordrecht, 1977.

[3] **Kaptein, R. & Oosterhoff, L.J.**
Chem. Phys. Lett. 4 (1969) 195

[4] **Closs, G.L., Forbes, M.D.E. & Norris, J.R.**
J. Phys. Chem. **90** (1986) 113

[5] **Buckley, C.D., Hunter, D.A., Hore, P.J., & McLauchlan, K.A.**
Chem. Phys. Lett. **135** (1987) 307

[6] **Anisimov, O.A., Grigoryants, V.M., Molchanov, V.K. & Molin, Yu.N.**
Chem. Phys. Lett. **66** (1979) 265

[7] **Trifunac, A.D. & Smith J.P.**
Chem. Phys. Lett. **73** (1980) 94

[8] **Avdievich, N.I., Bagryanskya, E.G., Grishin, Yu.A. & Sagdeev, R.Z.**
Chem. Phys. Lett. 155 (1989) 141

[9] **Atherton, N.M.** 'Electron Spin Resonance - principles and applications'
Ellis Horwood / PTR Prentice Hall, 1993

[10] **Pederson, J.B.**
J. Chem. Phys. **41** (1964) 994

Chapter 3

Behaviour of the radical pair in a magnetic field

3.1 Representation and evolution of radical pair spin-states

The previous chapter was concerned with introducing the radical pair and gave a simple introduction to the mechanism that can cause its spin-evolution. The radical pair is now treated in a more rigorous fashion to reveal the means by which a magnetic field can affect the yield of a radical combination reaction.

3.1.1 Temporal behaviour of the radical pair

Earlier discussion revealed that the behaviour of a radical pair is based on two major processes:

1. Separation and re-encounter of the radicals.

2. Spin-mixing of the radical pair by magnetic interactions.

In a complete mathematical treatment, these two processes are treated concurrently. Such a problem is handled by the Stochastic-Liouville equation which employs a density matrix in both spin and spatial co-ordinates. Practical use of such an approach allows analytical solutions only after severe approximations [1]. Even numerical solutions require certain assumptions [2].

As magnetic interactions are of little consequence unless the radical pair is sufficiently well separated, a reasonable approximation of the system can be obtained by treating the diffusion and spin-mixing of the radical pair separately.

Consider the singlet product of a radical pair reaction. The singlet product yield, φ_S, can be written as

$$\varphi_s(t) = \lambda \int_0^t P_s(t) f(t) dt \qquad \textbf{3.1}$$

where $P_S(t)$ is the probability of the the radical pair being in the singlet state (i.e. this is the spin-mixing term and is magnetic field dependent) and f(t) the probability of the radicals being at a suitable separation to react (i.e. this is the diffusion term and is magnetic field independent). λ accounts for the fact that not 100% of singlet encounters result in product formation. Mathematical treatments of spin-evolution and diffusion are now considered.

3.1.2 Quantum mechanical treatment of spin-evolution

To treat the spin-evolution of the radical pair, it is first represented in terms of the wavefunctions of the radicals. Employing the coupled representation of spins encountered previously, the radical pair wavefunctions can be represented as a linear combination of the individual electronic spin states α and β and the nuclear spins states, N;

Singlet

$$|S,N\rangle = \frac{1}{\sqrt{2}}(|\alpha\beta,N\rangle - |\beta\alpha,N\rangle) \qquad \textbf{3.2}$$

Triplet

$$|T_0,N\rangle = \frac{1}{\sqrt{2}}(|\alpha\beta,N\rangle + |\beta\alpha,N\rangle) \qquad \textbf{3.3}$$

$$|T_+,N\rangle = |\alpha\alpha,N\rangle \qquad \textbf{3.4}$$

$$\left|T_{-},N\right\rangle = \left|\beta\beta,N\right\rangle \qquad \textbf{3.5}$$

(These spin-states are strictly only correct when the external field dominates - the zero-field case is addressed later). The spin-evolution of the pair occurs due to the pair experiencing local interactions which are expressed in the form of a Hamiltonian operator. The radical pair spin-energy is obtained from the energies of the individual radicals and the spin-spin interaction that exists between them.

$$\hat{H}_{RP} = \hat{H}_1 + \hat{H}_2 + \hat{V} \qquad \textbf{3.6}$$

where $\hat{H}_1$ and $\hat{H}_2$ represent the individual radical spin Hamiltonians and $\hat{V}$ represents the interaction between the two radicals. The isolated radical spin Hamiltonians of the radicals can be considered as arising from isotropic and non-isotropic parts.

The isotropic parts of the Hamiltonian arise due to the Zeeman interaction of the electron spin with the external magnetic field (averaged over all the possible radical orientations) and with the magnetic nuclei present through the hyperfine interaction.

$$\hat{H}_{radical} = \hat{H}_{Zeeman} + \hat{H}_{Hyperfine} \qquad \textbf{3.7}$$

The Zeeman energy consists of the electron and nuclear Zeeman interactions represented by the Hamiltonians H_{ze} and H_{zn}.

$$\hat{H}_{Zeeman} = \hat{H}_{ze} + \hat{H}_{zn} = g_e \mu_B \underline{B}.\underline{S} + \hat{H}_{zn} \qquad \textbf{3.8}$$

The nuclear Zeeman energy is of no consequence to the electron spin dynamics and will be ignored.

The coupling of the electron with the nth magnetic nucleus has a hyperfine coupling constant a_n giving the hyperfine Hamiltonian as

$$\hat{H}_{hf} = \hbar \sum_n a_n . \underline{S} . \underline{I}_n \qquad \textbf{3.9}$$

The anisotropic part of the radical spin Hamiltonian has contributions from the dipole-dipole interaction of the electron with the magnetic nuclei, the spin-orbit interaction of the electron and the spin-rotation interaction. These anisotropic contributions are averaged to zero as the radical tumbles freely in solution - the reorientation time being of the order of 10^{-11}s [3]. The anisotropic interactions are responsible for the incoherent spin-relaxation mentioned in the previous chapter. The relaxation rate of the radical is determined by the mean square value of the anisotropic interaction and the rotational correlation time τ_0.

$$W_{relax} = \frac{< H^2_{anisotropic} >}{\hbar^2} . \tau_0 \qquad \textbf{3.10}$$

For organic radicals in solutions of normal viscosity, this gives a relaxation time of 10^{-5} to 10^{-6} s, far longer than the geminate phase of the reaction. Thus as observed previously, incoherent spin-relaxation is not usually of consequence to the spin-evolution of the radical pair.

This gives the overall radical spin Hamiltonian as

$$\hat{H}_{radical} = g_e \mu_B \underline{B} . \underline{S} + \hbar \sum_n a_n . \underline{S} . \underline{I}_n \qquad \textbf{3.11}$$

In order to complete the radical pair spin Hamiltonian, the electron-electron spin interaction must be included. The two electrons experience both exchange and dipole-dipole interactions, although the latter is averaged to zero due to re-

orientational movement of the radicals throughout the geminate phase. The Hamiltonian for the exchange interaction is

$$\hat{H}_{exch} = -\hbar J(r)(2\underline{S}_1\underline{S}_2 + 1/2) \qquad \textbf{3.12}$$

When treating spin and space separately, we consider intersystem crossing to occur only when the radicals have diffused sufficiently far apart for the exchange interaction to be negligible. Under these conditions then, the radical pair spin Hamiltonian can be written as

$$\hat{H}_{RP} = \mu_B \cdot \underline{B}\cdot(g_1\underline{S}_1 + g_2\underline{S}_2) + \sum_m a_{1m}\cdot\underline{I}_{1m}\cdot\underline{S}_1 + \sum_n a_{2n}\cdot\underline{I}_{2n}\cdot\underline{S}_2 \qquad \textbf{3.13}$$

Here S and I represent the electronic and nuclear spin vectors. g_i represents the g-value of the ith radical and a_{ij} represents the hyperfine coupling between the electron and jth nucleus on the ith radical. The summation terms then, represent the individual hyperfine couplings present. If the magnetic field is applied in the z-direction, the expression becomes

$$\hat{H}_{RP} = \mu_B B_z(g_1\underline{S}_{1z} + g_2\underline{S}_{2z}) + \sum_m a_{1m}\underline{I}_{1m}\underline{S}_1 + \sum_n a_{2n}\underline{I}_{2n}\underline{S}_2 \qquad \textbf{3.14}$$

The scalar product of the hyperfine terms $a\underline{I}\cdot\underline{S}$ can be expanded as follows

$$a\underline{I}\cdot\underline{S} = a(I_xS_x + I_yS_y + I_zS_z) \qquad \textbf{3.15}$$

Introduction of the raising and lowering operators $S^{+/-}$ and $I^{+/-}$ allows replacement of the $S_{x,y}$ and $I_{x,y}$ terms.

$$S^+ = S_x + iS_y \quad S^- = S_x - iS_y$$
$$I^+ = I_x + iI_y \quad I^- = I_x - iI_y \qquad \textbf{3.16}$$

These operators raise or lower the electron and nuclear spin angular momenta by one unit. Changes occur in opposite directions for the two radicals such that angular momentum is conserved. Thus equation 3.15 becomes

$$a\underline{I}\cdot\underline{S} = aI_zS_z + \frac{a}{2}(I^+S^- + S^+I^-) \qquad \textbf{3.17}$$

Applying this methodology to equation 3.14 yields

$$\hat{H}_{RP} = \mu_B B_z(g_1\underline{S}_{1z} + g_2\underline{S}_{2z}) + \sum_m a_{1mz}\underline{I}_{1mz}\underline{S}_{1z} + \sum_n a_{2nz}\underline{I}_{2nz}\underline{S}_{2z} \qquad \textbf{3.18}$$
$$+\frac{1}{2}\sum_m a_m(S_1^+I_{1m}^- + S_1^-I_{1m}^+) + \frac{1}{2}\sum_n a_n(S_2^+I_{2n}^- + S_2^-I_{2n}^+)$$

The operation of a Hamiltonian upon a wavefunction occurs according to the Schrödinger equation

$$\hat{H}\psi = E\psi \qquad \textbf{3.19}$$

Examination of the radical pair wavefunctions reveals the singlet state to be antisymmetric and all the triplets to be symmetric (with respect to particle interchange). Thus for singlet-triplet interconversion to take place, the operator must possess an antisymmetric component. It is useful then, to express the spin Hamiltonian as a sum of symmetric and anti-symmetric parts;

$$\hat{H}_{spin} = \hat{H}_+ + \hat{H}_- \qquad \textbf{3.20}$$

$$\hat{H}_{+} = \frac{1}{2}\left[(g_1 + g_2)\cdot\mu_B B_z + \sum_m^{(1)} a_m m_m^{(k)} + \sum_n^{(2)} a_n m_n^{(k)}\right]\cdot(\underline{S}_{1z} + \underline{S}_{2z}) \qquad \textbf{3.21}$$

$$\hat{H}_{-} = \frac{1}{2}\left[(g_1 - g_2)\mu_B \cdot B_z + \sum_m^{(1)} a_m m_m^{(k)} + \sum_n^{(2)} a_n m_n^{(k)})\right]\cdot(\underline{S}_{1z} - \underline{S}_{2z}) \qquad \textbf{3.22}$$
$$+\frac{1}{2}\sum_m a_m(\underline{S}_1^{+}\cdot\underline{I}_{1m}^{-} + \underline{S}_1^{-}\cdot\underline{I}_{1m}^{+}) + \frac{1}{2}\sum_n a_n(\underline{S}_2^{+}\cdot\underline{I}_{2n}^{-} + \underline{S}_2^{-}\cdot\underline{I}_{2n}^{+})$$

Examination of equation 3.22 reveals all the qualitative information necessary to understand the spin-evolution of the radical pair. There are three main terms to the Hamiltonian, each of which can cause spin-mixing of the pair. The terms will be considered individually.

1. $(g_1 - g_2)\mu_B \underline{B}\cdot(\underline{S}_{1z} - \underline{S}_{2z})$. This term is non-zero only if the radicals possess different g-values and corresponds to spin-mixing via the Δg mechanism described in the previous chapter. This term can only cause spin-interconversion between S and T_0 as the operator has no facility to alter the spin angular momentum in the direction of the applied field.

2. $(\sum_m^{(1)} a_m m_m^{(k)} + \sum_n^{(2)} a_n m_n^{(k)})\cdot(S_{1z} - S_{2z})$. This term, like term 1 can only cause rephasing of electron spins, and thus represents an S-T_0 interconversion process caused by the experiencing of different local magnetic fields due to different coupled hyperfine states in each radical. This then is the hyperfine mechanism of spin-evolution.

3. $\frac{1}{2}\sum_m a_m(\underline{S}_1^{+}\cdot\underline{I}_{1m}^{-} + \underline{S}_1^{-}\cdot\underline{I}_{1m}^{+}) + \frac{1}{2}\sum_n a_n(\underline{S}_2^{+}\cdot\underline{I}_{2n}^{-} + \underline{S}_2^{-}\cdot\underline{I}_{2n}^{+})$. $S^{+/-}$ and $I^{+/-}$ are shift operators that swap the spin-state of the electron and nucleus respectively.

Thus hyperfine interactions flip the nuclear and electron spin-states simultaneously, corresponding to an interconversion of the S,T_0 with the $T_{\pm}$ states.

Thus interconversion of all the spin-states is possible. The magnitude of the external magnetic field determines the extent to which mixing can occur and is considered in section 3.1.4. In order to aid this discussion, however, it is useful to consider the time-dependence of the spin-mixing process.

3.1.3 Time dependence of spin-mixing

It is convenient to consider spin-mixing as a transition between two of the four spin-states, for example, a transition between the S and T_0 states. This transition will possess a certain probability of occurring under the influence of the spin Hamiltonian. Thus the total wavefunction is time-dependent and is conveniently approached using perturbation theory.

The total time-dependent wavefunction of any system with multiple states can be written as

$$\psi(t) = \sum_n c_n(t)\psi_n \qquad \textbf{3.23}$$

$c_n(t)$ are time-dependent coefficients representing the relative contributions of the time-independent pure states, ψ_n. These are strictly the individual spin states of the radicals in the absence of the exchange interaction, but are considered here as the high field coupled states for ease of representation i.e. as the singlet or triplet wavefunctions $|S\rangle,|T_0\rangle,|T_+\rangle \& |T_-\rangle$. Consider the mixing of the S and T_0 states. The radical pair is initially created in a pure spin-state which then evolves in time producing a mixed state of varying composition.

$$\psi_{Total}(t) = c_1(t)\left|S\right\rangle + c_2(t)\left|T_0\right\rangle \qquad \textbf{3.24}$$

Thus an initially triplet radical pair will possess $c_1(0)=0$ and $c_2(0)=1$. It is then necessary to solve for $c_n(t)$ in equation 3.18. This is achieved by employing the time-dependent Schrödinger equation

$$\hat{H}\psi = i\hbar\frac{d\psi}{dt} \qquad \textbf{3.25}$$

This has the formal solution

$$\psi(t) = \psi(0)e^{-\frac{-iEt}{\hbar}} \qquad \textbf{3.26}$$

Applying this methodology to equation 3.18 produces

$$\psi(t) = \sum_n c_n(t)\psi_n(0)e^{\frac{-iEt}{\hbar}} \qquad \textbf{3.27}$$

Thus the time dependence of the wavefunction is carried purely in the coefficients c_n. In order to solve for the coefficients, it is assumed that the application of the magnetic operator changes the initially well defined quantum state of the system by only a small amount i.e. the spin Hamiltonian acts as only a small perturbation on the system's total energy. Dirac introduced the mathematical technique to solve this equation, the variation of constants method - it is not included here but is widely recorded in the literature [4]. The results give the time dependence of the probability of transition to a singlet state after formation in a pure triplet state as

$$P_S = (c_0(t) \cdot c_0^*(t)) = \frac{2H_{S,T_0}^2}{\hbar^2\omega^2}(1-\cos\omega t) \qquad \textbf{3.28}$$

where ω is the energy separation of the two states and H_{S,T_0} is the matrix element $\langle S|\hat{H}_{RP}|T_0\rangle$ giving the mixing strength of the transition (the probability of transition between *any* two of the spin-states can be obtained by supplying the correct matrix element). It is thus clear that a system created initially in a triplet state will oscillate between this and the singlet state (assuming the matrix element H is finite) at a frequency dependent upon the energy separation of the two states and with a probability inversely proportional to the square of the separation. Thus the total wavefunction is a mixed state with the S and T_0 contributions oscillating as indicated in figure 3.1.1.

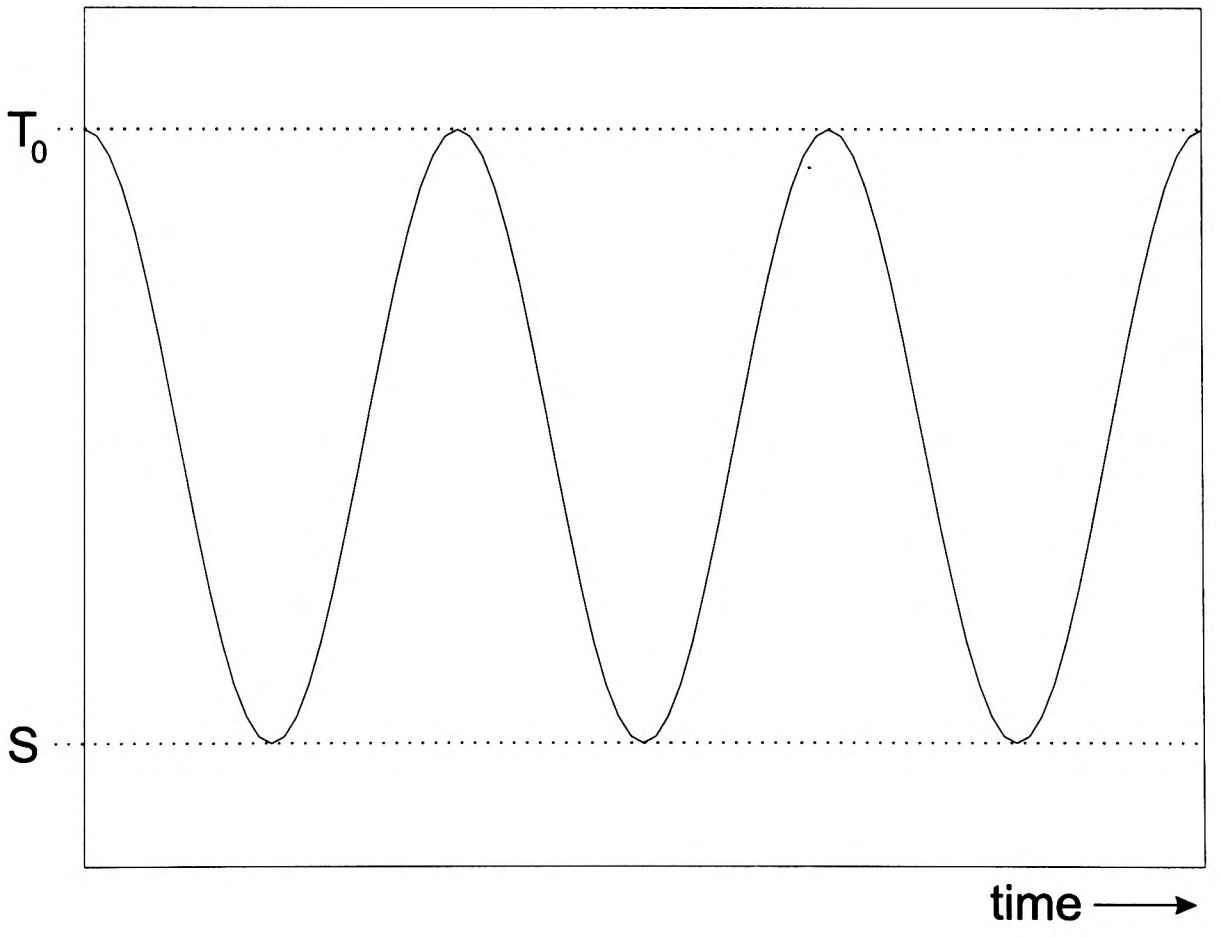

Figure 3.1.1. The time dependence of the total wavefunction predicted by perturbation theory for the S and T_0 states of a radical pair under the ST_0 matrix element of the spin Hamiltonian.

There are two more significant points that must be made in reference to this oscillatory behaviour.

First, real radical pair systems exist in many hyperfine states and thus spin-mixing occurs with many different interfering frequency components. This means that the spin-evolution of the pair from its inital state to a statistical distribution occurs with a sigmoidal, rather than oscillatory function.

Second, it is important to note that as the separation of states increases, the amplitude of the spin-mixing is decreased, but the frequency increases. However, the amplitude shows a much stronger dependence on ω than does the frequency, and thus, as the separation of energy levels increases, the probability of transition between them is decreased and the efficiency of singlet-triplet mixing is reduced.

3.2 Magnetic field regimes and spin-mixing

The complexity of the spin-evolution of a radical pair means that different magnetic field regimes are best treated individually. They are now discussed in terms of increasing magnitude of the applied field.

3.2.1 The zero-field regime

In the absence of any magnetic field, all the B_0 dependent terms are removed from the spin Hamiltonian, and only hyperfine terms remain. Solution of the Schrödinger equation under these conditions is almost intractable for real radical pair systems with many different hyperfine couplings: however good approximations exist [5]. Equation 3.23 implies that the amplitude of spin-mixing ought to be infinite, but accompanied with a mixing frequency of zero. However, even for J(r)=0, the S and T states are non-degenerate due to the difference in hyperfine levels present.

Thus although spin-mixing can occur between most states, many of the eigenstates are degenerate and thus are not temporally interconverted. This implies that the efficiency of singlet-triplet mixing is not at its maximum, and hence the rate at which the 3 : 1 triplet : singlet statistical distribution ratio of the radical pair is obtained is also not at its theoretical maximum. This is of great significance to the work in this thesis as will be revealed shortly.

3.2.2 The low-field regime

Applying a very small magnetic field (for instance one of environmental magnitude) serves to remove many of the eigenstate degeneracies described in 3.2.1. If the field is sufficiently small, the energy gap between the S,T_0 and $T_{\pm}$ states does not significantly reduce the mixing rate, and thus in the presence of a small field, the efficiency of singlet - triplet interconversion is **increased** relative to the zero-field case. This is then the origin of the mechanism by which environmental magnetic fields can alter the yield of a radical reaction. It is discussed further shortly.

As the field magnitude is increased, the $T_{\pm}$ states become increasingly removed in energy and thus (as described above), the amplitude of spin-mixing decreases and the rate of singlet - triplet interconversion is reduced. Ultimately, only the S and T_0 states are capable of mixing and the singlet : triplet statistical ratio now becomes 1 : 1. Once again, calculations at fields below this cut-off value are complex.

3.2.3 The high-field regime

The situation has now arisen where only $S\text{-}T_0$ mixing can occur and thus the mixing efficiency is now magnetic field-independent until the field is sufficiently large

to allow significant contribution from the Δg term. The effect of this term, once active, is to enhance the efficiency of $S\text{-}T_0$ interconversion, producing a field effect in the opposite sense to that produced by the separation of the $T_{\pm}$ states. Calculations in this region become much more simple as the Hamiltonian matrix becomes independent of specific nuclear states.

3.3 Spatial motion of the radical pair

It is now clear how the magnetic nature of the radical pair gives rise to varying behaviour at different applied field strengths. However, to understand the time evolution of a radical pair, its spatial motion must be considered and the spin-mixing processes convoluted to the diffusional behaviour of the pair. Random radical encounters in solution give rise to a randomisation of radical pair spin-states (the so-called 'freely-diffusing' or f-pairs) to produce the 3 : 1 statistical ratio of triplet : singlet (assuming no reaction from singlet and triplet channels). Thus any experiment will detect this non-magnetic background behaviour unless the detection technique is magnetic field-sensitive (see chapter 9). This reduces the overall effect of any magnetic field present. However, in order to understand the magnetic field behavior, we need only consider the geminate phase of the reaction with regard to radical separation and re-encounter.

The concept of the geminate phase of a reaction results from a consideration of the cage effect - first discussed by Franck and Rabinowitch [6]. Two molecular fragments in solution do not always separate. They can recombine and yield the parent molecule or react in some other sense to produce different molecular products. These products are referred to as 'geminate products' occuring as a result of in-cage recombination. Alternatively the fragments can leave the cage and react in the bulk, such products are referred to as 'escape products'. These processes were illustrated earlier in figure 2.1.4.

Thus, intuitively, the fragments are considered to be held together in a cage. The cage is considered to consist of solvent molecules and has two characteristic properties:

1. The cage ensures the reactant pair remain as partners for longer in condensed media than in the gas phase.

2. The cage allows for the re-encounter of the same radicals after radical diffusion.

The nature of the solvent cage is characterised by its radius, and by the in-cage lifetime of the reactants, τ_D. The value of these parameters is affected by a number of factors, including radical reactivity and concentration. However, two key factors to the nature of the cage are the viscosity of the solution and the long-range attraction between reactants. Indeed radical ions with opposite charge massively increase the cage radius.

A number of different approaches have been used to describe the in-cage radical motion. They are outlined below.

3.3.1 Diffusional models

Chandrasekhar [7] developed a theory of diffusion by jumps in continuous media. This assumed that species move in discrete steps of constant distance in an arbitrary direction i.e. to any point on a spherical surface of radius λ_D the jump length. This model was later employed by Noyes [8] in the calculation of re-encounter statistics. Two partners (e.g. the members of a radical pair) are only considered in contact if their separation is less than the radius of contact b, often assumed equal to the total van der Waals radii of the partners. Calculations show [8] that in the case of $\lambda_D >> b$, the situation is analogous to diffusion in the gas phase

(i.e. no cage effects) whereas the probability of re-encounter given λ_D<b tends towards unity in the extreme case of continuous diffusion. The re-encounter probability is approximately 0.5 when λ_D=b, i.e. when molecules jump by steps approximating their contact radius. In real systems, the jump length of reactant species is unlikely to exceed molecular sizes considerably and so continuous diffusion and diffusional jumps of $\lambda_D \approx$b are the most commonly used models for re-encounter. Both models agree in a number of significant areas

1. The long time contact probability can be described by a function of the form $f(t) \sim t^{-\frac{3}{2}}$ irrespective of the molecular jump length. However, on time-scales of the order of individual jump steps, the distribution depends upon the detailed particle motion. Since spin-mixing is slow on the timescale of molecular jumps, it is the long-time behaviour which is relevant to the type of study described here.

2. Using functions of the form described above, produces spin-state yields dependent upon the square root of the hyperfine coupling elements and the jump length. These are used in both the modelling of magnetic field effects and the polarisation patterns of CIDEP spectra.

3. The use of the different models is dependent upon the exact nature of the chemical system under scrutiny. As is often the case with the comparison of theory and experiment, different models are employed and the greater their match with experimental results, the more likely they are to describe the microscopic picture responsible.

The models described above in both their basic and highly refined forms give good agreement with experimental results for neutral radical pairs in isotropic solution, although their complete solution is complex. An alternative approach is the

exponential model which can be employed with much greater ease of calculation and more relevance to radical ion pairs or pairs with restricted motion, for example those encapsulated in a micelle or microemulsion.

3.3.2 The exponential model

This model is considerably simpler than the diffusional models described above. It effectively assumes unimolecular decay of the ensemble of radical pairs with a Poisson distribution of the pair lifetimes. The function f(t) (from equation 3.1) can then be written as

$$f(t) = \frac{1}{\tau} e^{-\frac{t}{\tau}} \qquad \textbf{3.29}$$

where τ is the radical pair lifetime. This gives a good approximation to the observed kinetics of a pair of charged radicals [2] where the diffusion is affected by the strong electrostatic forces between the radicals. In fact studies in solutions of various permittivities show that the model fits well even in solutions of high dielectric constant.

For neutral radical pairs, the model may provide good agreement when the diffusion of the radicals is restricted. This is of particular relevance in biological systems where radicals may be created within small biological structures, for example inside a cell membrane or trapped within a supercoil of DNA (see later).

In the short time limit, the exponential model shows a strong, squared dependence on the hyperfine couplings and the pair lifetime compared to the much weaker square-root dependence predicted by the diffusional models.

One feature that all the models of spatial motion share is that although radical re-encounter is quite likely at early times after pair formation, the probability of re-encounter decays rapidly in time.

3.4 Magnetic field effects

The effect of a magnetic field on the spin-mixing of a radical pair along with the pair dynamics has been considered. It is crucial now to determine what this means in practice. How do the mechanisms described affect the measurable characteristics of a chemical system? This thesis is concerned with photochemical reactions. Observable quantities include product yields and radical yields, measured both transiently and by collection. The former are usually measured by optical techniques - either by emission detection (fluorescence and phosphorescence decay signals) or by absorption spectroscopy. Steady state techniques include the NMR of products and other standard analyses e.g. gas chromatography. Radical yields can also be detected transiently using EPR or optical spectroscopy. Alternatively spin-trapping can be employed to collect radicals for subsequent analysis. Regardless of the detection technique employed, the ultimate measurable quantity is related to either the singlet or triplet yield of the radical pair, the specifics depending upon the system under scrutiny.

Consider a reaction that involves the creation of a triplet radical pair and the observation of a molecular product arising due to singlet recombination of the radical pair e.g.

$$^1M \xrightarrow{h\upsilon} {}^1M^* \xrightarrow{ISC} {}^3M + S \rightarrow {}^3\{R_1^\bullet + R_2^\bullet) \xleftrightarrow[Spin\ mixing]{} {}^1\{R_1^\bullet + R_2^\bullet) \rightarrow X$$

Figure 3.4.1 Formation of a triplet radical pair and recombination from the singlet state after spin mixing.

where X is the product under observation.

It is possible to predict the effect of a magnetic field on the yield of X using the ideas described in section 3.2. Figure 3.4.2 shows the field dependence of φ_X, the yield of X on the magnetic field strength.

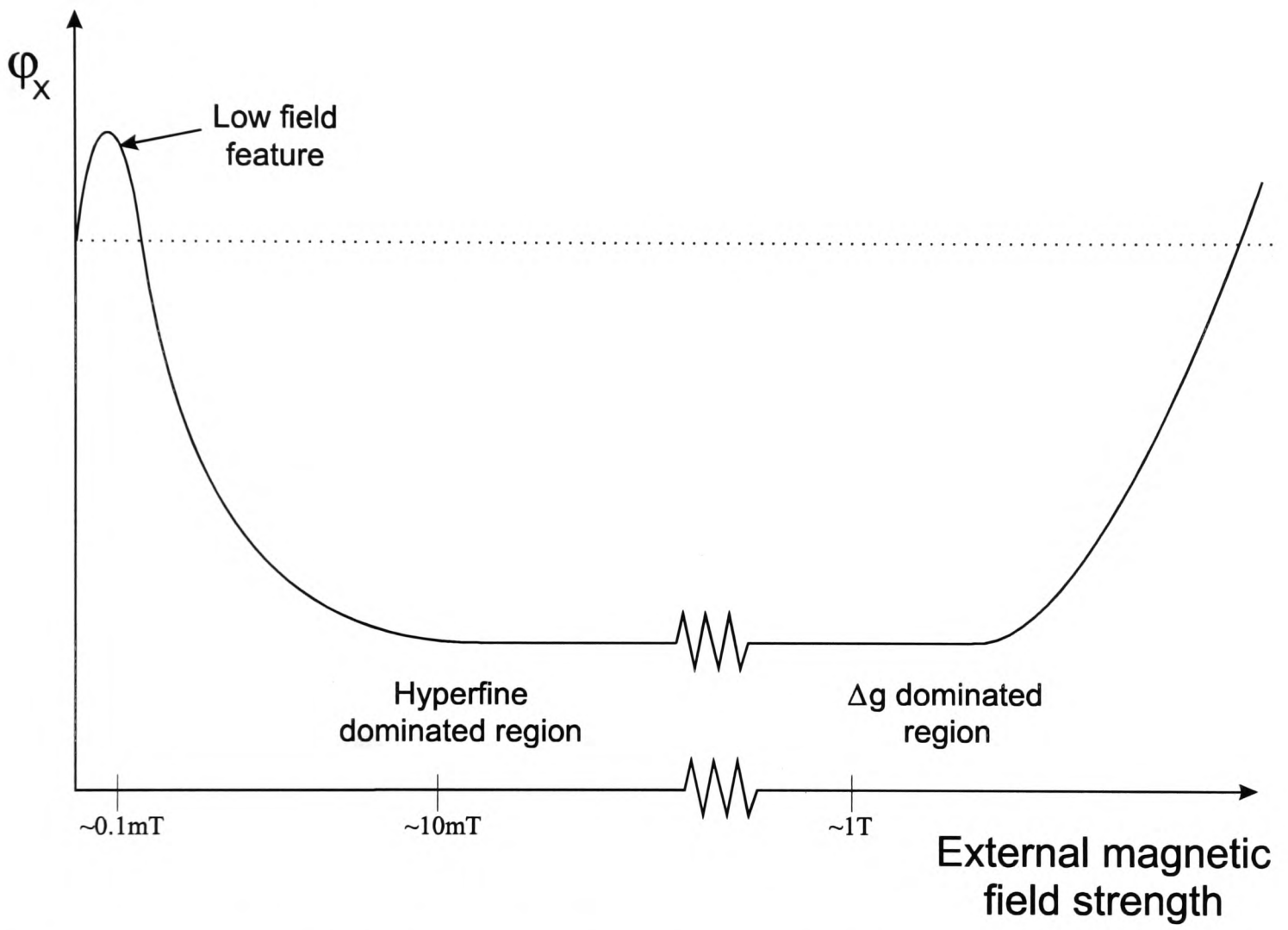

Figure 3.4.2. Variation of singlet product yield with magnetic field strength for an initially triplet radical pair. This diagram neglects relaxation effects.

The product yield is increased at low magnetic fields due to the enhanced rate of spin-mixing caused by the removal of degeneracies of certain spin-states. As the field is further increased, the singlet-triplet conversion efficiency is reduced as the $T_{\pm}$ states are removed in energy. At high fields, the Δg mechanism is responsible for enhancing spin-mixing and increasing the singlet yield once again.

This is only one possible situation that can arise. Often, the radical yield is of much greater relevance and the initial pair can be formed in either a singlet or triplet state. Figure 3.4.3 details the possible situations that can arise and the effect of the various magnetic field regimes upon them.

Initial radical pair spin-state	Radical pair spin-state yielding observed species	Effect of very low magnitude magnetic field	Effect of removal of $T_{\pm1}$ states by Zeeman splitting	Effect of Δg dominated spin-mixing (relative to Zeeman split condition)
Singlet	Singlet	Yield reduced	Yield increased	Yield reduced
Singlet	Triplet	Yield increased	Yield reduced	Yield increased
Triplet	Singlet	Yield increased	Yield reduced	Yield increased
Triplet	Triplet	Yield reduced	Yield increased	Yield reduced

Figure 3.4.3. Effect of magnetic field regions on product yield for varying initial RP and product spin states.

Numerically, the effect of a magnetic field on a reaction yield is handled by subtracting the product yield in the absence of a field, from the field present yield and normalising. This is known as the field effect (F.E.). It is also often expressed as a percentage.

$$F.E.=\frac{Yield(field\ on)-Yield(field\ off)}{Yield(field\ off)}x100\% \qquad \textbf{3.30}$$

In the situation of an initially singlet radical pair and observation of product via the singlet radical pair channel, the probability of singlet product formation P_s is given by

$$P_s = 1 - P(S \rightarrow T) \qquad \textbf{3.31}$$

Applying this to the integrated form of equation 3.30 yields

$$F.E. = 1 - \frac{P(S \rightarrow T)_{field\ on}}{P(S \rightarrow T)_{field\ off}} \qquad \textbf{3.32}$$

This allows a simple method for directly comparing experimental results with theoretical calculations. In zero field, the F.E. has a value of zero. Increases in product yield relative to zero field give the field effect a positive value (negative values arising for reduced yields). Thus the expected sign of the F.E. can be determined readily from figure 3.4.3.

References

[1] **a) Haberkorn, R.**
Chem. Phys. **19** (1977) 165
b) Haberkorn, R.
Chem. Phys. **24** (1977) 111
c) Haberkorn, R.
Chem. Phys. **26** (1977) 35

[2] **Werner, H-J., Schulten, Z. & Schulten, K.**
J. Chem. Phys. **67** (1977) 646

[3] **Salikhov, K.M., Molin, Yu.N., Sagdeev, R.Z. & Buchachenko, A.L.**
'Spin polarization and magnetic effects in radical reactions', Elsevier 1984

[4] **Atkins, P.W., 'Molecular Quantum Mechanics'.**
2nd Edition; Oxford University Press 1983.

[5] **Schulten, K. & Wolynes, P.G.,**
J. Chem. Phys. **68** (1978) 3292

[6] **Franck, J. & Rabinowitch, E.**
Trans. Far. Soc. **30** (1934) 120

[7] **Chandrasekhar, S.**
Rev. Mod. Phys. **15** (1943) 1

[8] **Noyes, R.M.**
J. Chem. Phys. **22** (1954) 1349

Chapter 4

Experimental Strategies

The motivation behind the work in this thesis is to take the knowledge of both experiment and theory regarding the effect of magnetic fields on radical pairs and to try to extend those ideas to encompass biological systems. The aim is to see if this mechanism may have significance in interpreting and predicting the effect of magnetic fields upon the human body.

Moving from chemical systems to biological systems is a significantly large step and within the course of the work contained herein, it has been approached in a number of ways. Before the strategies can be examined, the state of understanding at the starting point must be well defined. This provides a strong base, then, for the extension of ideas into new areas.

All the discussion in the previous two chapters refers to static magnetic fields. Magnetic fields generated by overhead power cables and electrical equipment, however, are oscillating fields with a frequency of 50 or 60 Hz. Chapter 2 discusses the relaxation and dynamics of radical systems and concludes that any effects on radical recombination occurs on timescales sufficiently small that field oscillating at 50 / 60 Hz appear static to the radical pair. All further theory and experimentation refers, then, to static magnetic fields only, but applies equally to environmental oscillatory fields.

4.1 Magnetic field effects in chemical systems

Much successful research has been carried out on the observation of MFEs. Both time-resolved and steady state experiments are common,

employing photochemical methods for the generation of free radicals and the detection of products. A review of the work performed in this field is not included here, but useful references include [1,2]. More important is to outline the key features discovered regarding the nature of experimentally observed effects.

1. The effect of the solvent 'cage' described earlier is of great significance in the observation of MFEs. The most prominent and readily measured effects tend to be in radical ion pair systems, in solutions of high viscosity or in compartmentalised systems such as micelles or microemulsions. The latter of these have significant bearing in biological systems as mentioned above.

2. In virtually all experimental cases, the magnitude of the field effect at environmental strength fields (the so-called 'low-field feature') is considerably smaller than the effect due to removal of the $T_{\pm 1}$ states by the Zeeman splitting. This region will henceforth be referred to as the high-field region and involves magnetic fields of magnitudes under 1T. This thesis is not concerned with fields of greater magnitude than this and so effects arising due to the Δg mechanism will not be considered further.

It is only in recent studies that the significance of the low-field effect (LFE) is commented upon. As it is this field region that is of concern for environmental field interaction, it is important to discuss exactly how such an effect arises and the properties of the system that may maximise it.

4.1.1 The low-field feature

Theoretical calculations and discussion on the nature of the low-field feature are available in a recent paper by Brocklehurst and McLauchlan [3] as a

result of a study carried out alongside the results contained in this thesis. A brief discussion of the conclusions is included here.

Although the origin of enhanced spin-mixing at low-fields was described in chapter 3, removal of some of the constraints on angular momentum conservation is not the only mechanism by which a low-field feature may arise. Referring to figure 2.3.1 reveals that for a non-zero value of the exchange interaction there is a crossing of S and T_{-1} levels with the possibility of enhanced spin-mixing in this region. In biological systems, it is feasible that the radical pair may not be mobile but anchored to a protein or other biostructure. If the radicals are indeed constrained in their movement with an average inter-radical difference corresponding to a small but appreciable exchange interaction, enhanced S-T_{-1} mixing (due to application of a small magnetic field of suitable magnitude) may have an effect on the extent of reaction and the number of radicals escaping. Such an effect is referred to as a J-resonance [4,5,6].

Calculations by Brocklehurst & McLauchlan [3] have revealed some key features regarding the factors influencing the magnitude of LFEs. Employing the exponential model described earlier to model the diffusion of a real radical pair, two main factors are discovered to alter the magnitude of any LFEs.

1. The radical pair lifetime significantly affects the LFEs observed, with longer pair lifetimes producing much more substantial effects. Although this effect has not been previously remarked upon, it is intuitively correct. The magnitude of the effect depends upon enhanced spin-mixing in the radical pair over the zero field case. If the pair lifetime is short in both zero- and low-field, little or no spin-mixing will be observed in either case and thus very little difference will exist between the two cases. If, however, the pair lifetime is increased, spin-mixing will become more efficient in zero and low-field and the difference between

the two cases will manifest itself. If this argument is a true one, the magnitude of the LFE is a measure of the efficiency of spin-mixing in zero field.

2. LFEs appear to be maximised in systems in pairs where one radical possess extensive hyperfine coupling and the other radical has little coupling. This is also illustrated in practice [7,8] and is useful in the choice of chemical system if maximisation of LFEs is the experimental aim.

The mechanism by which low-fields can affect radical recombinations poses the question of whether spin-mixing in zero or low-field can be enhanced by the application of radiation resonant with the energies of the singlet and triplet states. As described previously, different hyperfine states give rise to slightly different radical pair energies. Radiation in the radio-frequency region of the spectrum corresponds to the differences in energy of the hyperfine states and thus it is reasonable to suggest that the application of RF radiation of suitable frequency may also be able to affect radical recombination yields. The testing of this hypothesis has formed one of the large areas of work in this thesis and is discussed in chapter 7.

4.1.2 Experimental approach

Armed with a fairly comprehensive understanding of MFEs in chemical systems, there are a number of ways to approach the transition into biologically significant systems. The flowchart below reviews possible experimental strategies.

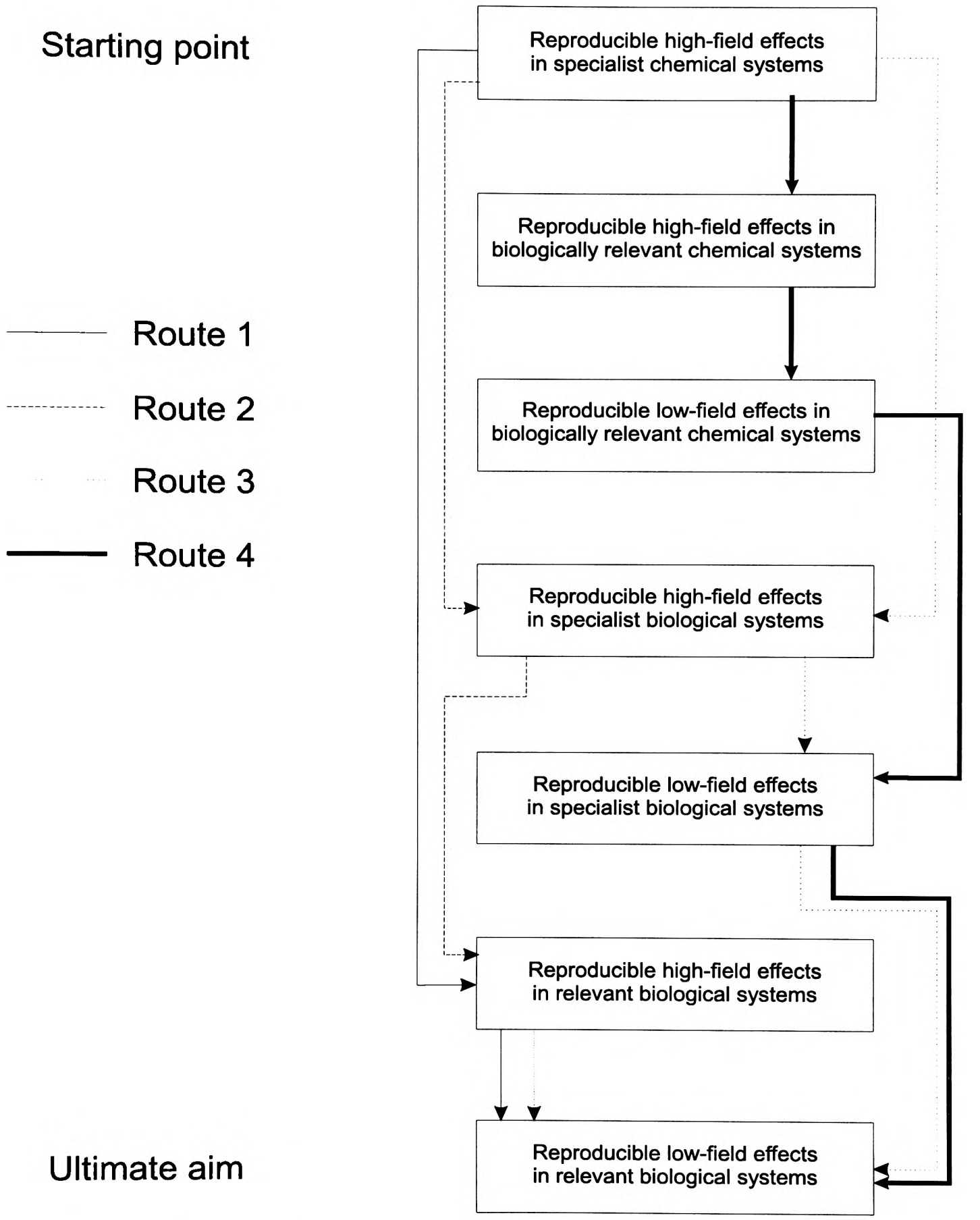

Figure 4.1.1. Flowchart illustrating logical strategies for the investigation of LFEs in biological systems.

Routes 1-4 indicated are sensible approaches to the problem. Route 1 relies on applying knowledge of radical recombination reactions to existing biological assays and was employed in early research on photochemical damage in yeast cells and in the behaviour of a known enzyme system suspected to operate via a free-radical mechanism (see chapter 5). Routes 2 and 3 involve designing biological systems tailored to allow convenient detection and as little deviation as possible from established chemical systems (see chapter 6).

The chemical systems studied previously by the Oxford group and elsewhere have concentrated on radical ion pairs in viscous solutions with fluorescence detection of products. In biology, most of the chemical systems are water based (although diffusion is often limited to the confinement of reagents with cells, membranes etc). Thus a worthwhile stepping stone to biological systems is with water based chemical systems involving neutral radical pairs (route 4). Such systems are unlikely to produce fluorescing products and so alternative methods of analysis must be employed. These problems are addressed in chapter 8.

It is also important to note that, although the initial motivation behind this work was to assess the potential interaction between environmental strength fields and biology, the observation of effects at any magnetic field strength is still of great significance.

References

[1] **Salikhov, K.M., Molin, Yu.N., Sagdeev, R.Z. & Buchachenko, A.L.**
'Spin polarization and magnetic effects in radical reactions' Elsevier 1984

[2] **Steiner, U.E. & Ulrich, T.**
Chem. Rev. **89** (1989) 51

[3] **Brocklehurst, B. & McLauchlan, K.A.**
Int. J. Radiat. Biol. **69** (1996) 3

[4 **Werner, H-J., Schulten, Z. & Schulten, K.**
J. Chem. Phys. **67** (1977) 646

[5] **Staerk, H., Kühnle, W., Treichel, R. & Weller, A.**
Chem. Phys. Lett. **118** (1985) 19

[6] **Tanimoto, Y., Okada, N., Itoh, M., Iwai, K., Sugioka, K., Takemura, F., Nakagaki, R. & Nagakura, S.**
Chem. Phys. Lett. **136** (1987) 42

[7] **Stass, D.V., Tadjikov, B.M. & Molin, Yu.N.**
Chem. Phys. Lett. **233** (1995) 444

[8] **Stass, D.V., Tadjikov, B.M. & Molin, Yu.N.**
Chem. Phys. Lett. **235** (1995) 511

Chapter 5

Investigations involving established biochemical systems

The logical starting point for the investigation was to select a biological system that had been studied previously in some detail, and was known to involve free-radicals. The experimental system chosen for study was selected particularly due to the fact that it was currently being used by another research group in Oxford when this investigation was undertaken.

5.1 The killing of yeast cultures by photoactive reagents

5.1.1 Introduction

The work described here has been carried out under the supervision of Dr J. Knowland in the Biochemistry department. Strains of yeast are known to be particularly sensitive to attack by free radicals [1], thus the basic strategy is to deliberately produce radicals in their presence and subsequently to assay their viability.

The assay system employed in these experiments utilises a strain of yeast that has been genetically altered to make it incapable of repairing certain types of damage caused to the DNA, where dimerisation of pyrimidine bases occurs forming cyclobutane dimers and 6-4 photoproducts [2]. Radicals are created in a photochemical reaction by exciting a photoactive molecule with ultra-violet radiation. At the onset of the experiment, pyrene was chosen as the radical source, chiefly because its photochemistry and role in magnetic-field dependent recombination reactions have previously been extensively studied by the group. Pyrene undergoes photochemical excitation (see appendix) to an excited singlet

state. This state then tends to donate or accept an electron to produce a radical ion pair as indicated in figure 5.1.1.

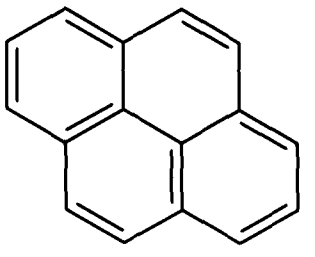

Pyrene = Py

$$Py \xrightarrow{h\nu} {}^1Py^* + A \rightarrow {}^1\{Py^{\bullet+}\ A^{\bullet-}\}$$

$$Py \xrightarrow{h\nu} {}^1Py^* + D \rightarrow {}^1\{Py^{\bullet-}\ A^{\bullet+}\}$$

Figure 5.1.1. Formation of singlet-correlated radical pairs by photoexcitation of pyrene and subsequent electron transfer.

Preliminary experiments showed that irradiation of a suspension of yeast cells to which pyrene had been added caused a large killing effect upon the yeast cells.

Figure 5.1.2 shows the UV absorption spectrum of DNA. The strongest absorption occurs at around 260nm, the so-called UVC region. This absorption results in damage to the absorbing bases.

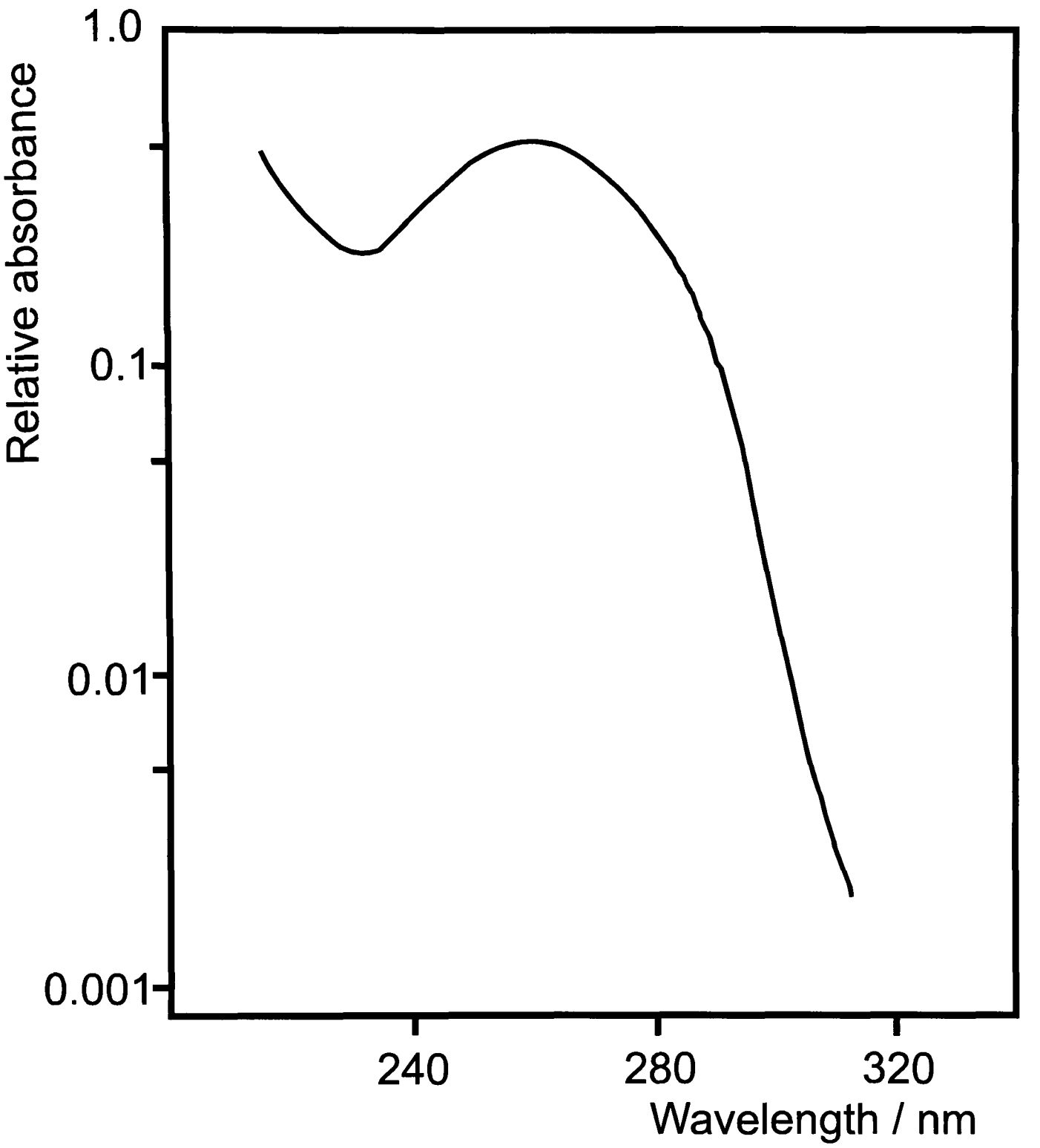

Figure 5.1.2. UV absorption spectrum of DNA in vitro

Absorption occurs until approximately 320nm, through the UVB and UVA regions, and although the quantum yields of DNA damage occurring at these frequencies are reduced, damage can still occur. Thus in any experiment where

DNA damage from photochemically generated free radicals is being assessed, these frequencies must be eliminated.

The yeast cells employed were eukaryote, budding cells of genotype *ade 2.1 can 1.100 SUPQ5 RAD1::LEU2 [psi⁻]* with a *rad1* disruption [3].

5.1.2 Experimental

For details of all buffer solutions, see appendix D.

Yeast cells were grown overnight in the dark, in rich (YEPD) medium until in the exponential phase of growth (approx 2 x 10^6 colony forming units (CFU) per ml) as they are particularly sensitive to radical damage at this stage [4]. Cells were harvested and twice washed in 20mM sodium phosphate pH 7.4. Two aliquots of 2.5ml of suspended cells were then taken for sample preparation.

Pyrene (supplied by Aldrich and recrystallised from ethanol) was dissolved in ethanol to give a saturated solution (0.054mol dm^{-3}). This solution was then diluted with ethanol and a number of preliminary experimental runs were performed to determine the approximate pyrene concentration required to produce a suitable degree of yeast cell death. A concentration of 1 / 50,000 of the saturated pyrene solution was observed to produce useful results and was employed in the subsequent experiment. 2.5ml of the pyrene solution was added to one of the 2.5ml cell aliquots giving an overall pyrene concentration of 10^{-5} times the saturated pyrene solution. This corresponds to an actual pyrene concentration of 5.4 x 10^{-7} mol dm^{-3} (determined by UV spectrometry). To the other aliquot, 2.5ml of ethanol was added to produce a control sample. The final cell density in the samples was 2 x 10^7CFU / ml. The cells were left (in the dark) to equilibrate with the pyrene or ethanol solutions for 15 mins prior to irradiation.

A 1.5ml aliquot of each sample was introduced to either side of a double-chambered quartz cuvette, allowing simultaneous irradiation. The cuvette was contained in a jacket with a silica window, kept at 28^0C by circulating water. Sterile air was continuously passed through the cells in order to keep them suspended.

The samples were illuminated with a 250W Xe arc lamp fitted with a WG320 Schott glass filter which removes all wavelengths shorter than 320nm and thus prevents any direct DNA damage. The irradiation apparatus is illustrated in figure 5.1.3.

2 experimental runs were performed resulting in 4 different samples;

1. Yeast cells without pyrene with magnetic field
2. Yeast cells with pyrene with magnetic field
3. Yeast cells without pyrene without magnetic field
4. Yeast cells with pyrene without magnetic field

The magnetic field was supplied by two ring magnets suspended above and below the sample cuvette. Magnetic field magnitude was measured using an F. W. Bell hand-held digital Gaussmeter. The field was reasonably constant throughout the sample region with an average field value of 300G. Such a field should allow the maximum effect on radical concentration in the hyperfine-dominated region of spin-mixing (figure 3.4.1).

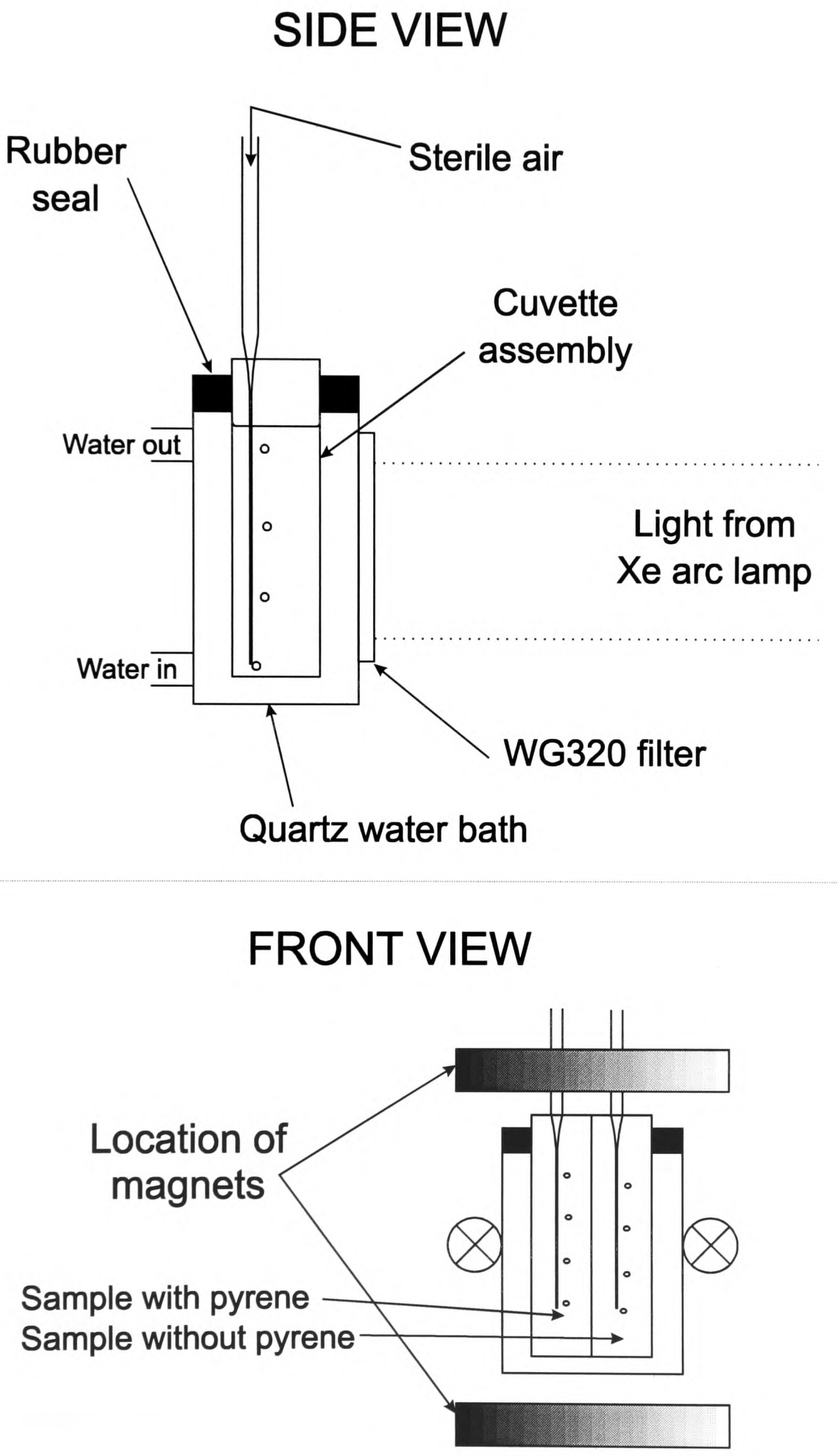

Figure 5.1.3. Apparatus used for irradiation of yeast cell samples

Sampling took place prior to irradiation and at various time intervals up to 30 minutes. It involved removal of 50μl samples, 10μl of which was serially diluted 10,000 fold. 3 samples of 100μl of the diluted sample were plated out on YEPD plates , giving 200 cell colonies per plate at 100% survival. This number can be scored and indicates viability. Whenever possible, aliquots were plated immediately. If there was a short delay, the cells were left on ice until plating was possible. All post irradiation manipulations were carried out under red light. The YEPD plates were incubated for 3 days at 28^0C in the dark. During this time, each healthy cell present on the plate would multiply to form a colony visible to the human eye allowing the surviving cells to be recorded. The recorded result for each sample is obtained by averaging the colony numbers for the three plates produced.

5.1.3 Results and discussion

After a number of trial runs to establish the pyrene concentration (see above) and the optimum experimental conditions, magnetic field experiments were performed. The first experiment produced good results, although the rate of cell killing was still slightly greater than ideal. Figure 5.1.4 shows a linear and a logarithmic plot of the killing curve. It is quite clear that the killing of the yeast cells is enhanced in the magnetic field case, particularly if the samples are examined after 4 or 7 minutes where there is a large discrepancy between the low and high field cases. It is important to note that samples with and without pyrene were also run for the time course in the dark. No killing was observed to take place in these samples.

This initially promising result was followed up with further experimental runs under almost identical conditions. The pyrene concentration was reduced slightly in order that the killing curve be better distributed through the time

course. In all subsequent experimental runs, no observable difference was observed between the pyrene samples in the presence and absence of a magnetic field. Figure 5.1.5 is a data plot from a typical one of these experiments.

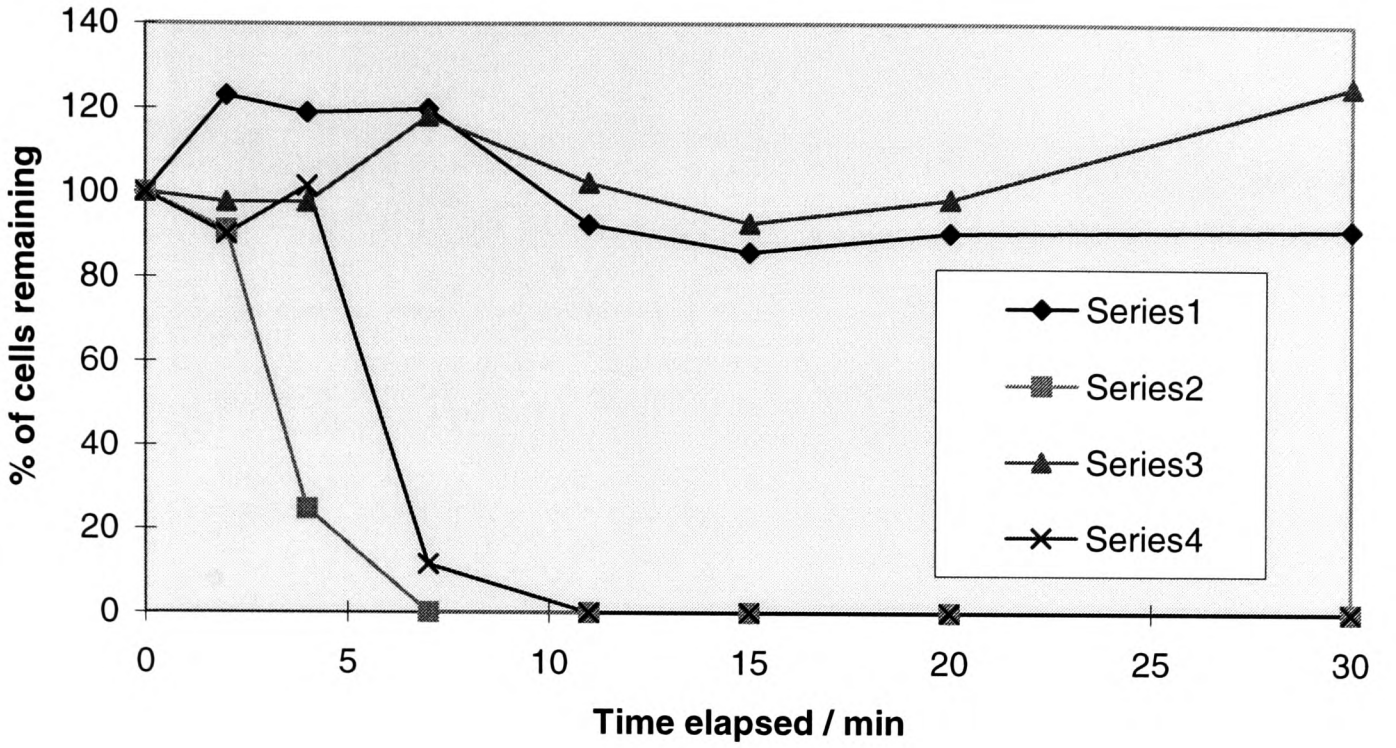

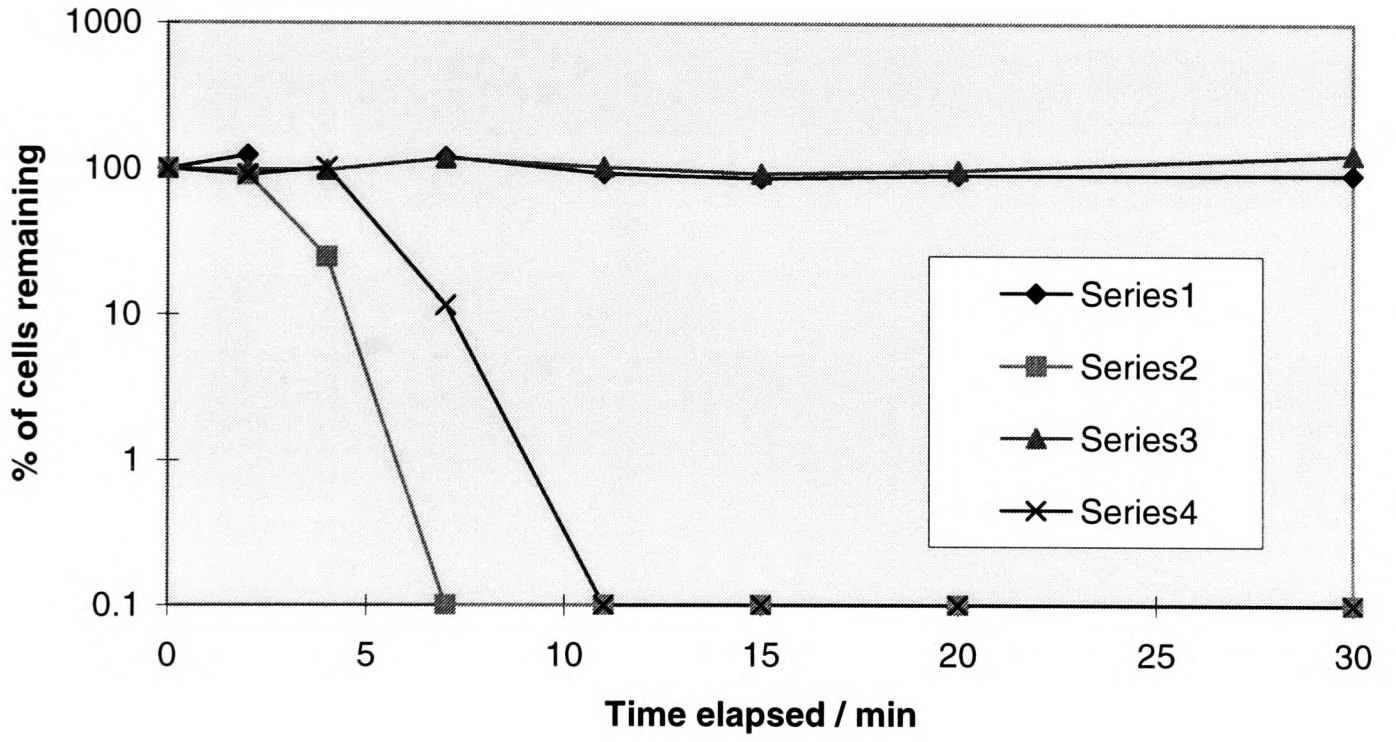

Figure 5.1.4. Linear and logarithmic plots of initial yeast killing results. Series 1 represents samples with no pyrene but a magnetic field present. Series 2 represents pyrene and magnetic field present. Series 3 represents no pyrene or magnetic field present. Series 4 represents pyrene present but no magnetic field. All results of 0% remaining cells are scored as 0.1% for ease of logarithmic representation

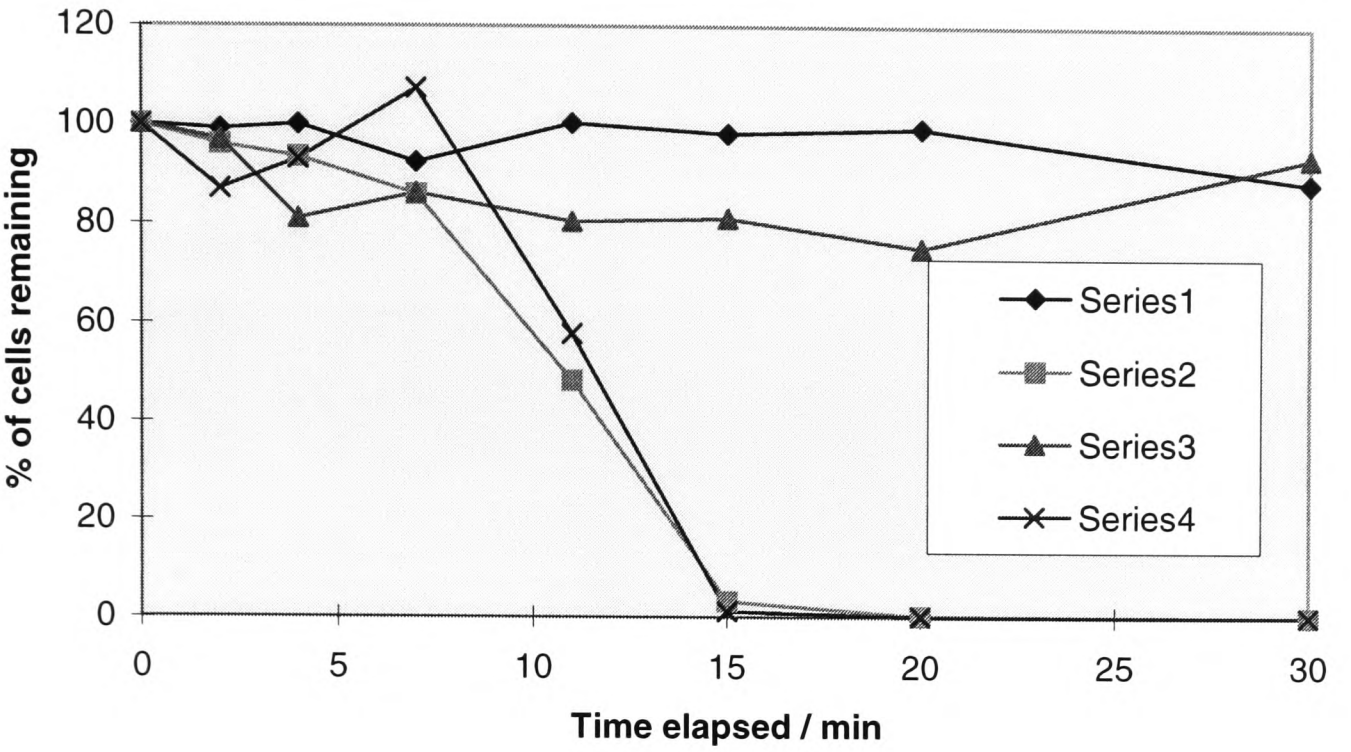

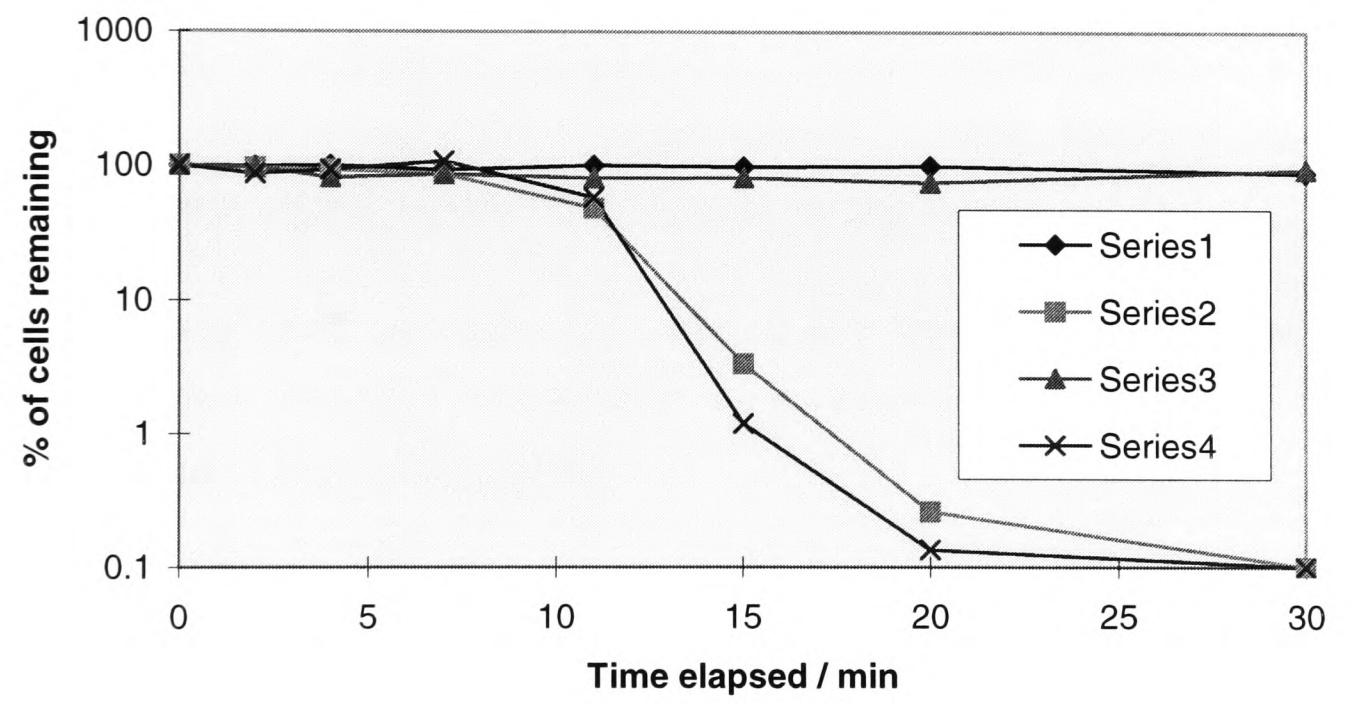

Figure 5.1.5. linear and logarithmic plots for a typical killing curve. Series are as for figure 5.1.4.

The data in figure 5.1.5. are typical results from a series of 4 identical experiments. Experimental data from other such experiments is available in appendix E. It is clear that

1. Any magnetic field effect present is significantly smaller than in the initial experiment. This implies that the difference in field present and field free curves in this experiment is due to some other external factor. As the total assay is relatively complex and involves many separate media transfer stages, it is likely that the experimental discrepancy has arisen somewhere within one of these stages.

2. The noise level in these experiments is fairly high. This is clearly shown by the samples containing no pyrene. There does not appear to be any significant killing effect throughout the course of the experiment, but the variation in the cell count, even after averaging over 3 plates, is quite high. Thus in the pyrene experiments, it is likely that any low-level magnetic effects will not be detectable via this assay.

This assay then, although not indicating any reproducible magnetic field effects, illustrated a number of significant points about the strategy for observing low level effects in biological systems.

Experimentally, the yeast killing system is a very powerful one as any detectable effects are affecting the biochemistry of the entire organism. An *in vivo* effect such as this is clearly of significance in the stray fields argument. The system also has its drawbacks, however, in that trying to alter the experiment to improve the chances of a reproducible field effect is made difficult due to the complexity of the system. Any subsequent experiments on this system employing different reagents, concentrations and reaction conditions are rather hit and miss as determination of essential parameters is highly difficult. For

example, are radicals actually being formed or is photodamage being incurred by a different mechanism? Where do the pyrene molecules reside, within the cell or in solution around the cell? Do any radical pairs formed remain correlated long enough for spin-evolution to occur? Experiments can be designed to investigate these questions, but the total process will be considerably time-consuming and perhaps a better approach is to design a similar system of lower complexity in which experimental parameters are more readily measured and modified. Perhaps armed with information from such an experiment, the yeast killing assay can be revisited with a greater understanding and an increased chance of success.

It is important to note that the lack of an observable field effect in this experiment may be a genuinely significant result. If the cell damage is radical induced (and it likely is given the observed behaviour of pyrene molecules in chemical systems), then there could genuinely be a magnetic field effect below the noise level of the experiment, or the change in radical concentration as a result of the magnetic field is somehow not translated into the observed damage in the cells. This stresses the point, then, that a positive result is as important as a negative one, as long as it can be justified that radical pair formation occurs within the system and that it is potentially affected by the presence of a field.

References

[1] **Hutchinson, F.**
Progress in Nucleic Acid Research and Molecular Biology **32** (1995) 115

[2] **Friedberg, E.C.**
Microbiol. Rev. **52** (1988) 70

[3] **Cox, B.S.**
Genet. Res. **30** (1977) 187

[4] **Knowland, J., McKenzie, E.A., McHugh, P.J. & Cridland, N.A.**
FEBS Lett. **324** (1993) 309

Chapter 6

Magnetic Field Effects on radical induced *in vitro* DNA damage

6.1 Approach and techniques

The majority of the biochemical work carried out during the research period involved *in vitro* DNA damage. The author is regretful to report that much of the experimental data accumulated during this period was lost in removal to a new laboratory. The results indicated by the data are included, but the data itself (namely many of the gel photographs) are not included.

The aim of the work described in this chapter was to design a biochemically relevant system in which photochemical damage could be observed, taking into account as many of the following points as possible:

1. Experimental parameters and conditions should be easy to alter and effects easy to detect.

2. The number of experimental stages between irradiation and detection should be as low as possible to remove the possibilities of interference by external factors.

3. The sensitivity of the assay must be as high as possible as the magnitude of potential MFEs is unknown. It is certainly the case that differences of damage between samples of 10% should reasonably be detected, with lower levels a distinct advantage.

4. The assay should be highly reproducible.

Taking the yeast killing assay as a starting point and stripping the concept to its bare minimum, a logical experiment is simply to take strands of DNA in solution along with a free radical source, to create free radicals in a controlled fashion for a known length of time and then determine the extent of damage caused to the DNA. The experiments described in this chapter effectively fit this description. The fashion in which the DNA is assayed is, perhaps, of greatest experimental interest.

6.1.1 Circularly closed, supercoiled DNA

Biologically active DNA is present in cells in a double-stranded, circularly closed, supercoiled state. DNA can be circularly closed either by physically linking the 3' and 5' ends (this is the case in bacterial and mitochondrial plasmids [1]), by holding the DNA loops together, e.g. on a protein scaffold [2] or simply by restricting free rotation at the ends of a long piece of DNA.

If a relaxed piece of DNA is closed into a circle by linking of its ends, no supercoiling occurs. Circular DNA molecules can exist in different isomeric conformations (called topoisomers) depending on the number of times the strands cross. Characterisation of these isomers is in terms of the *linking number Lk*. For a linear DNA molecule with *N* base pairs and *h* pairs per helical turn, joining the ends produces closed circular DNA with linking number Lk^0 (referring to the relaxed state of the DNA).

$$Lk^0 = \frac{N}{h} \qquad \textbf{6.1}$$

If torsion is applied to the double-strand, causing it to be overwound or underwound before the ends of the linear DNA are joined, supercoiling occurs and the linking number is altered. The linking difference ΔL, is given by

$$\Delta L = Lk - Lk^0 = Lk - \frac{N}{h} \qquad 6.2$$

Overwinding gives a positive value to ΔL (the DNA is positively supercoiled) and underwinding a negative value (the DNA is negatively supercoiled). Supercoiling can affect the shape of the circular DNA in two ways, changes in twist, *Tw*, which describes how the DNA strands are coiled around one another, and changes in writhe, *Wr,* describing the winding of the double strand about itself. ΔL can be defined in terms of these parameters.

$$\Delta L = Tw + Wr \qquad 6.3$$

Illustrations of circular DNA, supercoiling, writhe and twist are provided in figure 6.1.1. An arbitrary value of -4 has been chosen for ΔL in these examples.

The two supercoiled states illustrated in figure 6.1.1 are not the only possible states for such a supercoil with ΔL=-4. Electron micrographs of *in vitro* supercoiled DNA show that changes in the linking number tend to be accompanied by a 75% change in writhe and a 25% change in twist. Such a conformation is called plectonemic supercoiling as is adopted by DNA in plasmids, bacterial chromosomes, mitochondria and chloroplasts.

Supercoiling of DNA is performed by enzymes known as gyrases or topoisomerases [3]. Such enzymes accept double-stranded DNA and alter the linking number until a certain supercoiled state is achieved; in general about 1 supercoil per 15 double helical turns of the DNA [4].

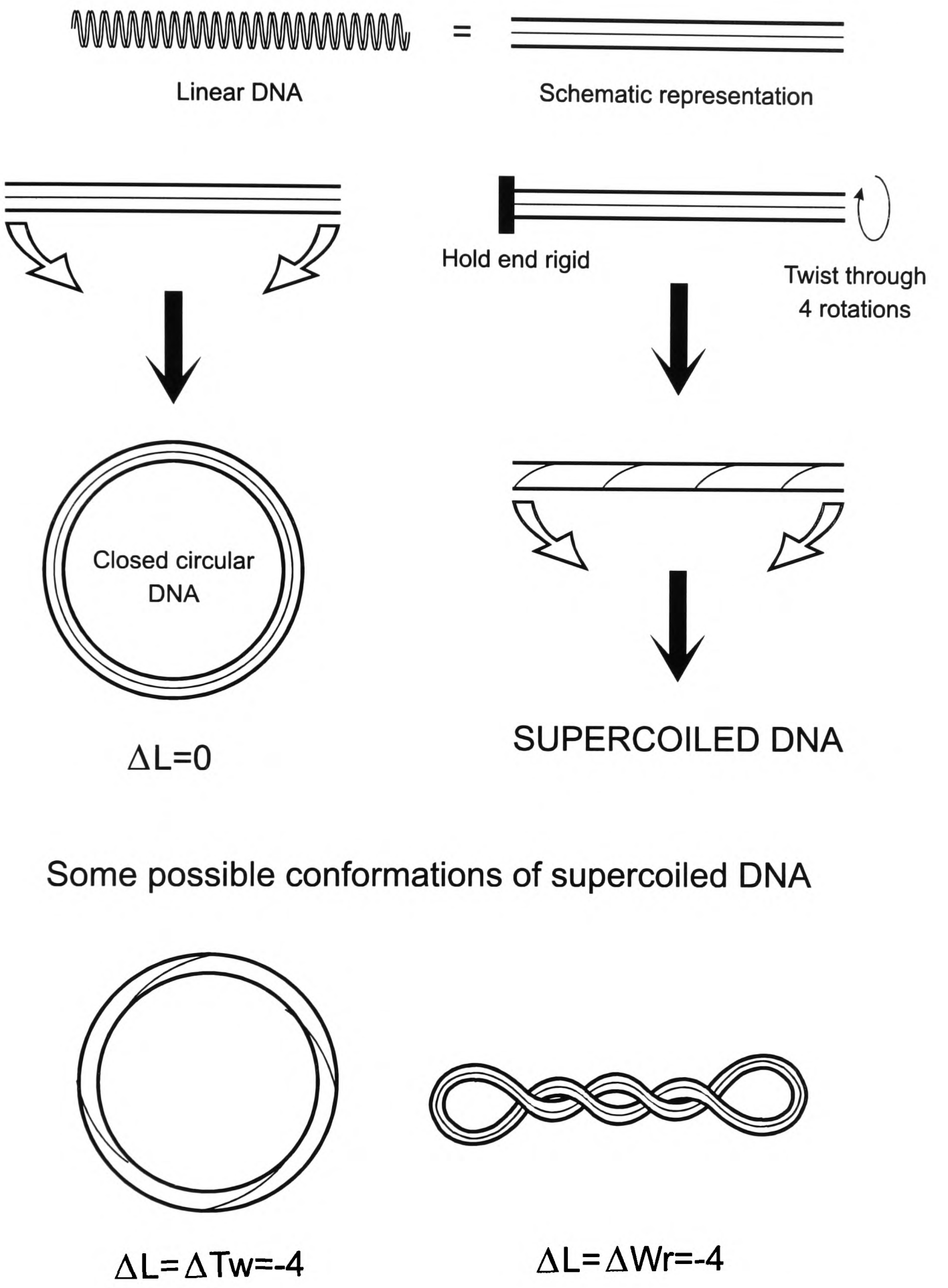

Figure 6.1.1. Schematic diagram illustrating closed circular and supercoiled forms of DNA.

6.1.2 Assaying of supercoiled DNA by gel electrophoresis

Clearly supercoiled DNA exists in a higher energy state than closed circular ('relaxed') DNA. Thus, if a strand break occurs in the backbone of a DNA supercoil, the DNA 'recoils', winding around itself until a relaxed conformation is achieved. This is the basis of the electrophoresis assay. Figure 6.1.1 indicates clearly the difference in shape between relaxed and supercoiled DNA. In aqueous solution at physiological pH, DNA is negatively charged and thus is subject to movement within an electric field. By mounting DNA into a gel and applying an electric field, supercoiled and relaxed DNA can be separated as their differing physical characteristics mean that the former migrates toward the anode at a greater rate than the latter.

The basic experiment, then, involves taking a sample of supercoiled DNA and subjecting it to free radical attack throughout a well-defined time course. Electrophoresis of the DNA after this period should reveal two bands corresponding to the supercoiled and relaxed DNA, their relative intensities indicating the extent of damage to the DNA backbone.

In practice, the assay provides even more information about the extent of damage caused. If a piece of supercoiled DNA receives a strand break, it will recoil to the relaxed state (the DNA is said to be 'nicked'). A second hit to the same piece of DNA will produce no significant change in the physical structure unless the breakage occurs on the opposite strand very close to the original strand break. In such a situation, the circular DNA becomes completely severed and opens up to form a piece of linear DNA. The probability of two adjacent strand breaks occurring is very low and thus the generation of linear DNA is an indication of a large number of strand breaks on an individual DNA supercoil. Thus in the experiment described above, one would expect to see purely supercoiled (S) DNA at time zero. Radical attack producing strand breaks

should cause conversion of supercoiled to relaxed (R) DNA with a commensurate reduction and increase in their band intensities in the electrophoresis gel. Continued attack should eventually see a reduction in the intensity of the R band accompanied by the appearance of a new band corresponding to linear (L) DNA. L DNA travels more quickly than R DNA under the electric field and appears as a band between the R and S positions. As the extent of the damage is increased still further, the linear DNA becomes reduced to smaller and smaller fragments which travel faster and faster under electrophoresis giving a 'smearing' of the DNA down the gel. A damage assay of this type is known as a 'DNA nicking assay'. The appearance of the different bands in a nicking assay is illustrated in figure 6.1.2

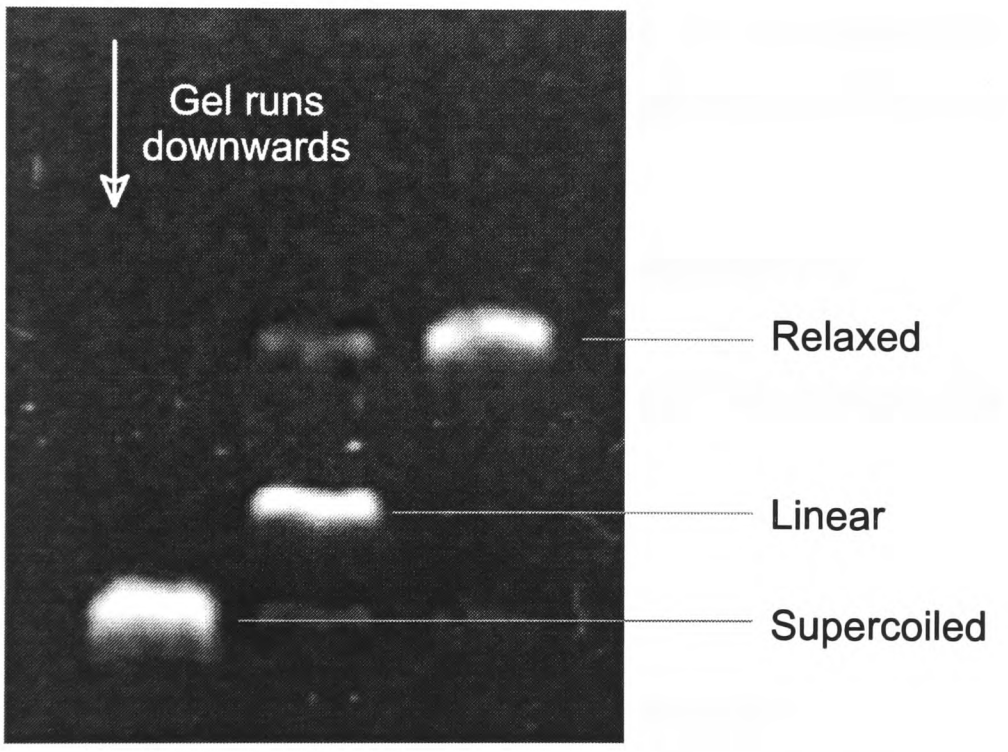

Figure 6.1.2. Diagram illustrating the fluorescence bands produced by electrophoresis of supercoiled linear and relaxed DNA. The bands are observed by staining the gel with ethidium bromide which binds to the DNA and causes it to fluoresce under UV irradiation.

6.2 DNA and electrophoresis gel preparation

6.2.1 Sterilisation

All solutions, buffers and media were sterilised, where possible, by autoclaving at 121^{0}C, 15lbs/in^2 for 15 minutes. All sample tubes, Gilson pipette tips, glass pipettes and pasteur pipettes were also subject to this sterilisation procedure prior to use.

6.2.2 Chemicals

All chemicals used were BDH AR quality or the equivalent. Water was purified using a Milli-Q system, and subject to autoclaving as described above.

6.2.3 Maxipreps - DNA large scale plasmid preparations.

Maxipreps were carried out with the Wizard^{TM} Maxipreps DNA purification system described below.

E-coli strain used

XL 1-Blue (Stratagene) containing the plasmid SK+.

Growth of bacterial cultures

Single colonies of XL1-Blue SK+ were grown as 10ml seed cultures in LB (Luria-Bertani medium; 10g Difco Bactotryptone, 5g Difco Bacto Yeast extract and 10g sodium chloride per litre water) containing ampicillin (50μg/ml), overnight at 37^{0}C.

This was used to inoculate a 500ml flask of LB with ampicillin (50μg/ml). This culture was grown up at 37^{0}C until the OD^{600} was 0.4. At this point, chloramphenicol (170μg/ml) was added to amplify the plasmid, and the culture incubated overnight at 37^{0}C.

Cell harvesting

The bacterial cells were harvested by centrifugation at 14,000g for 10 minutes at 4^{0}C. Cells were resuspended in 15ml of Cell Resuspension Solution.

Production of a cleared lysate

15ml of Cell Lysis Solution was added to the resuspended cells and gently mixed. The cells were left to lyse for approximately 20 minutes until the solution was clear and viscous.

15ml of neutralisation solution was added, followed immediately by mixing by inversion. The resulting suspension was centrifuged at 14,000g for 15 minutes at 4^{0}C producing a clear supernatant liquid above a white solid. The supernatant was decanted off and was mixed with 0.6 volumes of isopropanol. Centrifugation at 14,000g and 4^{0}C for 15 minutes produced a DNA pellet. The supernatant was removed and the pellet resuspended in 2ml of TE buffer.

Plasmid purification

10ml of Wizard Maxipreps DNA purification resin was added to the DNA solution. This is a proprietary silica-based resin. The mixture was pulled through a Maxicolumn under vacuum along with washings, using column wash solution. The resin which remained on the column was rinsed pulling 5ml of 80% ethanol through the column and then centrifuging the column within a reservoir for 5 minutes at 1,300g.

The DNA was eluted from the resin by application of 1.5ml of preheated TE buffer (65-70^{0}C). This was left for 1 minute and then centrifuged at 1300g. The resulting solution of purified plasmid DNA was stored at -20^{0}C. The plasmid was tested by running on an electrophoresis gel (see details below) in both supercoiled and relaxed forms (the latter being produced by the use of a restriction enzyme) alongside samples from a frozen test stock for comparison. The results are shown in figure 6.2.1.

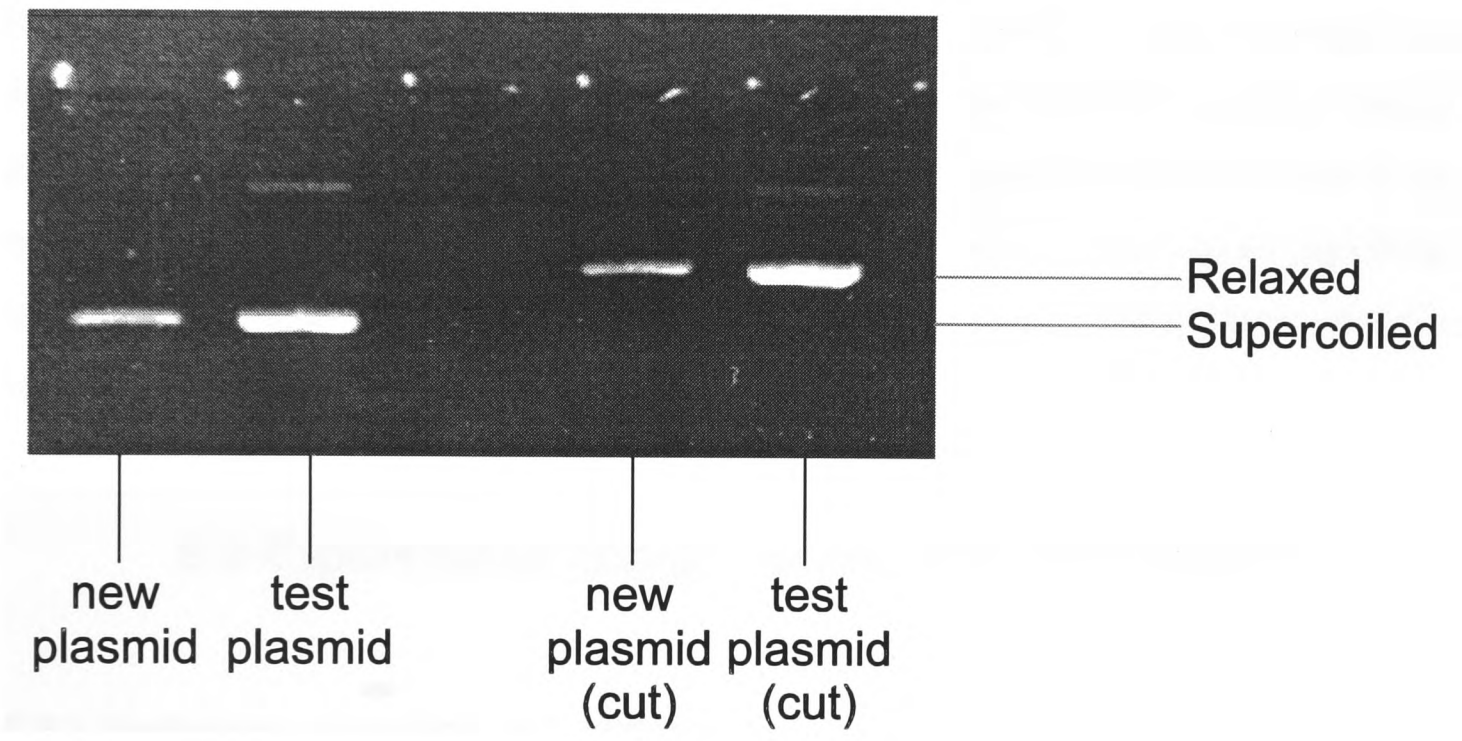

6.2.1. Test gel of DNA plasmid for use in assays.

It is clear that the sample is of high quality with no relaxed DNA present in the supercoiled sample.

6.2.4 Agarose gel electrophoresis

A solution of 1% w/v agarose (Sigma) in 0.5 x TBE buffer solution containing 0.5mg/ml ethidium bromide (which binds to the DNA and causes it to fluoresce under UV irradiation - this allows the bands of DNA in the gel to be observed by eye) was produced by heated to near boiling on a hot plate and

poured to set when cool enough to not cause damage to the plastic gel tray. Gels were run at 5 Vcm^{-1} on a Pharmacia GNA 200 gel apparatus in 0.5 x TBE also containing 0.5mg/ml ethidium bromide. Loading of samples into the gel was achieved using a buffer consisting of 0.04% bromophenol blue, 0.04% xylene cyanol and 7% sucrose (all w/v) in sterile double distilled water.

Examination of the gels took place on a 313nm transilluminator. In general gels were photographed using a computerised digital camera system producing instant hardcopy. Gels that were of particularly high quality, contained significant data or that were intended for statistical analysis were recorded using Polaroid photography. Unfortunately, it was all the Polaroid negatives that were lost in the laboratory removal process and thus no records remain of the most significant results. The more important of the instant digital printouts have been scanned and are included here.

6.3 Experimental design, results and development

6.3.1 Hydrogen peroxide experiments

Introduction

Initial experiments were carried out in the laboratory of Dr J. Knowland and were based on an assay currently being employed there. The assay involved observing the action of hydrogen peroxide on supercoiled DNA in the presence of Fe^{2+} and ascorbate ions.

The reaction of hydrogen peroxide with Fe^{2+} ions produces peroxy radicals ($HOO^{\bullet}$) which can attack DNA directly or via other radicals (namely $HO^{\bullet}$ in aqueous solution). This reaction oxidises Fe^{2+} to Fe^{3+}. To stop the depletion of Fe^{2+} throughout the course of the experiment, ascorbate ions are also added to

the solution to reduce the Fe^{3+} back to Fe^{2+}. The reaction is sampled at various times after peroxide addition and the samples are analysed on an agarose gel as described above.

Experimental

Sample tubes were prepared such that the final sample volume would be 50μl and the concentrations of the various reagents would be

Fe^{2+}	0.1μM
EDTA	0.1μM
Ascorbate	1mM
DNA	5μg in sample

upon addition of the hydrogen peroxide. Hydrogen peroxide samples of various concentrations were added to complete the samples and a stopwatch started. 10μl samples were removed at 0, 2, 5 and 10 minutes and immediately quenched by addition of an equal volume of thiourea solution at a concentration suitable to quench all the peroxide present. DNA was precipitated from the samples by addition of high concentrations of salt, and then centrifuged to produce a pellet. The pellet was washed and resuspended in phosphate buffer. The gel electrophoresis process then proceeded as described above.

Experiments performed applying this procedure revealed a number of important points in developing a suitable magnetic field assay. Initiating the reaction by adding the hydrogen peroxide and stopping it by quenching it with thiourea is not an ideal method of control. Particular problems lay in the reaction being incompletely quenched. An improved system would employ a photochemical reaction that could be effectively instantaneously switched on and off by adding or removing illumination. This would have the benefit of allowing reagents of well-documented photochemistry to be employed.

Precipitation of DNA, vortexing and resuspension can cause additional physical damage to the phosphate backbone inducing added noise to the experiment. Removal of the iron ions from the system might allow reaction samples to be loaded directly onto the gel, eliminating the need for DNA recrystallisation producing a simpler and cleaner assay.

6.3.2 A photochemical plasmid nicking assay

The logical experiment to perform given the shortcomings of the hydrogen peroxide experiments is simply to take supercoiled DNA in the presence of a photoactive molecule capable of producing free radicals upon irradiation and assess the extent of nicking for different irradiation times. Experiments can be performed in the presence or absence of a magnetic field and any difference between the experiments should be observed in the electrophoresis gel.

The initial experimental system selected utilised benzophenone (see figure 6.3.3) as the radical precursor. This was contained inside an SDS (sodium dodecyl sulphate) micelle in a phosphate buffered salt solution of pH7.4. DNA, being negatively charged in solution, resides outside the micelle, and thus only radicals escaping the micellar environment should be capable of DNA damage.

Experimental

Benzophenone (Aldrich) was recrystallised from methanol and added to hot (60^0C) pH 7.4 phosphate buffer (produced by combination of Na_2HPO_4 and NaH_2PO_4). The solution was vortexed, left for 1 hour to facilitate dissolution and vortexed again. Centrifugation allowed removal of the solution supernatant, a saturated aqueous solution of benzophenone. A sample of the saturated solution was diluted until it obeyed the Beer-Lambert law and its concentration

calculated by absorption spectrometry. The concentration of the saturated solution was found to be 4.6×10^{-4} mol dm^{-3}.

Samples were irradiated with an Oriel 150W Xe arc lamp as illustrated in figure 6.3.2.

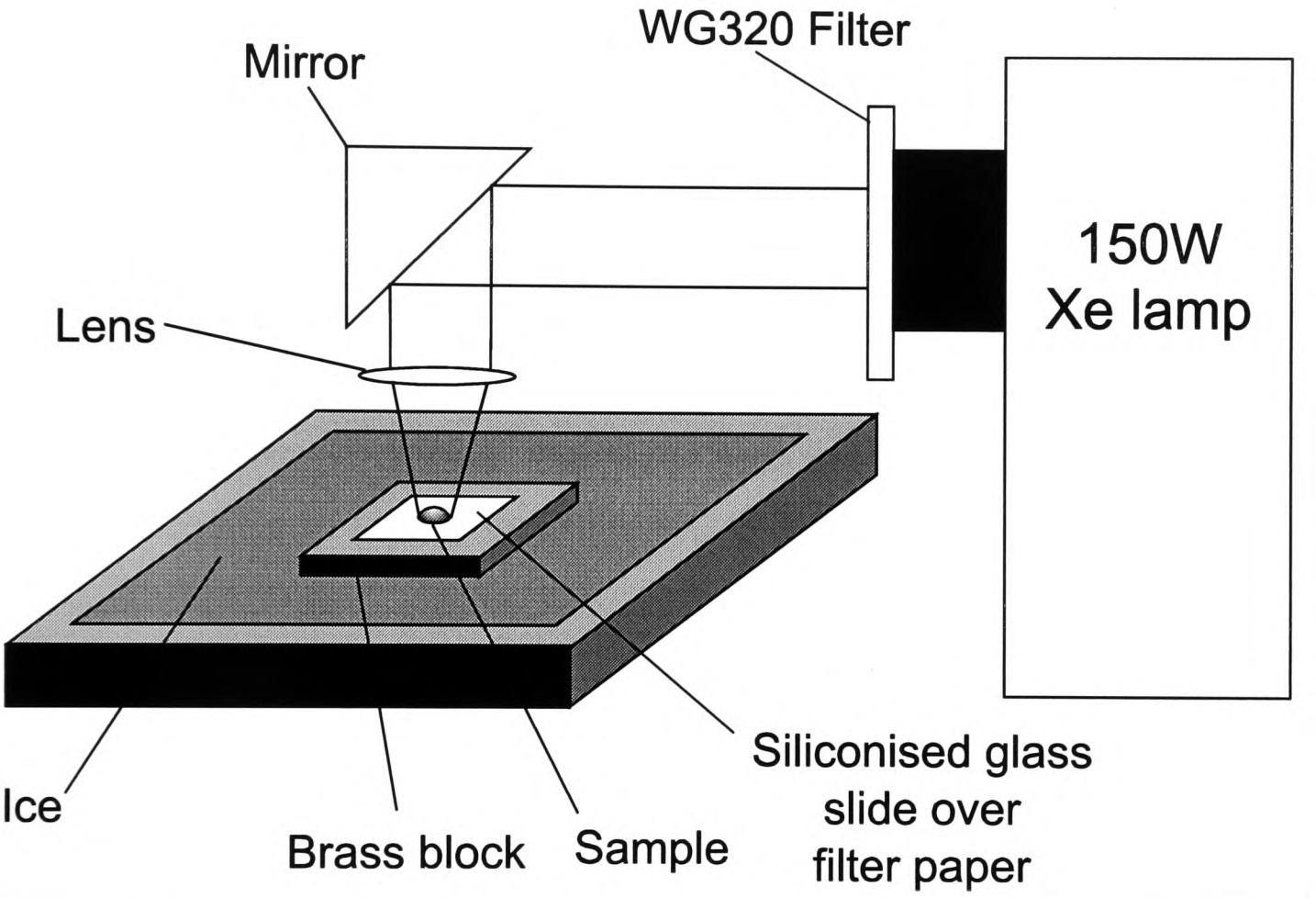

Figure 6.3.2. Apparatus initially used for irradiation of in vitro DNA samples.

The samples were pipetted onto a siliconised glass slide which was separated from a chilled brass block by a layer of damp filter paper. This served to allow good thermal contact between brass block and glass slide and also to provide a background of consistent reflectivity for the light. Maintaining a consistent 'background' is important as the brass block is replaced with a permanent magnet in the magnetic field experiments. The permanent magnet supplied a field of 450G at the sample location. The spot size of the focused light was consistent for all experiments and completely covered the sample in all

cases. The sample is cooled to counter heating effects from irradiation and to reduce evaporation throughout the course of the experiment.

In all experimental runs, controls were run in the dark, with photoactive molecules present, and throughout the irradiation course with no photoactive molecules present. No DNA damage was seen in these controls unless stated otherwise.

6.3.3 SDS / benzophenone results

The photochemistry of benzophenone is well documented [5]. In hydroxylating solvents, it undergoes excitation to the triplet state upon irradiation (with ε_{max} of 18,600 at 252nm). The triplet state abstracts an H atom from the solvent to produce a radical pair, one radical of which is the benzophenone ketyl radical. These processes are illustrated in figure 6.3.3.

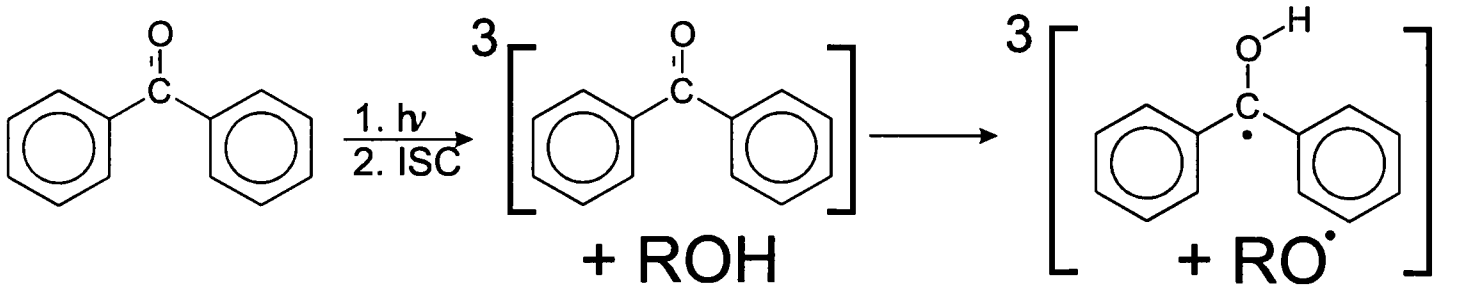

Figure 6.3.3. Photochemistry of benzophenone in a hydroxylating solvent.

Initial experiments involved assessing suitable time courses and reagent concentrations and included experiments to investigate the DNA damage caused by irradiation with benzophenone in the presence and absence of SDS micelles. Some typical results are illustrated in figure 6.3.4.

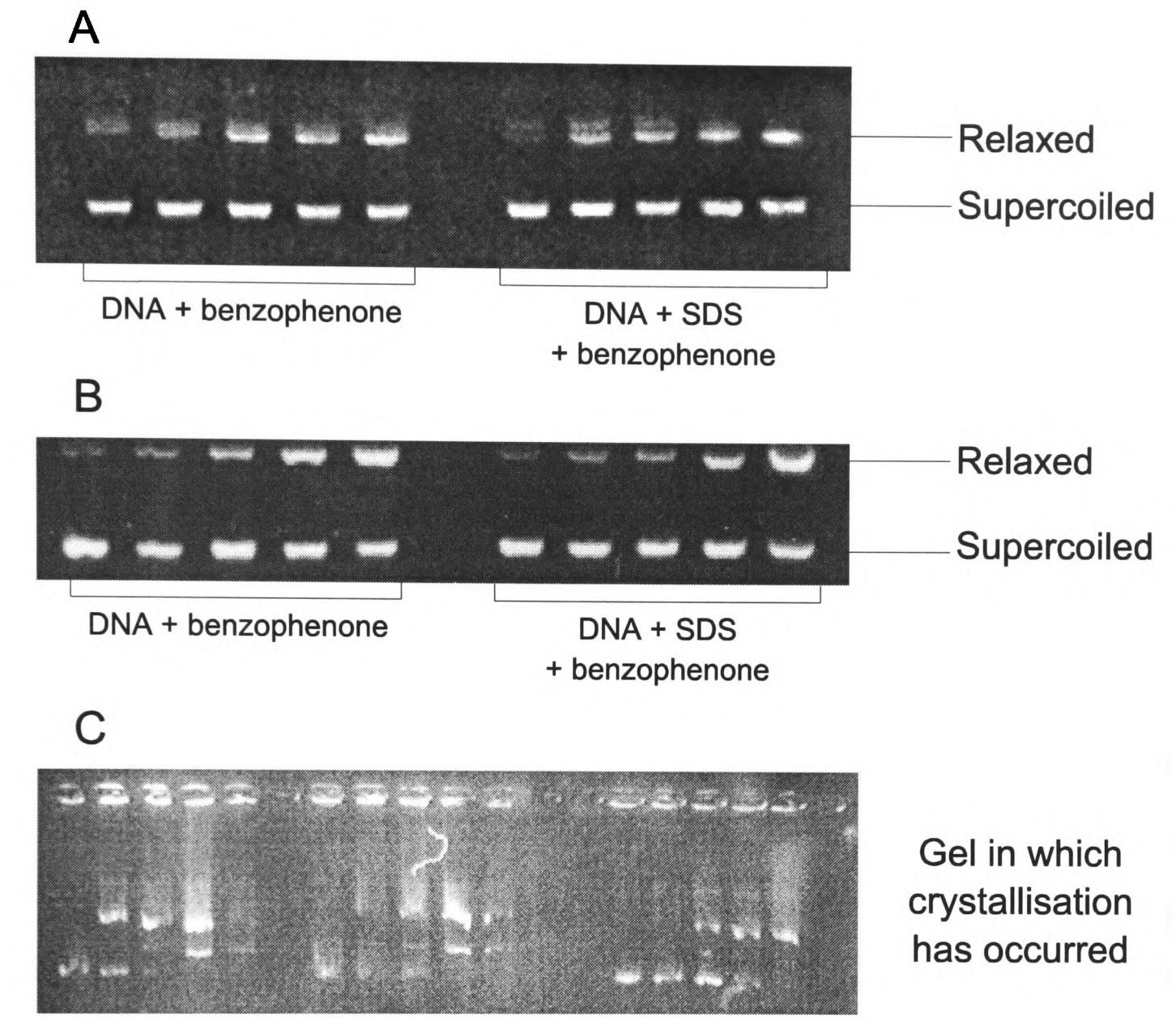

Figure 6.3.4. Some typical results for 1 hour irradiation courses of DNA with benzophenone with and without SD micelles.

From the results of the early experiments, the following points became clear:

1. The results from the gels have not suffered from the lack of the DNA separation process. The photochemical assay is simpler, cleaner and of greater utility than the initial hydrogen peroxide experiments.

2. Using a time course of total length 1 hour irradiation with saturated, buffered, aqueous benzophenone, a suitable degree of DNA nicking occurs.

3. Encapsulating the benzophenone inside an SDS micelle appears to reduce the damage induced by a small amount. This is an expected result as radicals need to escape the micellar environment before they can induce DNA damage.

4. Non-micellar solutions are much easier to use because they form a stable uniform droplet when placed on the siliconised slide. Micellar solutions, however, tend to 'spread out' due to their lack of surface tension. This makes removal of samples more difficult, and also leads to increased evaporation. Difficulties were also encountered due to the SDS samples foaming which made pipetting consistent volumes very difficult.

5. Storing the samples on ice often caused crystallisation to occur leading to very poor quality gel bands.

Taking the above points into account, it was clear that before magnetic field experiments were performed, the problems of surface tension, crystallisation and evaporation must be sorted out. This was done by redesigning the illumination system.

In order to remove the surface tension problem. Small sample holders were built which enhanced the uniformity of both micellar and non-micellar samples. These holders are illustrated in figure 6.3.5.

To stop crystallisation, the ice cooling was removed. For this to be possible, the evaporation problem must be well-addressed. The simplest way to reduce evaporation was to enclose the sample in an environment saturated with water vapour. This was achieved by placing the sample holder inside a glass vessel containing blotting paper soaked in water. The WG320 filter was then placed on top of the vessel and sealed airtight.

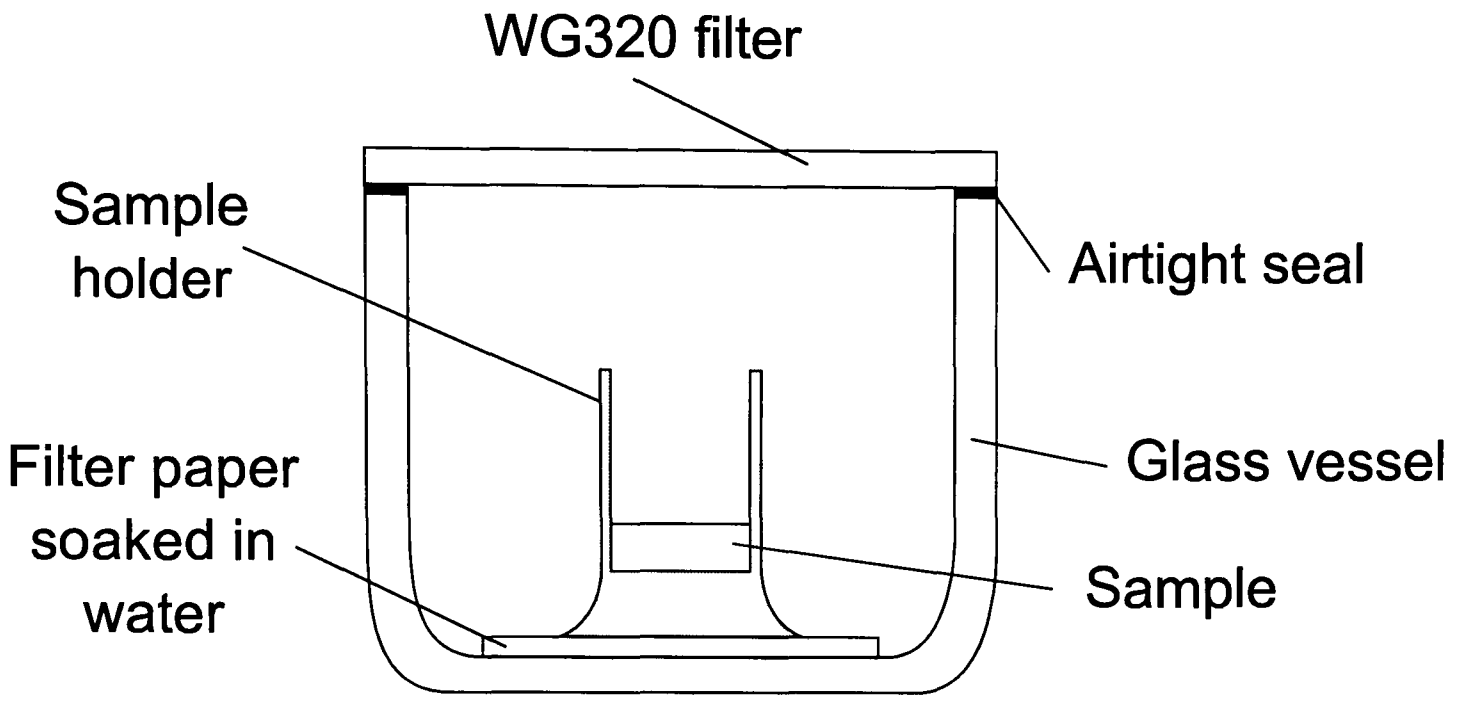

Figure 6.3.5. Enhanced illumination apparatus.

Experiments performed with this new apparatus showed no signs of crystallisation or evaporation and generally produced gels of higher quality than previously. Magnetic field experiments were undertaken. Some of the initial results obtained are shown in figure 6.3.6.

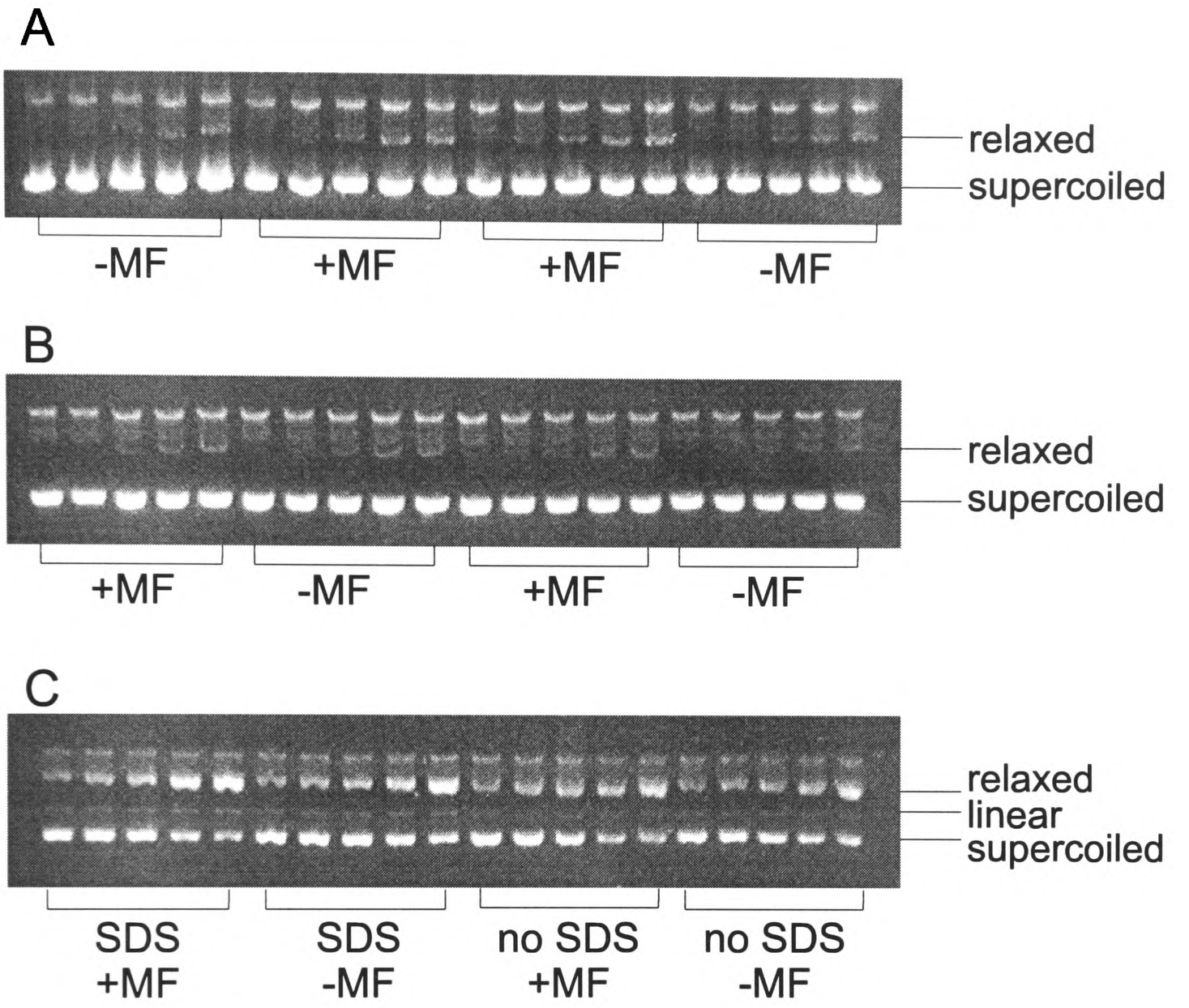

Figure 6.3.6. Sample experimental data from 1 hour irradiation courses of DNA with benzophenone in SDS micelles.

Gel A shows a clear discrepancy between magnetic field and no field samples. Examination of figure 3.4.2 shows that given a radical pair born in the triplet state, the yield of free radicals escaping to the bulk should be increased in a magnetic field of 450G. This should therefore give an increased degree of DNA damage. Gel B shows some indication of a discrepancy and Gel C shows no clear difference between the field and no field cases. It is thus difficult to say whether the magnetic field effects observed are genuine or not. The best way to determine for certain if an effect exists, would be to perform the experiment a

statistically significant number of times and quantitatively to analyse the results. Further discussion of this procedure appears in section 6.3.5.

6.3.4 Results from water / glycerol mixtures

The SDS micelle experiments, although much improved with the new illumination system, were still difficult to perform as the sample removal relies heavily on accurate pipetting and this was difficult to perform with surfactant solutions. As discussed in chapter 3 (and also in chapter 9), radical pair lifetime is of great importance in the development of magnetic field effects. Instead of achieving long RP lifetimes through micellisation, experiments were attempted with solutions of high viscosity. This was achieved using water / glycerol mixtures. Desire to produce viable solutions of the maximum viscosity led to initial experiments where the only water in the mixture was the buffer in which the DNA was resuspended. Figure 6.3.7 illustrates a gel obtained using such a sample. It is clear that the gel has run very badly and this was attributed to too high a glycerol concentration.

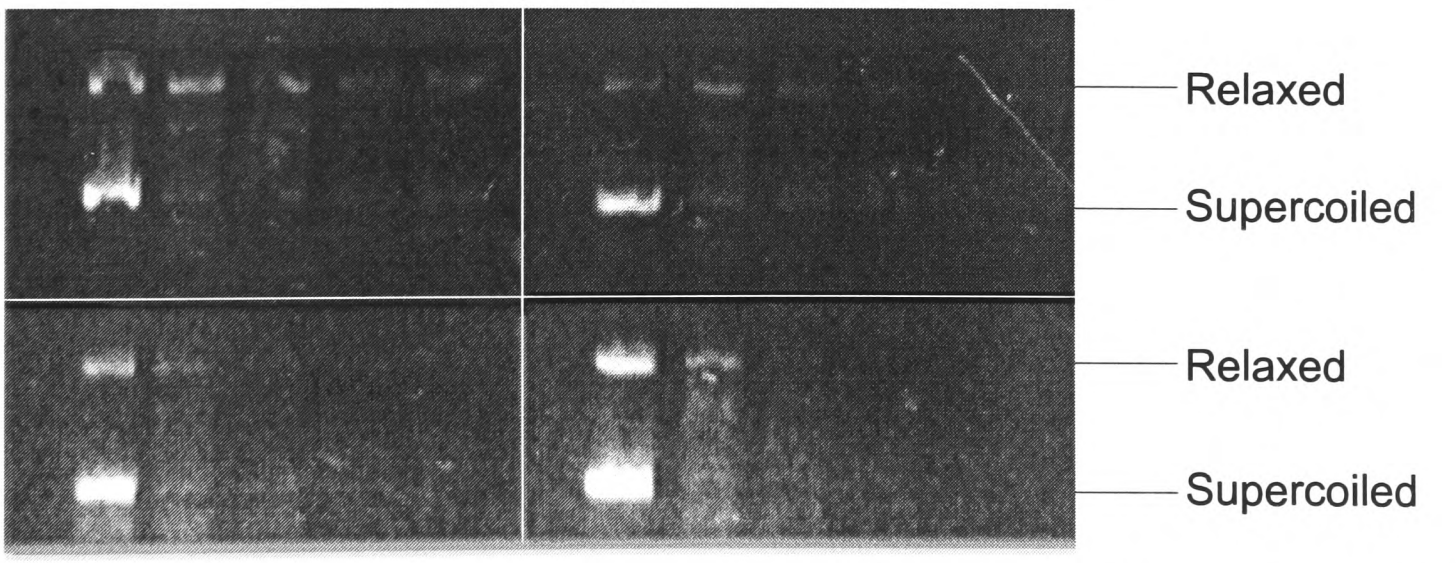

Figure 6.3.7. Experimental results obtained using the maximum possible glycerol / water ratio. The gel is clearly of no analytical value.

The highest glycerol content that produced satisfactory gels was found to be in a 9 : 1 glycerol : water (v/v) mixture. Dissolving recrystallised benzophenone in such a mixture and analysis by UV/VIS absorption showed the benzophenone concentration to be 2.6 x 10^{-3} mol dm^{-3}. This was found to give suitable gel damage courses without further dilution (figure 6.3.8).

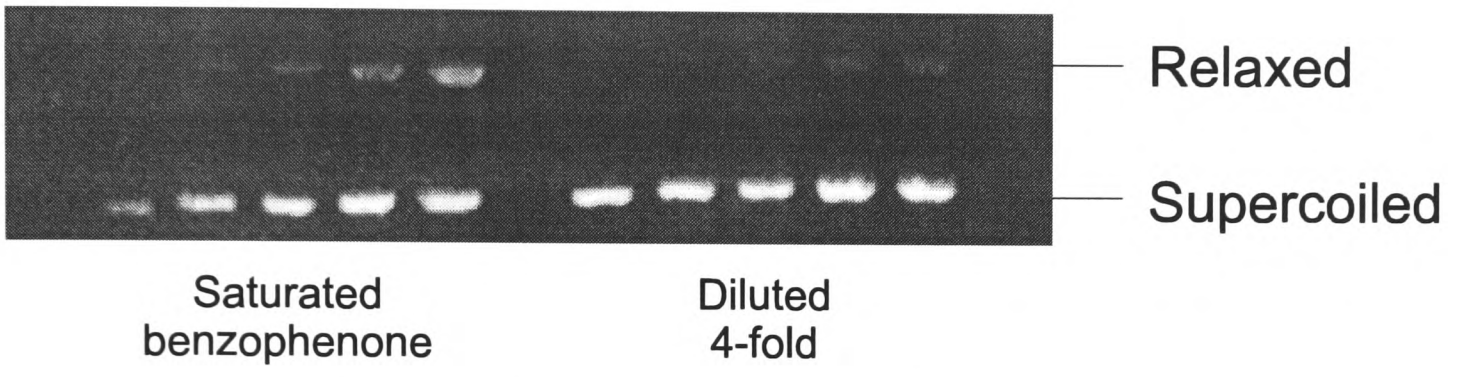

Figure 6.3.8. Damage courses obtained using a glycerol:water ration of 9:1.

Magnetic field experiments gave initially very promising results, again showing increased damage in the field present samples.

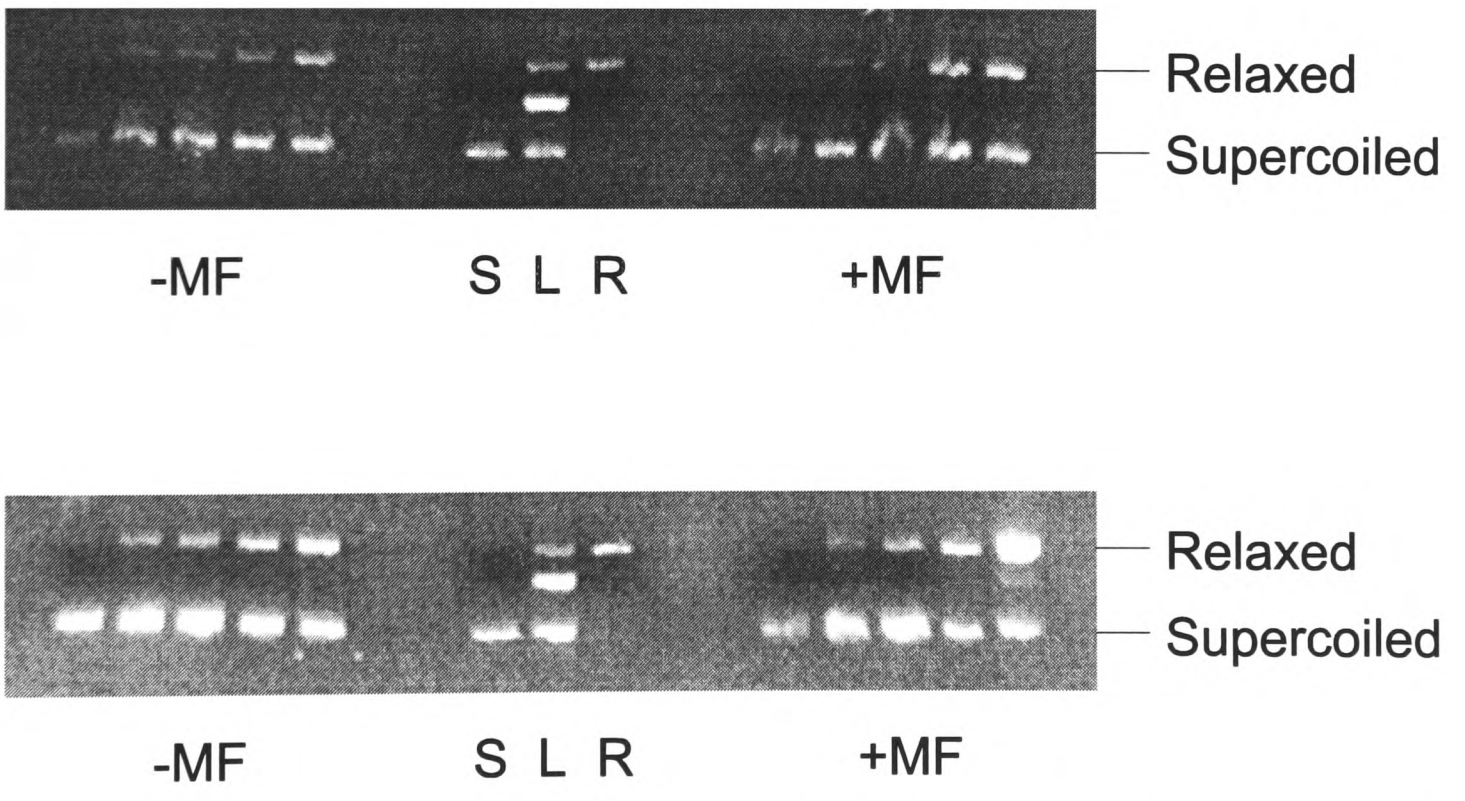

Figure 6.3.9. Magnetic Field experiments performed on 9 : 1 glycerol : water system. The bands labeled S, L and R correspond to supercoiled, linear and relaxed DNA and come from standard samples for comparison. +MF denotes the presence of a magnetic field. -MF denotes the absence of one.

The results are suggestive of a field effect and again point towards a statistical analysis for confirmation. It is difficult in these gels to obtain any feel for the magnitude of difference between the samples. Thus an experiment was performed to see if a controlled, small difference in DNA damage is readily observable in the gel. Thus using the standard glycerol / water mixture, two runs were performed with the second using 10% shorter irradiation times. There is a perceivable difference between the two runs (figure 6.3.10), implying that the assay ought to be sensitive enough to pick up differences of the order of previously observed chemical MFEs. It also indicates, however, that this is the top end of sensitivity of the assay and that, if the field effects expected are of this order or less, they may not be easy to reproduce. This again feeds the argument for a statistical study.

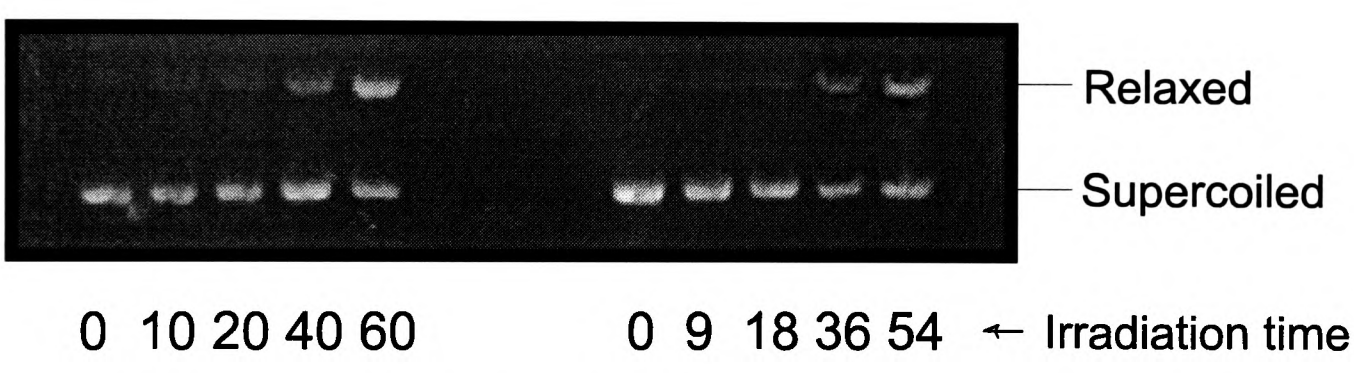

Figure 6.3.10. This gel indicates the reduction in damage caused by a 10% reduction in irradiation time.

6.3.5 TX100 micelle results

In order to perform a statistical analysis, the aim was firstly to find the system that gave the best results, the criteria for this being as follows:

1. The system should produce gels of high clarity. The bands must be distinct and well separated. Such gels should be reproducible and not suffer from DNA 'sticking' in the loading wells.

2. Ideally, the system would contain the most promising observed differences between field and zero-field samples.

3. A system that shows relaxed DNA at early times and linear DNA at later times is particularly suitable as it allows observation of differences in the early time samples as well as the later samples, increasing the degree of useful data produced in each experimental run. Such a system also allows the detection of a large degree of nicking. Sampling over a large number of DNA hits is effectively an averaging technique and will tend to remove the effects of any low-level random damage.

There are two basic techniques for quantitative statistical analysis of electrophoresis gels. The DNA can be radioactively labelled and the resulting bands can be cut from the gel and analysed with a GM tube. Alternatively, the negative obtained when photographing the gel can be scanned into a microcomputer and the intensity of the gel bands measured quantitatively by computer software. The latter technique was chosen as it can be conducted on the existing assay without modification.

During the work with SDS micelles and high viscosity solutions, experiments were also performed with the non-ionic surfactant Triton-X100. A saturated solution of benzophenone in 10% TX100 was initially employed and was found to give an excellent damage course, showing only relaxed DNA early in the assay, with linear bands appearing at later time. Figure 6.3.11 shows a gel obtained using the saturated benzophenone solution diluted 10 and 100 fold.

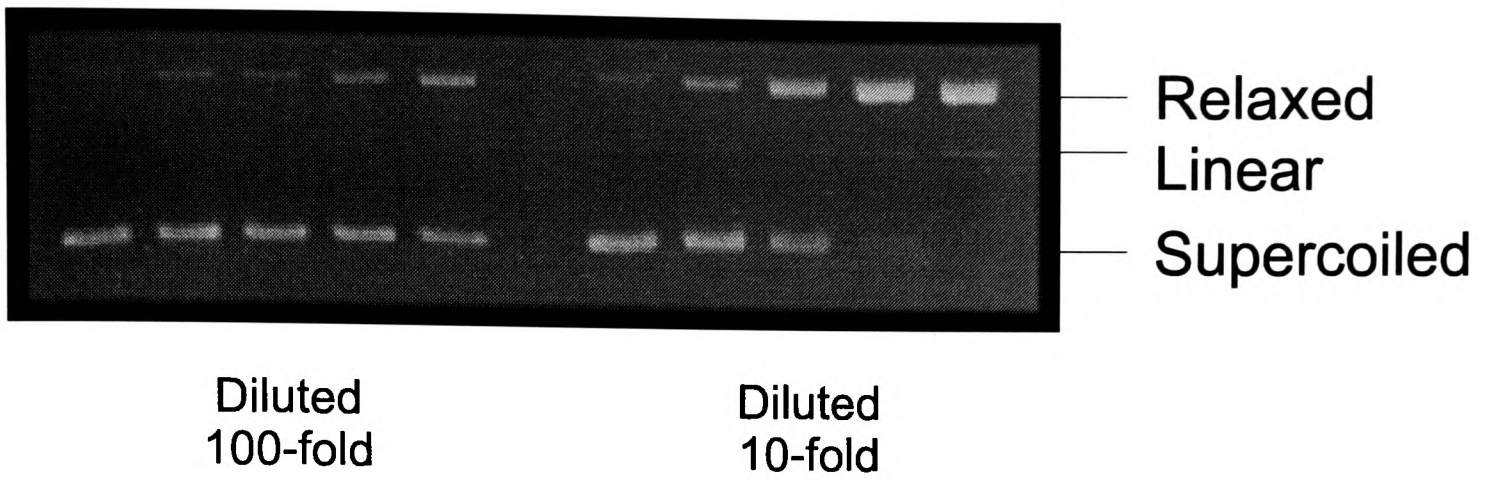

Figure 6.3.11. Experiments performed using solutions of benzophenone in TX100 micelles.

Early magnetic field experiments with the TX100 solution showed damage differences of similar magnitude to those observed previously. The assay proved to be consistent with this particular solution and thus was selected for the statistical analysis. Approximately 15 gels were run using a 1 hour time course and a saturated solution of benzophenone in 10% TX100 solution, with each gel containing two field-present and two field-absent experimental runs. All gels were recorded with Polaroid photography and the negatives labeled and filed ready for analysis.

Tragically, before any of the analysis work could take place, the negatives were lost during removal to a new laboratory and so no analysis was performed. Some negatives did appear (under the naked eye) to show some difference between field and no-field samples and in some the difference was less clear. It is impossible to speculate on whether the statistical analysis would have revealed a consistent field effect or not. It is much to the author's regret that this analysis could not be performed and the significance of this research is much reduced by its absence. It is hoped that future researchers in this field might return to this promising assay and repeat the experiments described.

6.3.6 Experimental variations and alternative systems

During the course of this research, studies were initiated on some different chemical systems and also on techniques of observing DNA damage that does not induce direct strand breaks. These are described below.

Alternative chemical systems.

Although benzophenone was an ideal reagent to use due to its well understood photochemistry and role in MFE experiments [5], it has the disadvantage of creating radicals by abstraction. In aqueous micellar systems, this can lead to some question over which radicals are being formed. Also, any non-micellised reagent molecules are likely to give rise to radical species other than the majority that are trapped inside the micelles. It is feasible that some reagent molecules become embedded in the DNA and again, the nature of the radical products is in question. Experiments were attempted to find a non-hydroxylated solvent that might solubilise both the benzophenone and the DNA. The search was fruitless as the DNA requires the energetically favourable hydrogen bonding interactions in order to enter solution.

The alternative, then, was to chose molecules that react by bond cleavage in the parent molecule to produce a well-defined radical pair. The molecules were chosen from transient ESR studies performed by the author and colleagues. The transient ESR spectrum of benzophenone shows transitions due to radicals derived from the solvent. 4-hydroxybenzophenone and 1,3-dihydroxypropanone however, show no such peaks and their photochemistry has been established to occur via Norrish Type 1 cleavage. Figure 6.3.12 shows the photochemical behaviour of these two molecules.

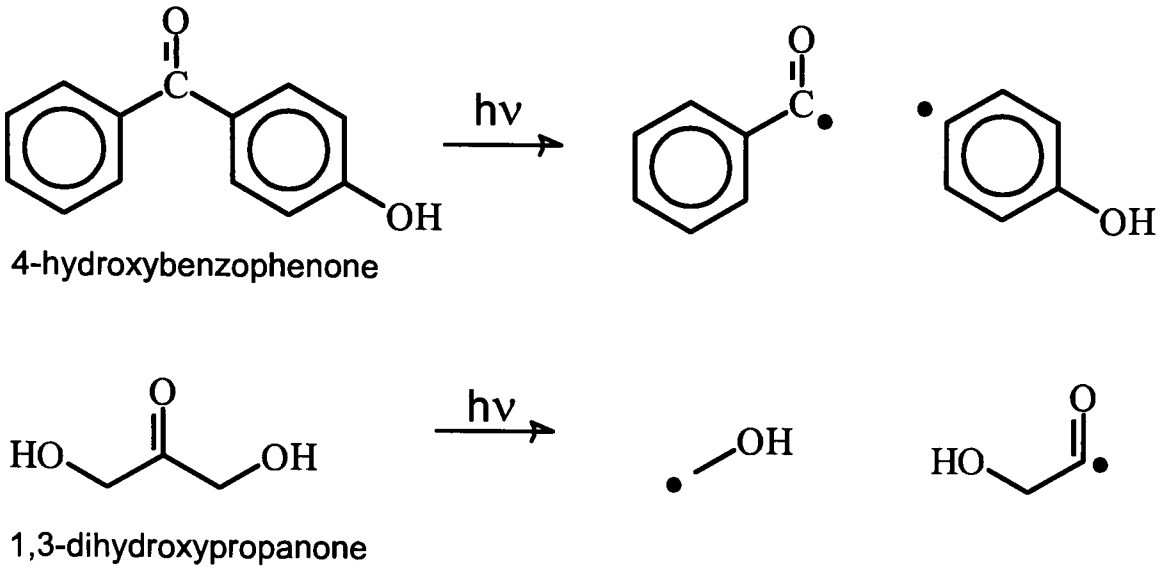

Figure 6.3.12. Norrish Type I cleavage of 4-hydroxybenzophenone and 1,3-dihydroxypropanone.

DNA damage time course experiments were performed using both of these molecules at saturation in aqueous TX100 solutions. The 1,3-dihydroxypropanone gave a suitable degree of damage, producing relaxed DNA in the later time samples. The results are illustrated in figure 6.3.13. 4-hydroxybenzophenone unfortunately gave very little damage in a 1 hour course with the light supplying the standard intensity. This is presumably due to its low solubility in the solution. Use of a stronger light source and / or longer time courses may mean that this molecule can be used in future experiments. No magnetic field experiments were performed with either of the molecules, but it is hoped that such studies will be performed in the future.

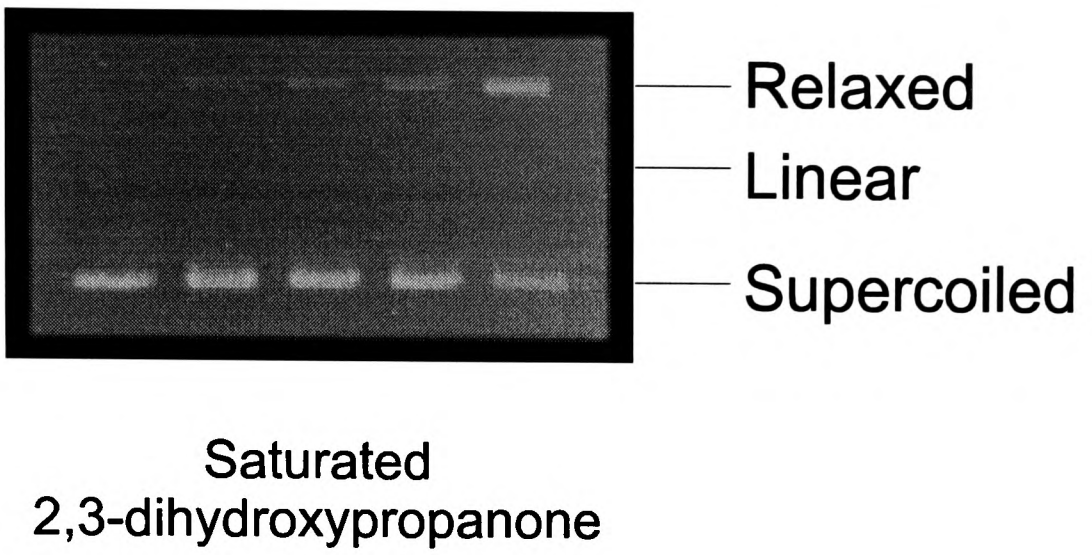

Figure 6.3.13. Results obtained employing a saturated aqueous solution of 1,3-dihydroxypropanone.

Analysis of non-strand breaking interactions

Although the DNA nicking assay is excellent as a means for analysing the extent of strand breaking, it gives no specific information on the means, location and type of damage. It is also limited to detecting damage to DNA that leads directly to cleavage in the backbone. Radical attack is likely to cause damage to other parts of the DNA molecule, producing products similar in nature to the photoproducts resulting from direct UV irradiation of DNA. The aim of this research is not to provide a detailed insight into the nature of the effects of benzophenone-derived radicals on DNA, however the possibility of analysing some of the non-strand break damage may reveal effects from different radical species or may simply provide a more suitable statistical sample.

The original technique used to produce strand breaks at sites of damaged DNA was to employ hot piperidine (approximately 90^0C). This method suffers from introducing non-specific damage to the DNA, presumably due to the high temperatures and the highly basic nature of piperidine producing siginificant concentrations of hydroxyl ions. An improved method, developed by McHugh and Knowland [6], employs N,N'-dimethylethylenediamine, which produces the same cleavage patterns as piperidine, but at 35^0C and pH7.4. It produces little

or no non-specific damage and thus can be used in the experiments described to produce other forms of DNA damage to strand breaks.

Piperidine treatment was introduced after the irradiation procedure to some damage courses obtained with benzophenone in TX100. In all experiments attempted, the gels obtained were of very poor quality with high levels of background damage and bands most unsuitable for the small differences that need to be detected in magnetic field experiments. It was unclear at the time of experiments the exact reason for the poor quality results. It is possible that the presence of the N,N'-dimethylethylenediamine interferes with the electrophoresis process and that it is necessary to recrystallise the DNA before loading for use in such experiments. It was felt that the time required to perfect this treatment was not warranted as their was no indication from the experiments performed that the results would provide any more information than those performed without the N,N'-dimethylethylenediamine.

References

[1] **Smith, G.R.**
Cell **24** (1981) 599

[2] **Gellert, M., Mizuuchi, K., O'Dea, M.H. & Nash, H.A.**
Proc. Nat. Acad. Sci. **73** (1976) 3872

[3] **Cozzarelli, N.R.**
Science **207** (1980) 953

[4] **Bauer, W.R. & Vinograd, J. Article in ' Basic Principles of Nucleic Acid Chemistry'**
Vol II p 265 Academic Press. New York (1974)

[5] **Turro, N.J. ' Moderen Molecular Photochemistry'**
University Science Books, Mill Valley, California (1991)

[6] **McHugh, P.J. & Knowland, J.**
Nucleic Acids Research **23** (1995) 1664

Chapter 7

Magnetic Field Effects on radical induced *in vivo* DNA damage

7.1 Single cell gel electrophoresis

7.1.1 Expansion from agarose gel techniques

The agarose gel analysis of strand breaks caused to supercoiled DNA is an excellent general assay for attempting to observe magnetic field effects in a simple designer biochemical system. The experiments performed using this assay led to the desire to find a system that would allow not only the simplicity of the experiments and analysis to be maintained, but also to observe the damage to DNA present in its natural state in the nucleus of a cell. This has the advantage of being a more biologically significant situation and also might adopt the naturally high viscosity of the cell nucleus to enhance any potential field effects.

7.1.2 Introduction to the comet assay

The comet, or microgel assay is a relatively new technique becoming increasingly used for detecting DNA damage in individual cells. It has a number of advantageous features

1. It is a simple and rapid technique for observing the production of strand breaks to DNA in the nuclei of whole cells.

2. It is readily adapted to suit many types of cell and is easily incorporated in most DNA-damaging systems.

3. It is currently the most sensitive technique for detecting strand breaks with a lower detection limit of one single-strand break per 2 x 10^{10} daltons of DNA [1].

As described in the previous chapter, the DNA present in a cell nucleus is supercoiled. If the nuclear membrane and most of the nuclear proteins are removed from a nucleus, a nucleoid (essentially a highly dense package of supercoiled DNA) is created [2]. If, prior to the formation of the nucleoid, any strand breaks have been inflicted on the nuclear DNA, the DNA strands containing nicks are released from the nucleoid while the undamaged strands remain supercoiled and bound into the nucleoid. This process is enhanced by alkaline unwinding which causes denaturation of the DNA strands and further protein removal, thus allowing further movement of the nicked DNA strands.

The comet assay was developed from original work by Rydberg and Johanson [3] on the nuclei of cells that had been subject to X-rays and thus contained strand breaks. The cell nuclei were lysed with alkali, embedded in thin layers of agarose on microscope slides and then stained with acridine orange. Acridine orange binds in high concentrations to single-stranded DNA to form polymers that fluoresce red under exposure to UV light. It binds in lower concentrations to double-stranded DNA, UV irradiation producing a green fluorescence. Denaturing of nicked DNA strands with alkali rapidly produces single stranded DNA, and thus analysis of the nuclei under a fluorescence microscope allowed DNA damage to be assessed by the comparison of the degrees of red and green colouration.

The comet assay has enjoyed many modifications since then. The first was the inclusion of an neutral electrophoresis step after alkaline unwinding [4]. This

step causes the nicked (and thus more mobile DNA) to become separated from the nucleoid, producing a tail of damaged DNA clearly visible under a fluorescence microscope. Undamaged nuclei produced no tail as the DNA remained supercoiled and tightly bound. It was also discovered that if the DNA strand breaks were created by irradiation with X-rays, the amount of DNA escaping the nuclei was related to the X-ray dose. The neutral electrophoresis conditions allow only the detection of double strand breaks. Use of alkaline conditions during electrolysis allows increased unwinding and removal of nuclear proteins allowing the detection of single strand breaks. Under these conditions, the DNA between two relatively close strand breaks becomes single stranded and can migrate completely out of the nucleoid as a free DNA fragment. This means that in an alkaline microgel assay, the comet tails are composed primarily of free DNA fragments, whereas in a neutral assay they are composed of loops of DNA that have lost their supercoiling, but are still attached to the nucleoid head [5]. The alkaline electrophoresis also produces strand breaks at alkali labile sites such as abasic sites and thus these also add to the comet tail.

The alkaline comet assay was chosen for use due to its high sensitivity and the protocol used was based on that published by Singh [6]. After DNA damage has been inflicted (either by the use of X-rays as a control or by irradiation with a free-radical precursor), cells are embedded in a thin layer of agarose on a microscope slide, creating a microgel. A surfactant solution is employed in a lysis step to damage the cell membrane. The DNA is then denatured by treatment with a mildly alkaline solution which also serves to remove most of the nuclear proteins. An alkaline electrophoresis step causes the unraveled, nicked DNA strands to migrate out of the nucleoid, leaving the undamaged DNA still coiled within. Analysis of the cells is carried out by staining with a fluorescent binding dye such as ethidium bromide and inspection with a fluorescence microscope. The nucleoids have the appearance of comets under the microscope, the undamaged and damaged DNA appearing as a 'head' and 'tail'

respectively. (Reviews of comet assay development and techniques are available in [7] and [8]).

7.1.3 Assessment of damage data

One of the most important (but subjective) parts of the comet assay is in the analysis of the results. The simplest method of doing this involves classifying the comets into groups according to the size of the tail (for example [9]). The greater the area of the tail, the greater the damage induced in the cell. There are a number of ways of measuring the tail area. A simple, but highly effective method is by eye using a fluorescence microscope. More sophisticated techniques use computerised image analysis to measure the fluorescence in the head and tail and thus estimate the DNA content in each. Such data is often presented as the 'tail moment', which is the percentage of DNA in the tail multiplied by it's length. This measurement is generally accepted as the most accurate method of DNA damage assessment in the comet assay [10]. Image analysis equipment was not available for use in these experiments, however, and thus the comets were classified into different grades by inspection and comparison with standards.

The comet assay appears to support the sensitivity required for magnetic field experiments and is of great significance as it allows the observation of DNA damage within a whole, living cell. Previously successful comet experiments (e.g. [6]) employing X-rays were used to first calibrate the procedure, allowing the formation of comets with a range of tail areas. Comets are classified on a scale of 0 to 4 with 0 indicating no DNA damage (0 comets possess no tail) and 4 indicating a comet in which there is virtually no head remaining. Sample comets from each classification group were obtained from the X-ray

experiments and were used to for comparison in the free-radical experiments. The sample comets are illustrated in figure 7.1.1

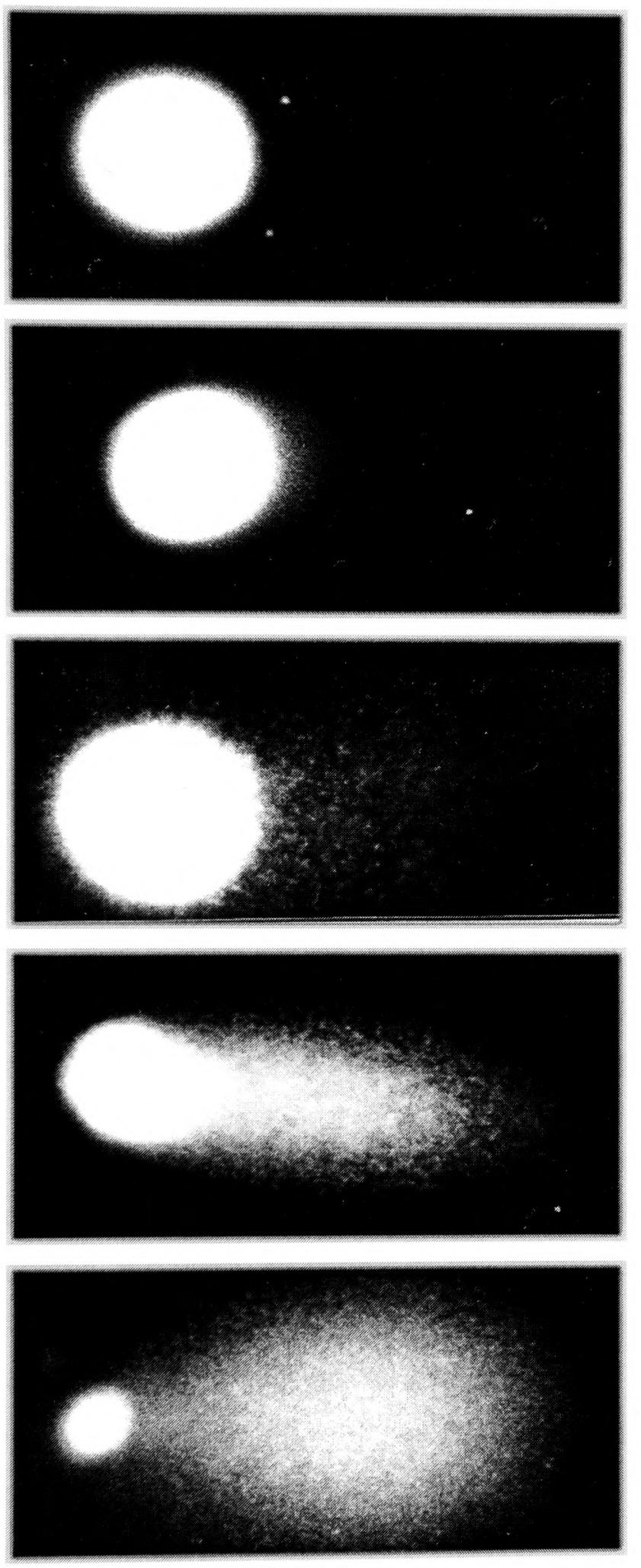

Figure 7.1.1. Fluorescence microscope photographs of ethidium bromide stained nucleoids showing various levels of DNA damage, The 'comets' are classified according to their tail area.

Next, experimental work commenced on producing a protocol that would give accurate time courses of radical induced DNA damage, maximising the spread of comet types throughout the assay. Much time was expended on optimising the concentrations of both cells and radical precursor. The aim of the research was to establish a working system in which magnetic field effects could potentially be measured consistently and reproducibly.

7.2 Experimental

All comet assay experiments were performed in the laboratory of Dr John Knowland, Oxford University Biochemistry Department.

7.2.1 Cell preparation

Human MRC 5 SV40 transformed fibroblast cells were grown as monolayers in vented plastic flasks (Falcon) at 37^0C in a 5% CO_2 incubator. The growth media was Eagles MEM plus Earles salts, supplemented with 10% Foetal Bovine serum, penicillin (final concentration = 100 U/ml) and streptomycin (final concentration = 100 μg/ml). (All media and solutions from Gibco BRL).

Cells were harvested initially using a cell scraper. This was found to give a high background level of non-zero comets due to physical damage caused when detaching the cells from the flask. Subsequently, cells were harvested by trypsinisation. The process involved incubation of the cells at 37^0C in PBS containing 0.25% Trypsin (Gibco BRL) for 15 minutes. They were then separated using a bench top centrifuge at 1400rpm for 5 minutes and resuspended in PBS at a concentration of 2×10^6 cells / ml (determined using a haemocytometer).

7.2.2 X-ray treatment of cells

The comet photographs in figure 7.1.1 were obtained by subjecting cells to X-ray irradiation. Slides containing untreated cells were placed horizontally in an ice filled box and treated with X-rays in a Gavitron RX 30 X-ray machine (^{137}Ce γ emitter) at a dose rate of 8.9 grays / minute for 0, 15, 30, 60 and 120 seconds. This corresponds to total doses of 0, 2.225, 4.45, 8.9 and 17.8 grays or 0, 222.4, 445, 890 and 1780 rads respectively. The cells were then treated as described in section 7.2.4.

7.2.3 Treatment by irradiation with benzophenone

Benzophenone was the logical choice of free radical source based on previous experiments. A solution of PBS was vortexed with solid, recrystallised benzophenone and left overnight. After a second vortexing, the remaining solid benzophenone was removed by centrifugation and decanting of the supernatant. The concentration of benzophenone was as for the aqueous solutions described previously.

The PBS benzophenone solution was diluted to twice the desired concentration and added to an equal volume of harvested cells in PBS (as described in 7.2.1). This gave a final cell concentration of 10^6 cells / ml. The cells were left in the presence of the benzophenone, in the dark, for 1 hour to encourage movement of benzophenone molecules into the cells.

Samples of 100μl were pipetted onto a siliconised slide and irradiated using the illumination system described in the previous chapter, but with an unfocussed beam. The beam does not need to be concentrated in this experiment as the greater amount of DNA present in whole cells presents a

much larger target for the damaging agent than the relatively small amount present in plasmid irradiations. 10μl samples were removed at 0, 20, 40 and 60 minutes. Experiments were also performed with samples left in the dark for the 60 minute period and with samples containing no benzophenone.

7.2.4 Slide preparation

Ordinary microscope slides will not allow microgels to adhere to the surface. Special slides with one side pre-frosted can be purchased (Micro Instruments ltd) but possess the disadvantage of being expensive and giving a high background fluorescence signal after electrolysis and drying. Instead, plain microscope slides (0.8 - 1.0mm thick, BDH) were precoated with 1% agarose (Sigma), by immersing the whole slide in melted agarose, wiping the underside clean and drying overnight in a warm oven. This method is cheap and produces no background fluorescence.

The first layer of the microgel is created by pipetting 100μl of 1% agarose in PBS onto the centre of the slide. A cover slip (22 x 22mm BDH) was placed on top of the liquid agarose producing a square of agarose on the surface of the slide. The slides were left for 10 minutes at 4^0C for the gel to solidify. The cover slips are then easily removed by sliding them sideways off the gel.

The 10μl cell samples were mixed with 85μl of 1% low melting temperature agarose (Sigma) made up with PBS and the sample was pipetted on top of the first square layer of agarose on the slide. As before, a cover slip was placed on top to create a square layer of microgel. The gels were again allowed to solidify by cooling the slides to 4^0C for 10 minutes and then the cover slips were removed as previously.

7.2.5 Lysis, alkaline unwinding and electrolysis

The slides were arranged horizontally in plastic trays, completely covered with lysis solution and left for 1 hour at 4^0C. The lysis solution contained 2.5M sodium chloride, 0.1M EDTA and 10mM Tris at pH 10. Iml of Triton X-100 was added for each 100 ml of this solution before applying to the cells.

After the cell lysis was complete, the slides were washed with PBS and then completely covered with alkaline solution at 4^0C for 40 minutes to allow the DNA to unwind and to remove some of the nuclear proteins. The alkaline solution contained 0.3M sodium hydroxide and 1mM EDTA. After unwinding, the slides were transferred to a horizontal gel tank (Pharmacia GNA 200) where they were arranged in rows and covered with an alkaline buffer solution of 10-fold dilution to that employed in the unwinding process (i.e. 0.03M sodium hydroxide and 0.1mM EDTA). Electrophoresis was carried out at 5 Vcm^{-1} for 30 minutes.

The slides were removed from the tank after electrolysis and washed 3 times with 0.4M Tris HCl, pH7.5. The nucleoids were stained by pipetting 100 μl of ethidium bromide (20μg / ml) on to the microgel square and applying a cover slip. Any slides that were not analysed immediately were stored by removal of the cover slip and overnight drying in a cool oven. They could then be stored at room temperature and rehydrated by the application of a new square of 1% agarose when required.

7.2.6 Comet analysis

Comets were counted by eye using a Dialux 200 EB fluorescence microscope at 10x magnification. For each slide, 100 comets were counted and

classified on the scale of 0 to 4 as described in section 7.1.3. In every case, a total comet score can be calculated by multiplying the number of comets of a particular type by the number of that type and summing over the different comet types. For instance, if a slide had 100 comets of class zero, the overall score would be zero. If it had 50 comets of class 1 and 50 comets of class 2, it would score (50 x 1) + (50 x 2) = 150.

The comet photographs in figure 7.1.1 were taken with a Ziess camera attached to a Ziess Axioplan fluorescence microscope. The film used was black and white Kodak 5053 TMY 400 ASA.

7.3 Results and analysis

7.3.1 Preliminary experiments

After initial experiments to establish protocol for cell harvesting, optimisation of lysis, unwinding and electrophoresis conditions, experiments were performed to obtain suitable trade off conditions between benzophenone concentrations, cell concentrations, light intensity and irradiation time. As described above, X-ray experiments determined a suitable cell concentration of 10^6 per ml. Using the UV filtered, unfocussed beam of a 200W Xenon arc lamp, experiments were performed at various concentrations of benzophenone with a time course of total 1 hour, to establish the concentration that gave the best spread of comets throughout the experiment. An ideal result would give a comet score of 0 in the zero time samples increasing smoothly throughout the time course to produce at least a reasonable proportion of 4 comets in the 1 hour sample. (The maximum possible score for the assay is 400). Achieving a score

of 400 in the 1 hour sample is not the desired situation as this might disguise the difference between samples containing similar (but not identical) degrees of damage.

An experiment performed with a saturated, buffered solution of benzophenone produced very large degrees of damage early in the time course and so subsequent experiments looked at a series of dilutions to maximise the comet range. Figure 6.3.1 illustrates the results obtained with saturated benzophenone solutions diluted 10 and 100 fold (and also control samples).

	10 fold dilution	100 fold dilution	No benzophenone	Dark sample
0 minutes irradiation				
Comet type 0	99	97	97	
Comet type1	1	3	3	
Comet type 2	0	0	0	
Comet type 3	0	0	0	
Comet type 4	0	0	0	
20 minutes irradiation				
Comet type 0	15	93	99	
Comet type1	62	7	1	
Comet type 2	22	0	0	
Comet type 3	1	0	0	
Comet type 4	0	0	0	
40 minutes irradiation				
Comet type 0	0	61	98	
Comet type1	11	38	2	
Comet type 2	31	1	0	
Comet type 3	51	0	0	
Comet type 4	7	0	0	
60 minutes irradiation				
Comet type 0	0	7	99	97
Comet type1	0	51	1	3
Comet type 2	5	36	0	0
Comet type 3	54	6	0	0
Comet type 4	41	0	0	0

Figure 7.3.1. Data obtained from dilution experiment. Total comet scores are given in figure 7.3.2. The data is plotted graphically in figure 7.3.3.

Irradiation time /min	10 fold dilution	100 fold dilution
0	1	3
20	109	7
40	254	40
60	336	141

Figure 7.3.2. Total comet scores for benzophenone dilution experiments.

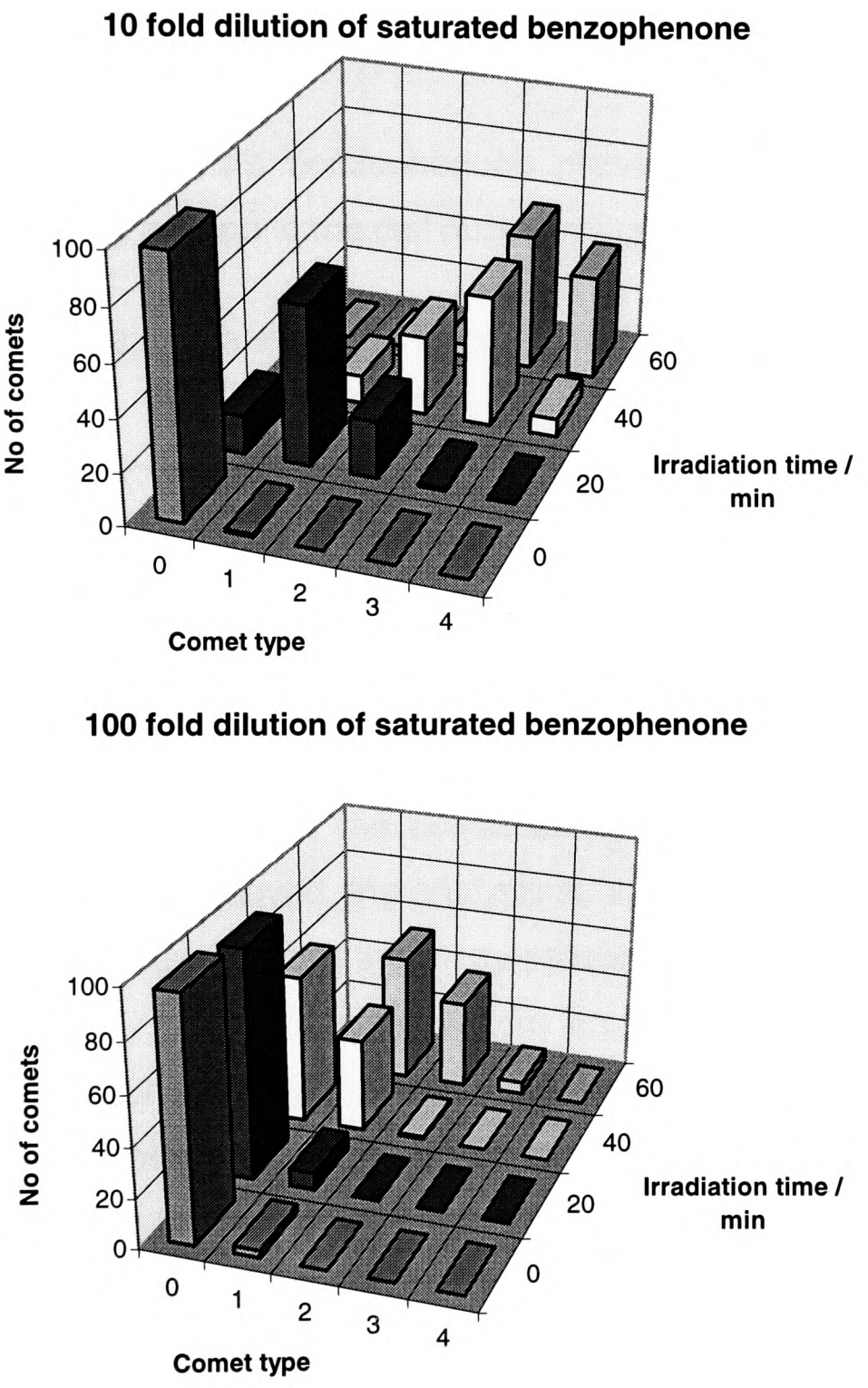

Figure 7.3.3. Three dimensional column plots of comet data from dilution experiments.

The most important points that can be deduced from these results are as follows;

1. The solution of 10 fold dilution appears to have an excellent spread of comet types throughout the time course.

2. The dark experiment and the time zero samples indicate that the level of background damage is very low.

3. The samples with no benzophenone present show that there is no damage being caused to the cell nuclei by irradiation alone.

4. The data obtained is very promising. It clearly indicates the increase in damage with time and with benzophenone concentration. It also appears to allow a suitable scale for the detection of relatively small differences in the extent of damage.

7.3.2 Magnetic field experiments

An inherent shortcoming of the comet assay is that even when image analysis techniques are employed, the analysis is, to some extent, subjective in that 100 comets are selected from the many present in the microgel. The best way to do this is simply to start from the bottom left of the microscope slide and move from left to right, classifying every comet encountered. There are still problems, however, when a comet is difficult to classify or if two (or more) are very close together. More significant, however, is the level of subjectivity when comets are being analysed by eye. When analysing the comets from the same time sample in magnetic field and no field experiments, it is possible to err towards the higher or lower comet classification depending upon the desired result. This may be a conscious or subconscious action and must be countered

either by not allowing the scientist performing the analysis to be aware of the desired result or by not allowing the scientist to be aware of which microgel is being considered as any given time. For consistency, all comet analyses were performed by the author but each microgel was coded by another member of the laboratory and thus the identity of each slide was unknown to the author throughout the analysis.

The 10 fold diluted benzophenone system was chosen as described above. A magnetic field of magnitude 450G was supplied from a ceramic doughnut magnet present beneath the sample. The first successful experiment produced the results tabulated below.

	No magnetic field present	450G field present
0 minutes irradiation		
Comet type 0	99	99
Comet type1	1	1
Comet type 2	0	0
Comet type 3	0	0
Comet type 4	0	0
20 minutes irradiation		
Comet type 0	99	94
Comet type1	1	6
Comet type 2	0	0
Comet type 3	0	0
Comet type 4	0	0
40 minutes irradiation		
Comet type 0	86	65
Comet type1	13	33
Comet type 2	1	2
Comet type 3	0	0
Comet type 4	0	0
60 minutes irradiation		
Comet type 0	46	28
Comet type1	50	65
Comet type 2	4	7
Comet type 3	0	0
Comet type 4	0	0

Figure 7.3.4. Experimental data from magnetic field comet experiments

Irradiation time /min	No magnetic field	450 gauss field
0	1	1
20	1	6
40	15	37
60	58	79

Figure 7.3.5. Total comet scores for magnetic field experiments

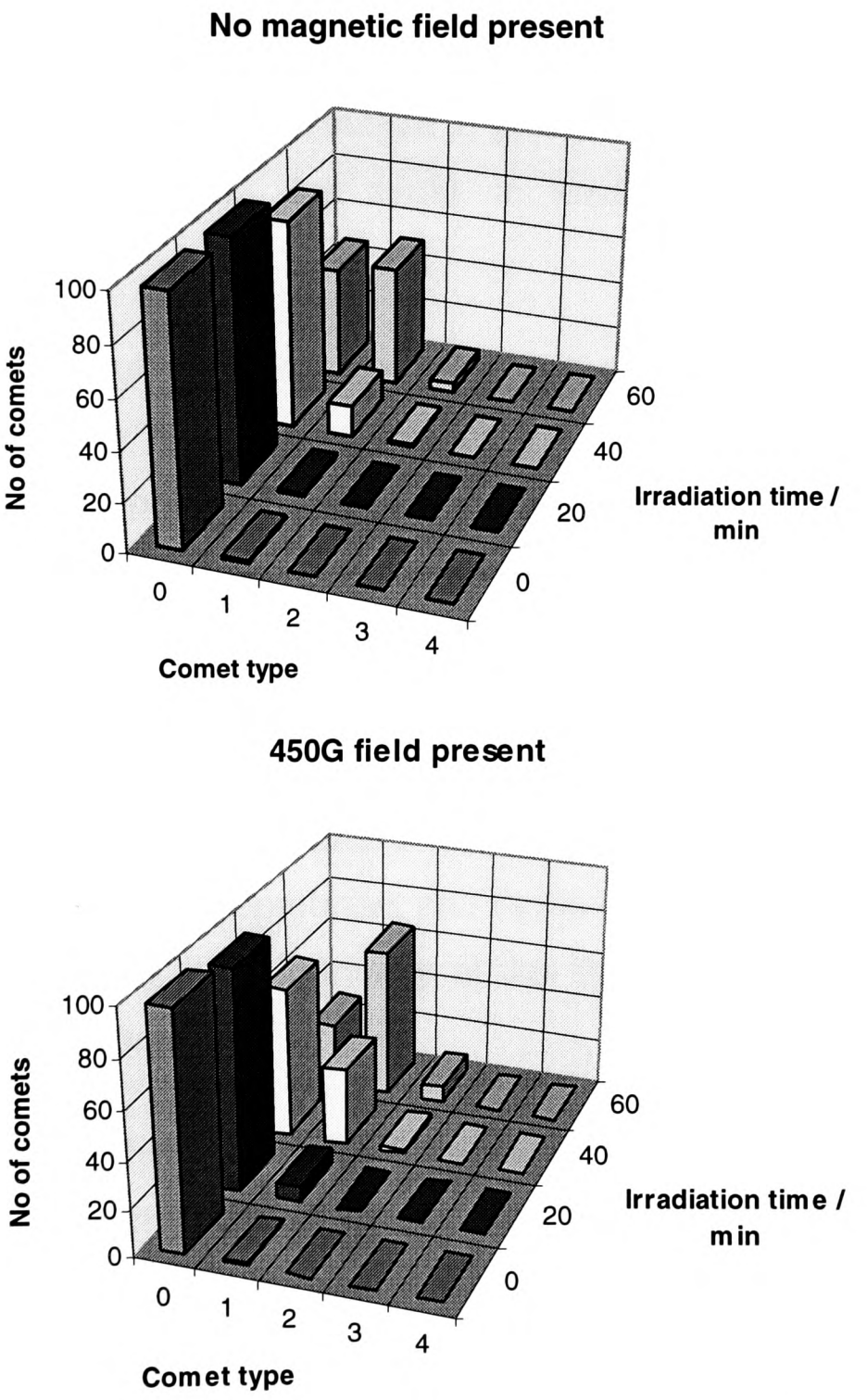

Figure 7.3.6. Three dimensional column plots of comet data from magnetic field experiments.

The most striking feature of the magnetic field experiments is that the overall damage level is considerably less than in the dilution experiments for a 10 fold dilute benzophenone solution. This has been attributed to the fact that in the two experiments, the cells may have been in different periods of their growth cycle which can have a significant effect on their susceptibility to DNA damage. This clearly adds to the experimental difficulty as it is very difficult to determine a suitable concentration of benzophenone for optimum use. Clearly, to produce results with consistent amounts of damage, the cells must be harvested and used at a controlled time after the culture is grown. This causes some logistical problems for experimentation, but could, in theory, be applied if deemed necessary.

Although the results only show a small spread of comet types, they are most promising. There is a distinct difference between the field present and absent data at all time points. This would indicate that the difference is not just due to random variability but to a genuinely increased amount of radical induced damage in the presence of a field. The experiment was performed again, a number of times, with the intention of testing the reproducibility of this result. Significant problems were encountered with contamination in the growth stage of the cells leading to results unsuitable for analysis. At this time, Dr Knowland moved laboratory within the department and tissue culture work was moved to a new location. There was no opportunity at the time to continue work on the magnetic field experiments.

It is hoped that this work will be revisited in the future as the result, if genuine, is of much significance. A modification of the assay employing human red blood cells (erythrocytes) eliminates the cumbersome tissue culture work, significantly speeding up the experimental process and allowing data to be obtained at a greater rate. The data included will remain unpublished until extra confirmatory data can be obtained.

References

[1] **Singh, N.P., Stephens, R.E. & Schneider, E.L.**
Int. J. Radiat. Biol. **66** (1994) 23

[2] **Cook, P.R. & Brazell, I.A.**
J. Cell Sci. **22** (1976) 287

[3] **Rydberg, B. & Johanson, K.J.**
'DNA Repair Mechanisms' p465 Academic Press, New York, 1978

[4] **Ostling, O. & Johanson, K.J.**
Biochem. Biophys. Res. Commun. **123** (1984) 291

[5] **Klaude, M., Eriksson, S., Nygren, J. & Ahnstrom, G.**
Mutat. Research - DNA Repair **363** (1996) 89

[6] **Singh, N.P., McCoy, M.T., Tice, R.R. & Schneider E.L.**
Exp. Cell. Res. **175** (1988) 184

[7] **McKelvey-Martin, V.J., Green, M.H.L., Schmezer, P., Pool-Zobel, B.L., De Méo, M.P. & Collins, A.**
Mutat. Res. **288** (1993)

[8] **Fairburn, D.W., Olive, P.L. & O'Neill, K.L.**
Mutat. Res. **339** (1995) 37

[9] **Gedik, G.M., Ewen, S.W.B. & Collins, A.R.**
J. Radiat. Biol. **62** (1992)

[10] **Olive, P.L., Banath, J.P. & Durand, R.E.**
J. Natl. Cancer Inst. **82** (1990) 779

8.2 Field effect magnitudes and consequences

All the potential MFEs observed in biological systems are small, to the extent that they can only just be detected. It is important to note that these effects are all obtained in the magnetic field region where one might expect the $T_{\pm}$ states to be completely decoupled from the S and T_0 ones. In all experimentally observed chemical systems (except one recent one [1]) and theoretical calculations, the magnitude of the effect in this region is considerably larger than any LFE, i.e. any effect that may be of environmental significance. Logically then, it seems likely that the effect of environmental strength magnetic fields on radical recombination in biological systems is very small indeed. All the experiments considered here have monitored the direct damage caused to DNA by free-radicals created photochemically (or by radicals created a small number of steps away from the parent radicals). The generation and concentration of radicals in complex biological systems is usually carefully controlled by the organism and often the concentration of radicals is determined by a complex series of reactions. It is possible that, in such a system, the reaction chain may produce a non-linear amplification of a small effect in any single stage. This might allow significant changes to the concentration of important species arising from only a small change in the rate of radical recombination step produced by a magnetic field.

The results then are, to some extent, ambiguous. The experiments suggest that magnetic fields are capable of interfering with radical processes in biological systems, but that the effect that they have is only very small. The techniques developed in this thesis are certainly significant and it is the author's hope that they might be used and developed further such that more forceful evidence on the subject might be produced.

Chapter 8

Summary of MFE experiments in biochemical systems

8.1 Comparison of results

The experiments discussed in chapters 5, 6 and 7 have one main feature in common, that they suggest the possibility of a field effect, but do not conclusively prove that one exists. The main reasons for the uncertainty are

1. The small size of any field effect present relative to the inherent inaccuracy level of the assay.

2. The variability of the biological system under question. Much effort was employed to remove potential variability from the systems but in some cases (e.g. the effect of the cell cycle on DNA damage) the problem was difficult to avoid.

Recording statistically large numbers of results appears to be the only way of producing convincing results in these systems. This was attempted with the supercoiled plasmid assay, and will hopefully be attempted in the future with the comet assay.

It is true of the research field as a whole that experiments will always attempt to observe small effects at the same level as the senisitivity of the assay. This is perhaps why a multitude of papers have been published with both positive and negative results. Quality of experimentation is critical and every effort must be made to ensure that any observed effects are completely reproducible. The author has discovered that this is often not the case.

It is interesting to note that a recent epidemiological study [2] has employed rigorous techniques upon a large sample of homes belonging to sufferers and non-sufferers of ALL (Acute Lymphoblastic Leukemia) and has shown no correlation between the directly measured residential magnetic fields and the incidence of the disease. Also, no correlation was found for fields calculated from power supply information using techniques employed for previous studies (a classification scheme known as 'wire coding'). The debate over the effect of environmental magnetic fields will no doubt continue and hopefully spawn high quality research in its wake. A recent review of the biological response to electromagnetic fields is given by Valberg, Kavet and Rafferty [3].

8.3 A technique to compare biological and chemical response

It would be very useful to be able to observe directly the concentrations of radicals created in the systems considered in this thesis. Some of the work performed during the research period focused on building an experiment that could observe the creation of free-radicals and their subsequent depletion by means of their absorption spectrum.

8.3.1. Experimental information

The work is not discussed here in detail, mainly because the bulk of it involved constructing apparatus and the optimisation of optics to allow the observation of transient radical absorption signals. The experiment is based on the time-resolved fluorescence detected MFE experiment described in [4]. The absorption detection system is experimentally more difficult in that

1. Two different sources of irradiation are used, one for the creation of radicals (in this case an excimer laser) and one to supply the incident light for absorption (in this case a xenon arc lamp). The irradiation beams must be perpendicular and preferably contain no common frequency. This is achieved by the use of filters and / or monochromators.

2. The size of an absorption signal is many times smaller than the fluorescence signal and in the opposite sense to that from scattered laser irradiation. This makes the detection considerably more difficult.

3. Radicals must be created in a suitable position to allow absorption of the analysis light. This means that solutions must be optimised such that radicals are created throughout the width of the analysis beam.

Significant progress was made, producing an experiment that allowed observation of the decay of the benzophenone ketyl radical. The experimental setup is indicated in figure 8.3.1.

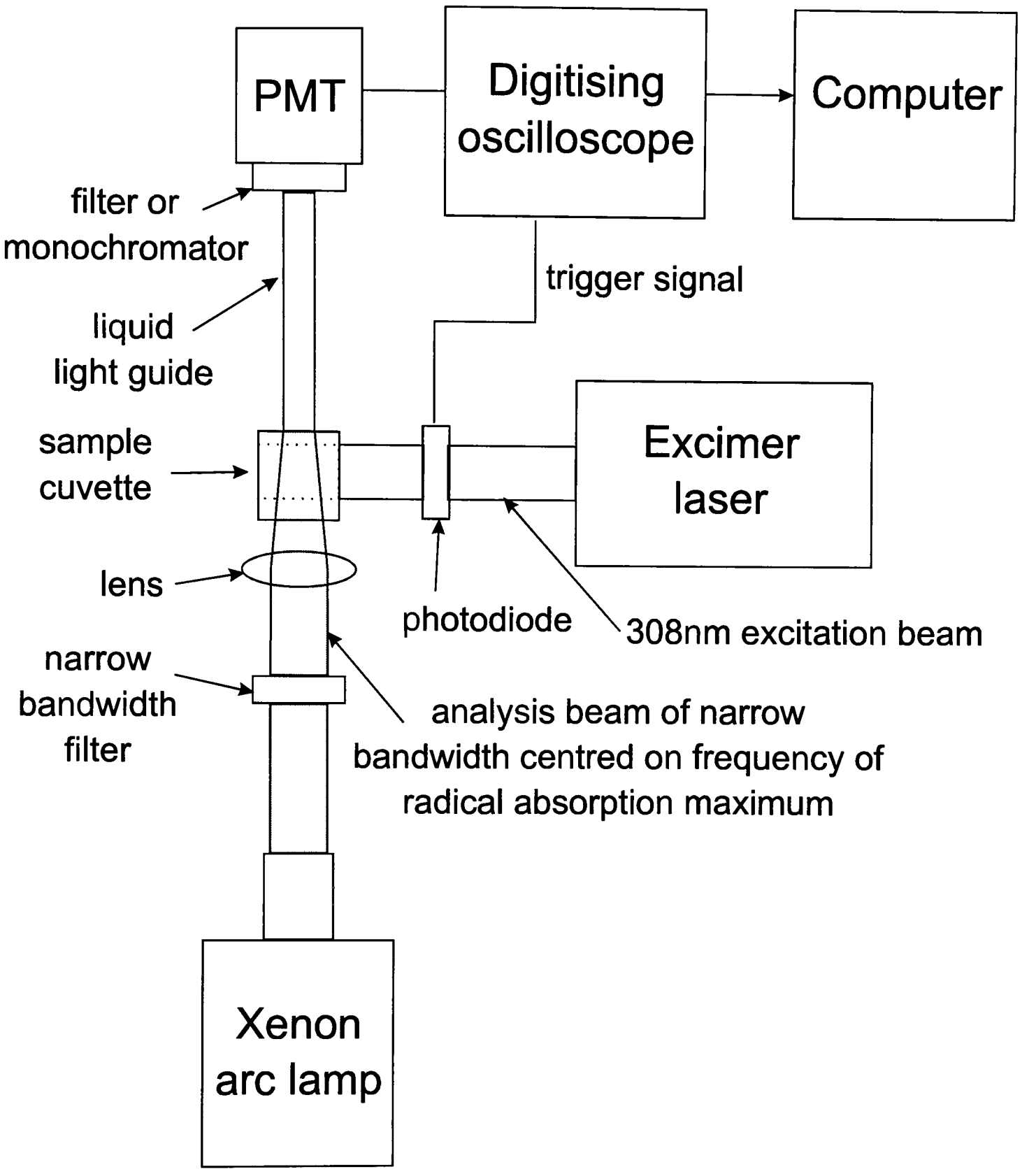

Figure 8.3.1. Schematic diagram of the apparatus used for the detection of transient free radicals by their absorption in the visible region of the spectrum. Radicals are created in the sample cuvette by the 308nm laser flash. They are continuously irradiated with an analysis light at the radical absorption frequency. Any absorption by the radicals causes a change in the light intensity reaching the photomultiplier. The digitising oscilloscope is triggered by the laser flash and records the subsequent light intensity of the analysis light. The complete experiment encloses the sample cuvette within a pair of Helmholtz coils, allowing the observation of the effect of a magnetic field on the transient absorption signal.

Figure 8.3.1 contains no magnetic field generating equipment. All the work performed by the author was concentrated upon obtain reproducible absorption signals suitable in magnitude for quantitative analysis. Other members of the group have recently optimised the optical system further and added magnetic field capability. The apparatus is now being used for MFE experiments and it is hoped that valuable results will be obtained in the near future.

Figure 8.3.2 shows a typical absorption signal obtained from the apparatus. The solution used was a 0.4 g dm^{-3} solution of benzophenone in octan-2-ol. The absorption signal of the radicals decays sharply at early time with a longer lived signal dominating after about 5μs. This would appear to correspond to the freely-diffusing period of reaction. The curve indicates that the absorption signal from transient radicals can be successfully recorded using the apparatus.

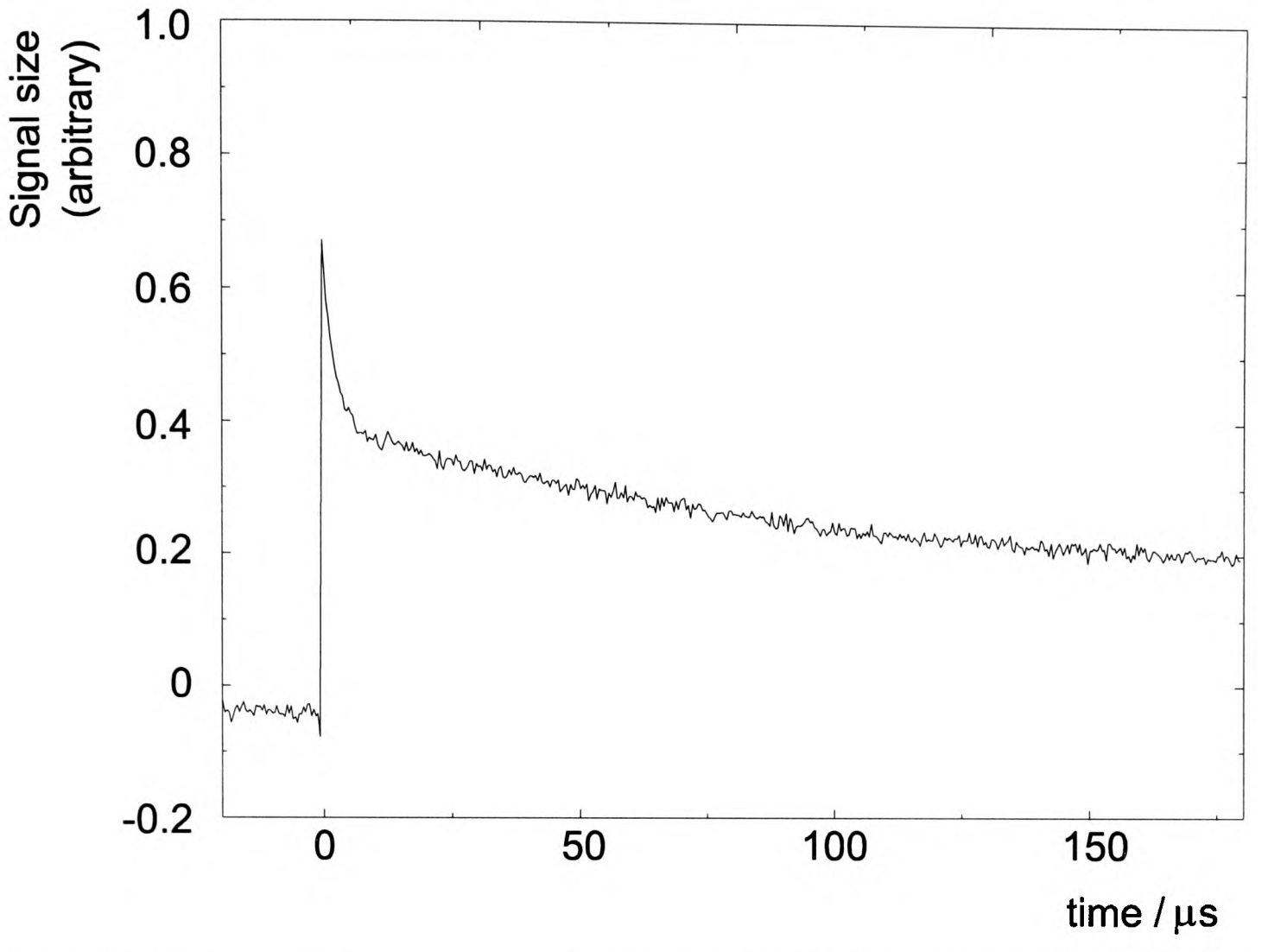

Figure 8.3.2. Transient radical absorption signal from the benzophenone ketyl radical (created by the excitation of benzophenone in octan-2-ol by laser irradiation at 308nm) recorded at 545nm using the apparatus indicated in figure 8.3.1.

8.3.2 Applications

The absorption apparatus has a number of uses in the investigation of magnetic field effects in biological systems.

1. Until now, the only chemical systems which could be studied necessarily possessed a fluorescing product. This meant that the scope of the experiment for studying radical pairs that might occur in real biological systems was virtually zero. The absorption experiment allows the study of neutral radical pairs with no limitations placed on the radicals involved. MFEs observed in such systems should mirror much more

closely the type of effect that might be observed in biological environments

2. Direct absorption measurements can be performed in tandem with biochemical experiments, observing the effects of certain radicals on DNA and other bio-molecules and allowing direct comparison with the known effects of magnetic fields on the actual radical concentration. This reveals whether or not an organism is actively enhancing MFEs or adjusting to the change in radical concentration, removing the effect of the field.

3. More experimental information can be gleaned on the factors that optimise the effects of magnetic fields in the various different domains of field magnitude.

4. In principle, real-time studies of intact biological systems can be made. That is, the response of the system to an instantaneous pulse or to a modulated perturbation, can be detected directly. This overcomes the problem of conventional biological methods, that the accuracy of the assay may be insufficient to detect small effects.

References

[1] **Sacher, M. & Grampp, G.**
Ber. Bunsenges. Phys. Chem. **101** (1997) 971

[2] **Linet, M.S., Hatch, E.E., Kleinerman, R.A., Robison, L.L., Kaune, W.T., Friedman, D.R., Severson, R.K., Haines, C.M., Hartsock, C.T., Niwa, S., Wacholder, S. & Tarone, R.**
The New England Journal of Medicine **337** (1997) 1

[3] **Valberg, P.A., Kavet, R. & Rafferty, C.N.**
Radiat. Res. **148** (1997) 2

[4] **Batchelor, S.N., Kay, C.W.M., McLauchlan, K.A. & Schkrob, I.A.**
J. Phys. Chem. **97** (1993) 1325

Chapter 9

The effects of radiofrequency radiation on radical recombination.

9.1 Introduction

Chapters 2 and 3 discussed the theory of radical pair recombination and the mechanisms by which static magnetic fields of various magnitudes can affect the radical yields of such reactions. This chapter is concerned with the idea that, as the yield of such reactions is influenced by the extent of interconversion between singlet and triplet states, then in zero or low field, a change in the rate of spin mixing might affect the proportions of singlet and triplet radical pairs and thus alter the yield of the reaction. This can be illustrated by a thought experiment.

Consider the following reaction scheme.

$$M + h\nu \longrightarrow {}^1M^* \xrightarrow{ISC} {}^3M^* + S \longrightarrow {}^3\{R_1^\bullet + {}^\bullet R_2\}$$

Figure 9.1.1. Creation of a triplet radical pair by production and reaction of an excited triplet molecule.

If recombination can only occur from the singlet radical pair, then no singlet product can be formed at the moment of pair creation. Now consider the situation after separation and re-encounter within the geminate cage. If the spin mixing process is 100% efficient, 75% of the radical pairs will re-encounter in a triplet state and 25% in a singlet state. Making the assumption that all singlet radical pairs recombine, then 25% of the radical pairs recombine after re-encounter. If, however, the spin-mixing process is only 10% efficient, then

97.5% of the radical pairs will re-encounter in a triplet state and only 2.5% in a singlet state. This gives only a 2.5% recombination.

If we now consider the average geminate pair lifetime of a radical pair to allow 4 re-encounters (this is completely arbitrary), then the total percentage of recombination in the 100% efficient case is

$$100(1-(0.75)^4) = 76.3\%$$

and in the 10% efficient case is

$$100(1-(0.975)^4) = 9.6\%$$

It is thus clear that the efficiency of spin-mixing has a significant effect on the number of radicals recombining within the geminate cage and thus in the number of radicals escaping to the bulk.

The rate of spin-mixing in zero or low field is driven by electron nuclear hyperfine interactions whose energies correspond to frequencies in the radiofrequency (RF) region of the spectrum. It is proposed that the application of a suitable radiofrequency could enhance the rate of spin mixing and be manifest as a change in the yield of the radical recombination reaction.

9.2 The chemical system

The chemical system chosen for study was pyrene (Py) / dicyanobenzene (DCB) radical ion pair / exciplex system. It was initially chosen for a number of reasons.

1. It has been studied extensively in the past by the group and elsewhere, and has reproducibly exhibited magnetic field effects due to both

removal of $T_{\pm1}$ states via the Zeeman interaction, and also the 'low field feature' described in chapters 2 and 3.

2. MFE experiments built by the group all currently rely on fluorescence detection to observe the product yield (although some of the authors time during the research period was employed in building a MFE experiment that allows detection of escaping radicals via their absorption spectrum - this is discussed in chapter 8). The product yield of this system is monitored by exciplex fluorescence and thus any experiments can be performed by modification of existing apparatus.

3. As the system involves a radical ion pair, the geminate pair lifetime is extended relative to a neutral pair, potentially increasing the size of any effect induced by enhanced spin mixing.

4. The 1,3-DCB radical anion has a dominant hyperfine coupling which is somewhat greater than those in the Py radical cation. It was hoped that resonance effects might occur near to this frequency.

The formation of the radical ion pair and its subsequent behaviour is illustrated in figure 9.2.1.

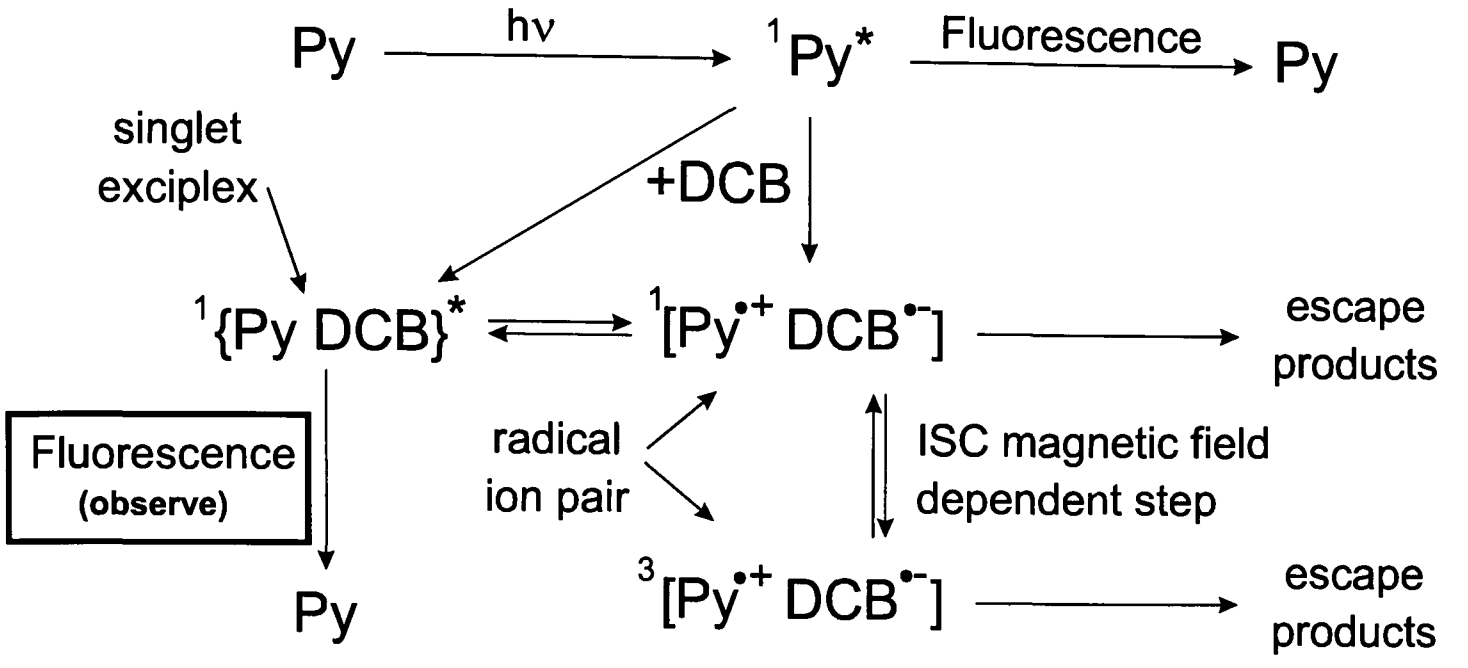

Figure 9.2.1. Reaction scheme for the pyrene and dicyanobenzene system showing all processes significant to the observation of MFEs.

Experiments are performed by measuring the fluorescence signal from the singlet exciplex, the magnitude of which is a measure of the singlet channel. Fluorescence maxima for the pyrene and exciplex fluorescence are at approximately 390nm and 435nm respectively and selective filtering of the exciplex fluorescence is sometimes beneficial.

DCB exists as three positional isomers indicated below

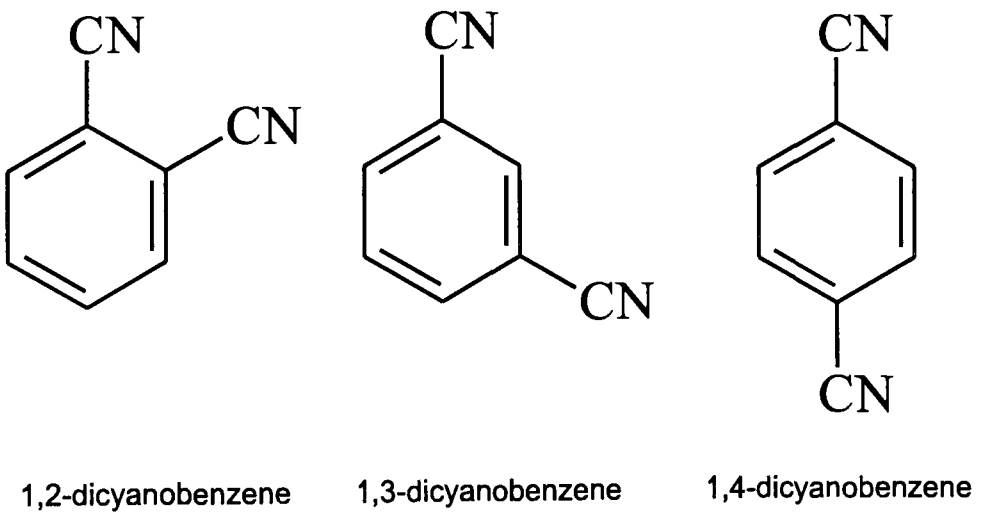

1,2-dicyanobenzene 1,3-dicyanobenzene 1,4-dicyanobenzene

Figure 9.2.2. The three isomers of dicyanobenzene (DCB).

Previous experiments [1] have shown the largest field effects to be observed with the 1,3 isomer and thus this was selected for use in the radiofrequency experiments.

The choice of solvent is crucial for the maximisation of field effects. To observe field effects, both the exciplex and the radical ion pair must exist. Previous studies have shown that very low polarity solvents allow formation of the exciplex exclusively [2] and highly polar solvents only allow direct electron transfer to the radical ion pair, bypassing the exciplex formation [3,4]. As a highly viscous solution extends the lifetime of the pair, solvent mixtures of cyclohexanol (low dielectric, high viscosity) and acetonitrile (high dielectric, low viscosity) have been used to provide a suitable polarity for both exciplex and ion pair to exist, while maintaining a high enough viscosity to enhance the probability of observing a field effect.

Py, DCB and solvents were supplied by Aldrich and used as supplied. All solutions used were thoroughly degassed with argon prior to use, as dissolved oxygen readily quenches exciplex and radical ion pairs.

9.3 Radiofrequency experiments in the presence of an applied static field.

9.3.1 Approach

It was suggested earlier that radiofrequency radiation that could interact with the hyperfine levels of the radical pair might cause an increase in the rate, and therefore efficiency, of spin mixing. Each radical in the Py / DCB radical ion pair possesses a number of different hyperfine couplings. The largest hyperfine coupling is in the 1,3-DCB radical anion and is reported to have a magnitude of about 8.3G [5]. This corresponds to an RF frequency of 23.2MHz. RYDMR

experiments involving 1,3-DCB have been interpreted in terms of the mean hyperfine coupling in the system, defined in a quasi-classical way, of 34.3MHz [6]. These frequencies encompass the range at which one might expect to find resonance effects.

When the experiment was first attempted, a precise expected frequency was unknown since no theoretical treatment was available. Therefore the experiment was designed to allow irradiation at a fixed RF frequency and to apply a variable static magnetic field in order to bring the system to resonance. Thus the experiment effectively attempts to observe the effect of radiofrequency radiation on the normal MFE curve of the system.

9.3.2 Experimental

The experimental design was a modified version of the normal pulsed MARY experiment used by the group. MFE curves are generated by recording exciplex fluorescence decay curves following flashes of 308nm from an excimer laser in the presence and absence of an applied static magnetic field and the field effect is calculated as described in equation 3.3.1. The apparatus is modified to allow MFE curves to be obtained with or without the application of RF radiation.

The apparatus used is illustrated in figure 9.3.1 and its operation is described below.

Application of RF and static magnetic fields

The sample was held in a normal silica UV cuvette within a 12mm diameter coil wound into two halves to allow light to enter (this is illustrated in the inset of figure 9.3.1). This was held inside an earthed copper gauze shield (not shown) in an attempt to minimise RF interference. The whole was enclosed in a

Helmholtz pair, via which the static field was created and stepped through chosen increments within a selected total range.

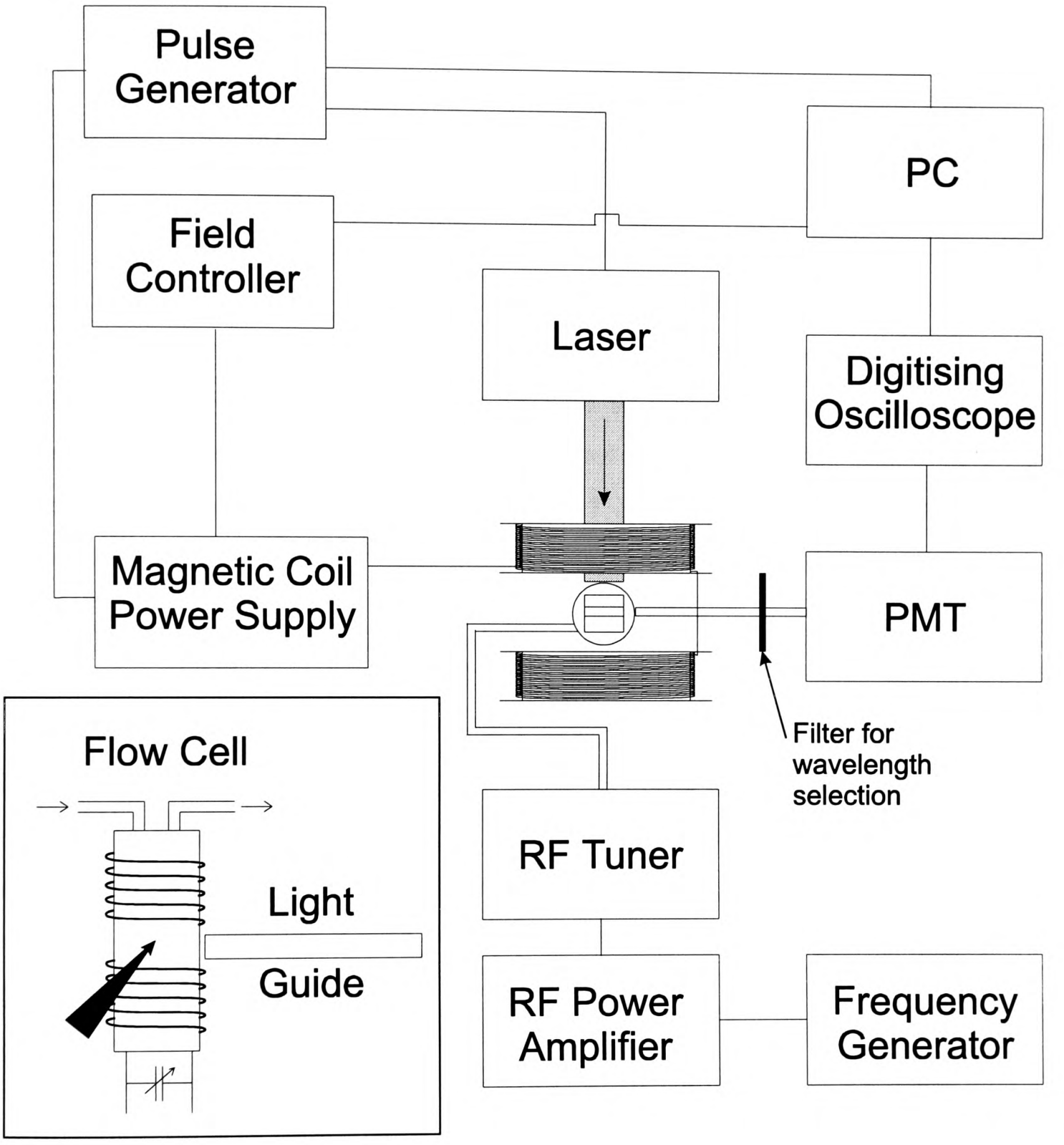

Figure 9.3.1. Time-resolved MARY apparatus modified for the investigation of the effect of RF fields. The RF coil was surrounded by an earthed copper shield which is not shown.

The RF coil was tuned with the aid of a capacitor in parallel, whilst the whole was further tuned and matched to the RF source using an inductor / capacitor circuit (Vectronics K300DLP antenna tuner). The solution was fairly lossy due to its relatively high dielectric and thus the VSWR (voltage standing wave ratio) achieved was about only 1.2, and 5W of continuous wave power was applied. This was measured by monitoring the incident and reflected power to and from the coil directly. The value was maintained in experiments performed at different frequencies of the applied RF radiation, implying that the strength of the field in the rotating frame did not vary greatly between them. This assumes that the Q-factor of the coil (which was not measured) was low. The absolute magnitude of the RF field applied was undetermined. Experiments were also performed at fixed RF frequency but at various power levels. The RF signal was supplied from a Marconi 6311 frequency generator, and was amplified using a nominally 100W Wessex RC114-100 RF amplifier.

Radical creation and detection

The radicals were created in a flowing system by laser pulses from a Lambda Physik LPX100 excimer laser of about 90mJ per pulse (although not all of this was absorbed by the sample). Pyrene was used at a basic concentration of 5×10^{-5}M with 1,3-DCB at 10^{-2}M in a 9 : 1 cyclohexanol : acetonitrile mixture, although these concentrations were adjusted such that the laser light was absorbed throughout the sample.

Fluorescence was detected, via a liquid light guide at a right angle to the laser beam, by a Hammamatsu R1913 fast photomultiplier tube and the signal recorded by a 500MHz digital oscilloscope (Tektronix TDS 520). Data acquisition was controlled by a dedicated computer running operating software written by the author. 10 fluorescence traces are recorded in the presence of the static field, averaged by the digital oscilloscope and transferred to the computer.

This process is then repeated for 10 traces in the absence of a static field and this average trace is subtracted from the field on signal by the computer. This sequence was repeated 20 times for each static field value. To obtain the field effect value, the difference signal is averaged over the range for which it has a positive value (0.4 - 1.3 μs post flash) to increase the S / N ratio further. This is then divided by the sum of the field absent signal over the same period and stored. This procedure means that the percentage field effect value does not represent the overall effect of the field on the product of the reaction. The computer then increments the static field (a normal spectrum consists of 20 field points over 150G) and the process is repeated until the entire MFE curve is obtained. The experiment was finally repeated in the presence of a radiofrequency field, with experiments being performed over a range of RF frequencies and powers.

9.3.3 Results

The results obtained from this experimental system were startling. Figure 9.3.2 illustrates the field effect curves obtained from the system in the presence and absence of RF applied at 25MHz and an arbitrary power of at least 5W.

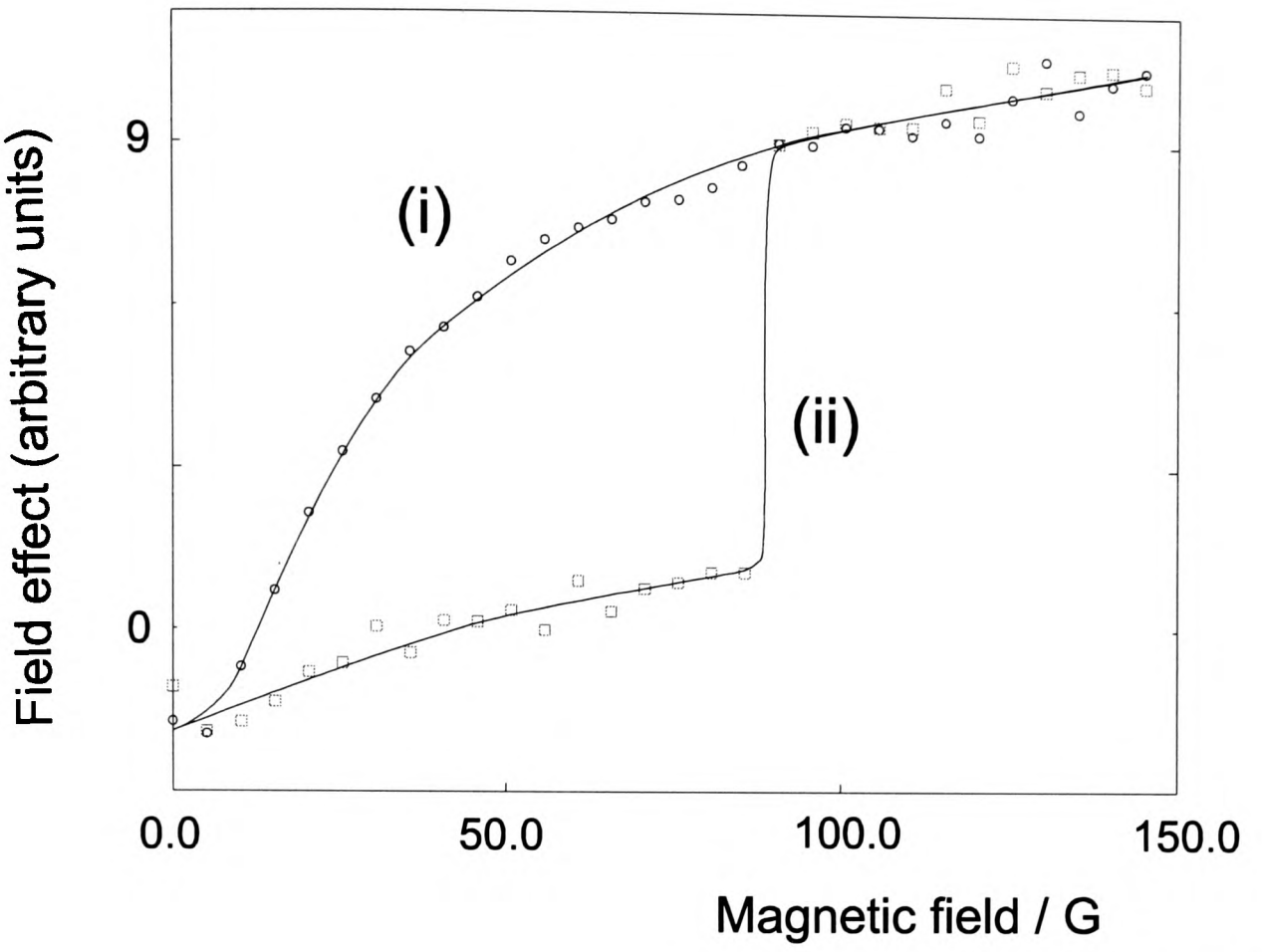

Figure 9.3.2. MFE curves obtained from the Py / 1,3-DCB system (i) in the absence of RF radiation and (ii) with RF applied at 25MHz.

Curve (i) represents the normal MFE curve for the system reported previously [7]. It indicates that the yield of singlet exciplex is increased in the presence of a magnetic field, in agreement with figure 3.4.2. The RF-present curve is strikingly different in shape, with the MFE decreased at low static field values, but reaching the same asymptote as the RF-absent curve at high values (within experimental error).

The difference can be emphasized by analysis of the time-resolved fluorescence curves in the presence of an 80G static field. Figure 9.3.3 illustrates these curves in the presence and absence of RF and also the curve obtained by subtracting the RF-on curve from the RF-off one.

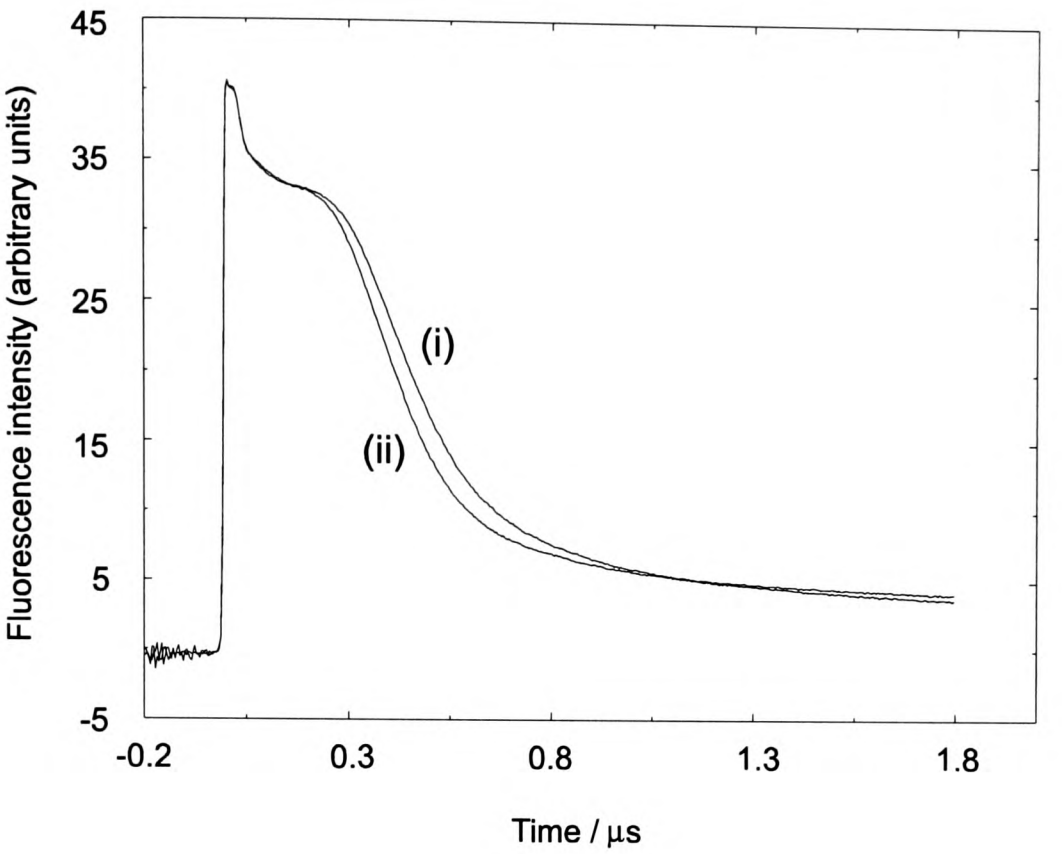

(a)

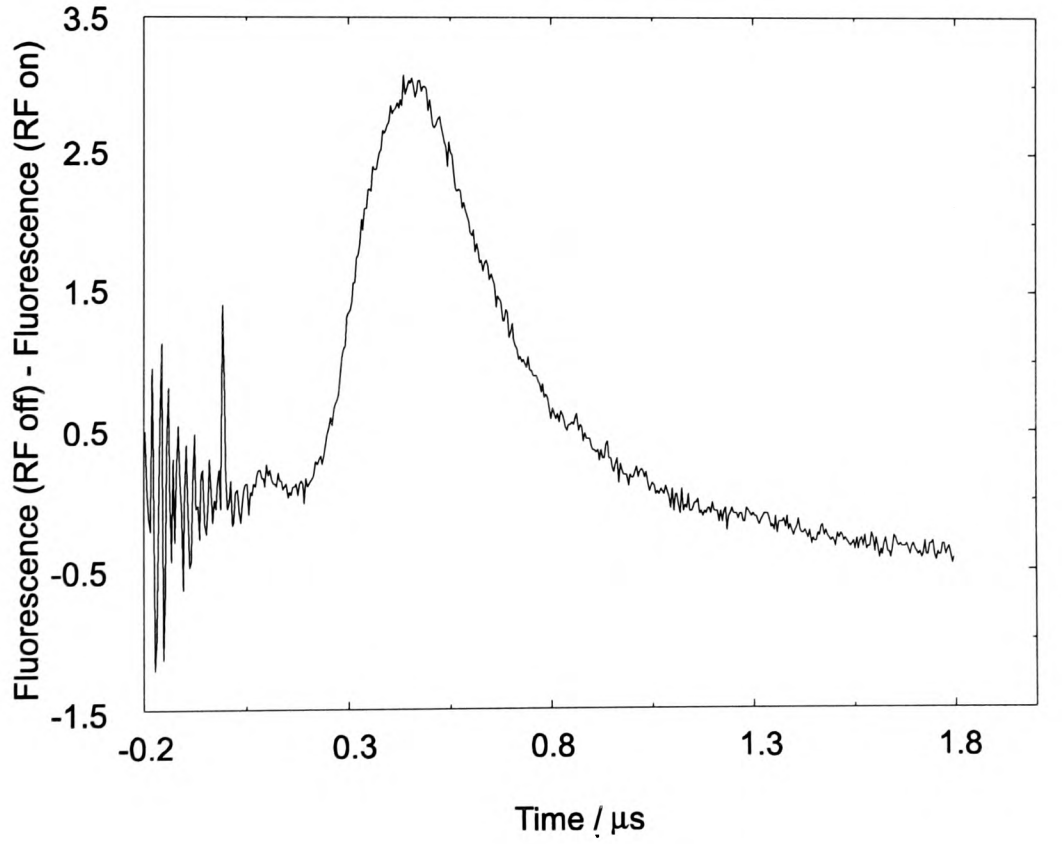

(b)

Figure 9.3.3. (a) Fluorescence decay curves from the Py / 1,3 DCB system in an applied, static field of 80G (i) In the absence of 25MHz radiation and (ii) in its presence. (b) The difference between the two curves in (a).

The result of these experiments is not of the form expected and thus there was some question over its authenticity. Many careful checks were performed to ensure that the effect was not instrumental in origin. The greatest fear was that the RF coil radiates freely in the 25MHz region and there is the possibility of interference with almost all parts of the experimental system. The earthed copper screen minimised the radiation produced from the coil, but was incapable of removing it completely. All the electrical equipment appeared to behave normally when the RF field was applied. One potential explanation of the effect is that the unit supplying current to create magnetic field pulses was affected. It is conceivable that the field is not incremented properly when the rf is applied to the experiment, but instead jumps from a low to a high field value once some threshold has been reached. This was checked by direct monitoring of the current steps produced by the unit, and no discontinuity in the current pulses was discovered in the presence of the RF field. No mysterious effects of instrumentation appeared to exist and so other experiments to investigate the nature of the effect were performed. Figure 9.3.4 illustrates the effect of changing the frequency of RF in the 25MHz region. This was achieved by a retuning and matching of the coil at the desired frequency until the total absorbed power was 5W. The curves were obtained over a smaller static field range and with fewer data points than in figure 9.3.2.

As the RF frequency is increased from 22MHz, the static field value at which the RF curve returns to the RF-free curve increases, achieving a maximum value at 28MHz, where the static field required lies outside the observation range.

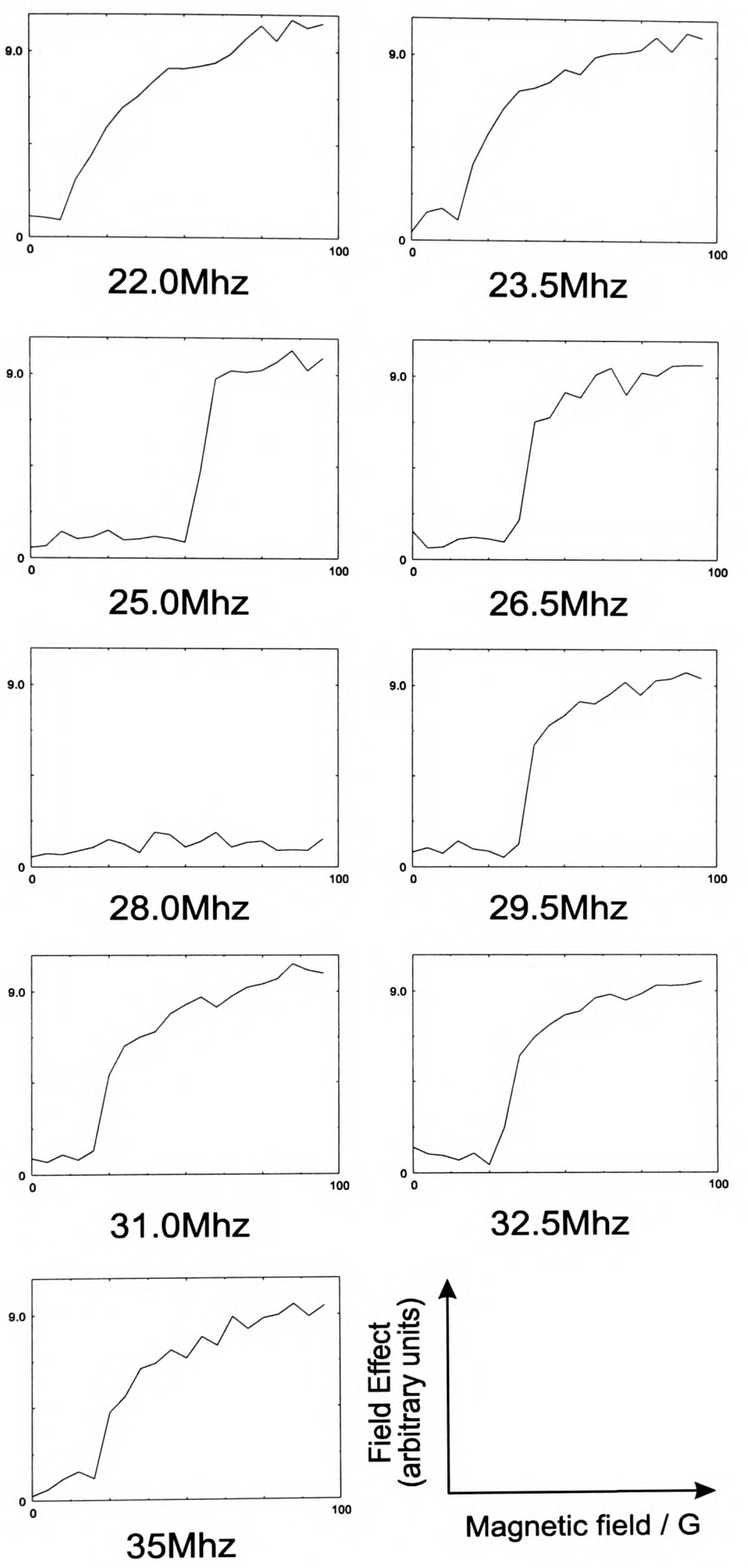

Figure 9.3.4. MFE curves obtained in the presence of 5W of RF radiation at a series of frequencies.

At increased RF frequencies, the static field required is reduced, indicating the effect to be a resonant one and there even appears to be evidence for fine structure with the discontinuity occurring at a lower applied field at 26.5MHz than at 25 or 28MHz. This behaviour compounds the evidence for the non-instrumental nature of the effect with the only possible remaining trivial explanation being an unfortunate resonant instrumental response in this range. The clock frequency in the field stepping unit is only 30Hz and thus the origin of any such resonance is unclear.

The static field at which the discontinuity is manifest was also found to be dependent upon the RF power. Figure 9.3.5 shows the effect of 0, 4 and 10W of applied 25MHz radiation.

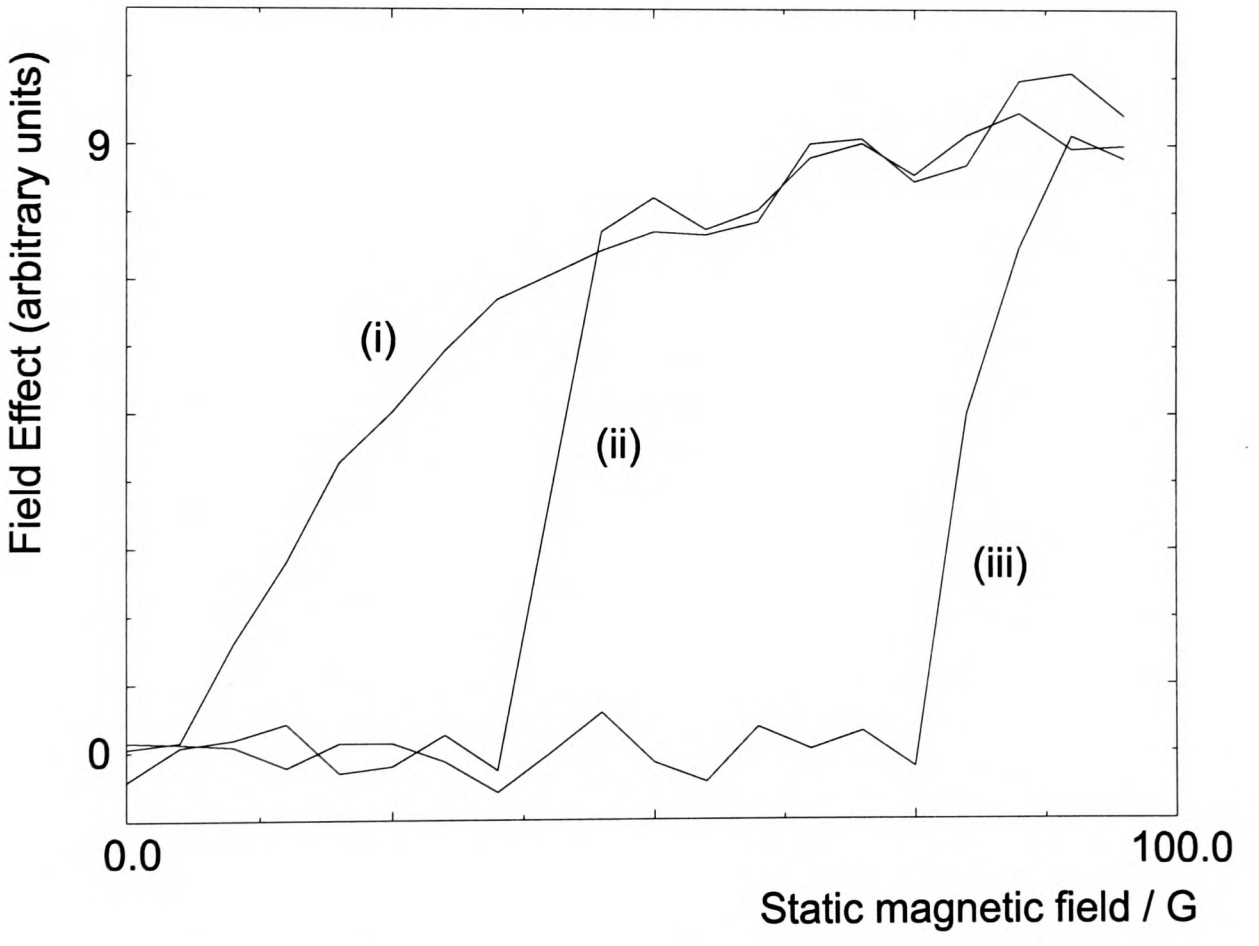

Figure 9.3.5. MFE curves obtained using 25MHz radiation at applied RF powers of (i) 0W, (ii) 4W and (iii) 10W

9.3.4 Discussion

The results obtained above, when published [appendix F], were discussed in terms of a process which conserves the zero-field mixing whilst the RF field is the dominant one present, with reversion to normal MFE behaviour once the static field exceeds it. This was a conjectural explanation as no measurement of the power of the rotating component of the RF field was performed. Even though extensive work had been performed to ensure that the result was non-instrumental, tests were continued even after publication. A final test attempted by the author was to supply the static field from a permanent magnet, rather than an electromagnet as there could be no possible way that RF could interfere with a field generated in this way. A large horseshoe magnet was used to provide the field whose magnitude was controlled by the separation between magnet and sample. As in figure 9.3.3, fluorescence curves were obtained in a static field of 80G in the presence and absence of 25MHz radiation, with the permanent magnet generating the static field. Figure 9.3.6 contains subtracted fluorescence curves obtained with the static field from both sources. It is clear that in the presence of both static magnetic field and RF radiation, the difference observed when the magnetic field is generated electrically is no longer present when a permanent magnet is employed. This means that the results are indeed experimental in origin although the precise nature by which the static field generation is affected is unclear.

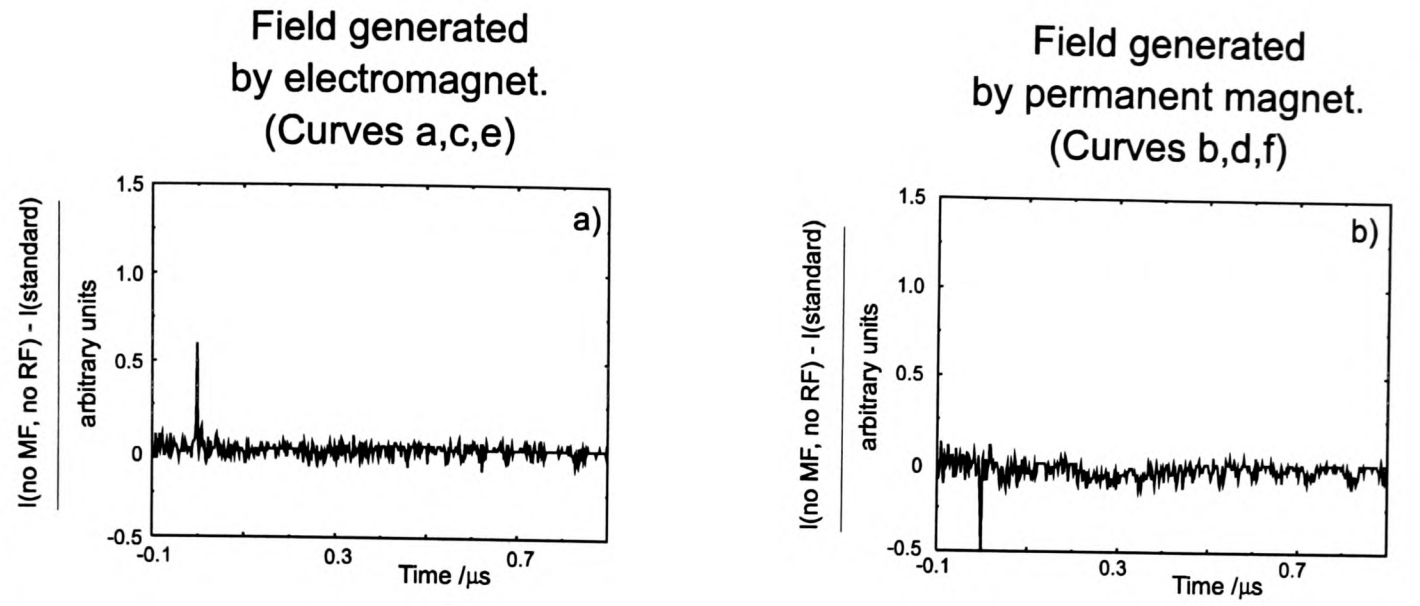

Figure 9.3.6. Subtracted fluorescence curves from the Py / 1,3-DCB system. Curves a) and b) illustrate the subtraction of similar fluorescence traces. Curves c) and d) show the MFE created by an electromagnet and a permanent magnet. In curve e) the effect is removed by the application of RF, however in curve f) the effect is not removed when the static field is generated by a permanent magnet.

It was felt imprudent to spend large amounts of time trying to determine exactly where the fault lay as this would likely provide little experimental and no theoretical insight. The experiment provoked much interest, however, prompting a theoretical investigation into the effects of RF magnetic fields on radical reactions [8], which showed that substantial resonance effects (up to 25%) might be expected. The resonances appear at frequencies corresponding to hyperfine energy-level splittings, which are not necessarily the same as the energy differences observed by EPR in a strong magnetic field. The influence of the RF field on the reaction yield was found to be considerably more straightforward in the absence of a static magnetic field: the spectra were simpler and more obviously related to the hyperfine coupling constants. Also, a necessary, but not sufficient, condition for the observation of an oscillating magnetic field effect (OMFE) was found to be the existence of an appreciable low-field effect (LFE). Armed with this information, experimental efforts were directed away from the initial RF experiment and towards designing a new one which would take the above theory into account.

9.4 Radiofrequency experiments in zero magnetic field.

9.4.1 Approach

The RF experiments described above provided valuable practical experience in the design and operation of RF circuitry and also a healthy skepticism of the results obtained in such experiments. The following points had to be taken into account in the building of a new experiment attempting to produce results for comparison with the theoretical work performed.

1. No static magnetic field is required for this experiment. This makes the design considerably easier than previously. Also, it appears that the instrumental resonance in the previous experiment was associated with the static field generating part of the apparatus. This problem is absent in the zero field experiment.

2. It was stated in chapter 3 that LFEs appear to be enhanced in systems with extensive hyperfine coupling in one radical, and little in the other. Thus the choice of chemical system was based on the Py / 1,3-DCB system for the reasons described in section 9.2. It was, however, modified to take the above information into account.

3. The size of a potential zero-field RF effect, although theoretically substantial when maximised, was unknown and thus the experiment was designed with sensitivity at the forefront. In order to achieve high sensitivity, the experiment was built, from the outset, to detect only the part of the exciplex fluorescence that was RF-sensitive using a modulation technique described below.

9.4.2 Modifications to the chemical system.

As described in section 9.2, the Py / DCB exciplex system had highly desirable properties, but suffered the drawback of the pyrene-derived radical possessing small, but significant hyperfine couplings. In order to maximise the LFE and simplify the theoretical calculations, one member of the radical pair should possess little or no hyperfine coupling. A potential solution to this problem was to use completely deuterated pyrene. Unfortunately, this was not readily available and thus a different electron donor molecule was found. Previous MFE experiments had been performed on a corresponding system of

anthracene (An) (figure 9.4.1) and DCB [9] and effects had been recorded, albeit somewhat more difficult to detect than in the Py / DCB system.

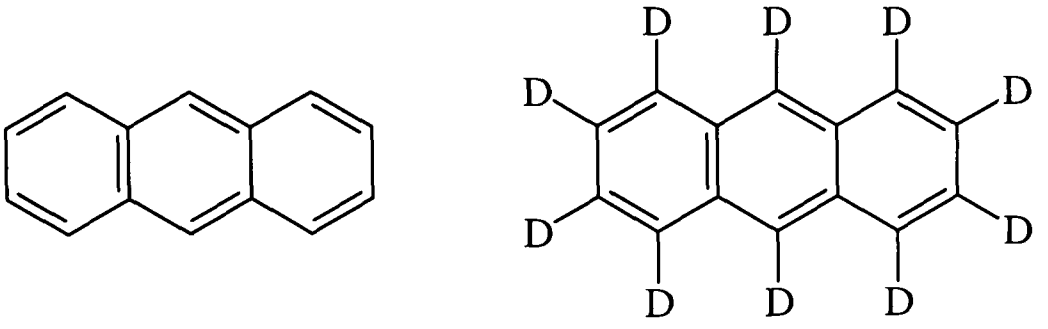

Figure 9.4.1. The structures of anthracene and deuterated anthracene.

Fully deuterated anthracene was available and thus MFE experiments were performed with d_{10}-An and 1,3-DCB using the apparatus described in [7], in an attempt to observe both MFEs due to Zeeman splitting and LFEs. These experiments were successful (see figure 9.4.6) and thus the An / DCB system was selected for theoretical calculations and experimentation.

9.4.3 Use of RF amplitude modulation

The principles of modulation and its effect upon observed signals are discussed in the references [10,11]. The static MFE curves presented in this chapter were obtained using modulation of the static field at an audiofrequency [11]. This technique was modified for use in the new RF experiment.

An amplitude-modulated RF signal was generated by supplying an audiofrequency to the voltage ramp input of the RF frequency generator. The audiofrequency was generated by a synthesizer circuit built into a lock-in amplifier and was fed-back to the amplifier for comparison with the fluorescence signal (obtained by detection using a photomultiplier tube), via phase-sensitive

detection. This means that any effect of the radiofrequency on the radical pair recombination will cause a modulation in the fluorescence signal obtained from the exciplex. By only observing the component of the fluorescence that varies at the audiofrequency applied to the RF, a large increase in signal to noise is obtained as signals are detected with narrow bandwidth. This effect is illustrated in figure 9.4.2. The power level of the audiofrequency entering the RF generator was controlled by a home-made unit such that the RF signal applied to the sample was modulated 100%. This was determined by direct observation of the RF signal applied to the sample, and the audiofrequency voltage had to be altered whenever the RF circuit was retuned to ensure that the modulation was always 100%.

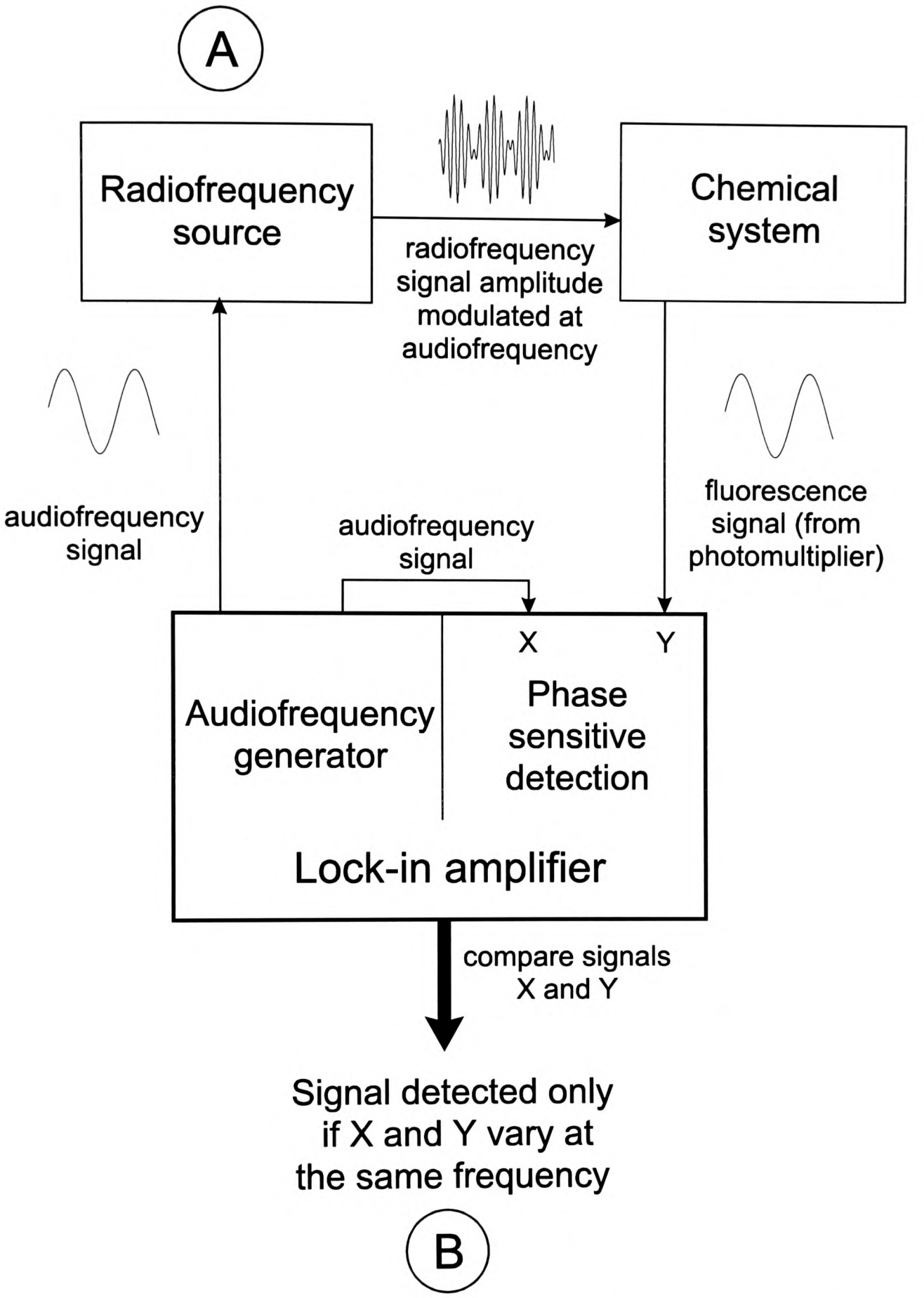

Figure 9.4.2. Schematic diagram illustrating the function of the modulation detection system as applied to the RF experiment. The experiment involves altering the frequency of RF supplied at A and monitoring the signal at B. Any effect of the RF on the chemical system will result in the observation of a non-zero signal at B, proportional to the amplitude of the OMFE. (The amplitude modulated RF signal is a simple pictorial representation and does not represent the actual relative frequencies of the RF and AF).

As well as providing enhanced sensitivity over direct changes in the fluorescence signal, the modulation technique is an excellent method for ensuring that chemical and instrumental effects are not confused. If the radiofrequency signal is in any way affecting other parts of the apparatus, this will be manifest as a non-zero signal from the lock-in amplifier (B in figure 9.4.2) regardless of the behaviour of the chemical system. Thus the apparatus can be tested by simply using a fluorescing system in which no form of MFE is expected and ensuring that the lock-in signal is zero. This was performed with a solution of pyrene in acetonitrile and the lock-in signal was recorded as zero throughout the range of RF frequencies under consideration.

9.4.4 Experimental

The non-flowing sample was irradiated in an air-cooled quartz tube using a continuous-wave radiofrequency source (Marconi Instruments 6311 programmable sweep generator) and a pair of Helmholtz coils (figure 9.4.3). Radicals were produced using a continuous-wave 300W Xenon lamp (Oriel) with an optical filter to discriminate against wavelengths longer than 350nm. Sample fluorescence was detected by an IP28 photomultiplier using a quartz light-guide coupled to a liquid light guide outside the earthed and screened box (which provided complete isolation of the radiofreqeuncy radiated from the coils) containing the irradiation cell. No wavelength selection of the fluorescence was used, except for observations of the static field effects on 1,2- and 1,4-DCB for which a band pass filter was used to improve the signal-to-noise ratio. The RF field was 100% amplitude modulated at 381Hz, a frequency found to give satisfactory signal-to-noise. As described in section 9.4.3, the modulation depth was checked using a fast oscilloscope prior to each measurement.

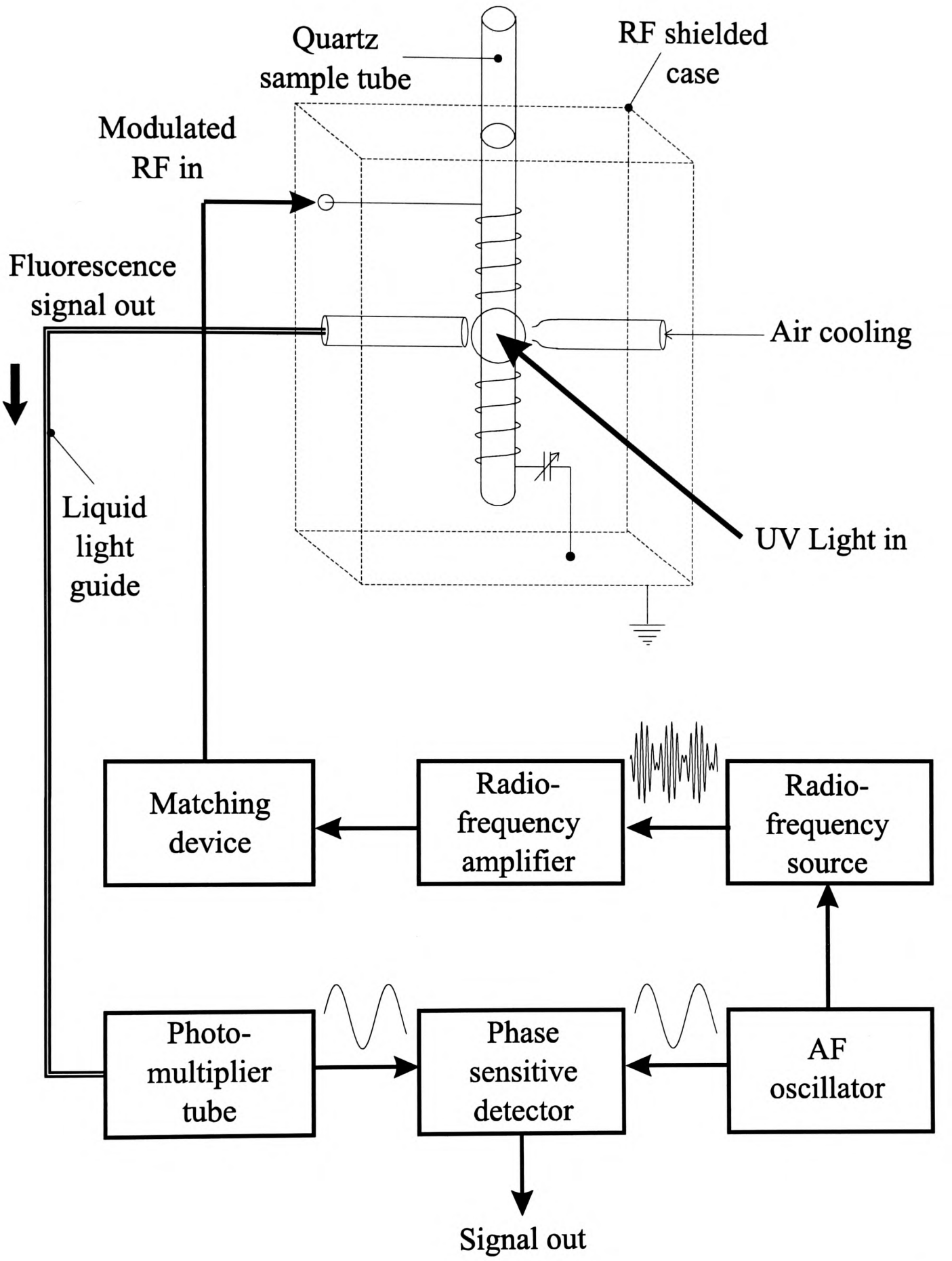

Figure 9.4.4. A schematic diagram of the apparatus used to measure oscillating magnetic field effects.

The modulated RF signal was passed through a 100W amplifier (Wessex Electronics RC114-100) to a matching unit (VCI Electronics VC300DCP Antenna Tuner) in series with a variable capacitor which allowed the coil to be tuned across a 25-50MHz range. As in the previous RF experiment, the tuning / matching unit displays both the incident and reflected RF power, permitting the power absorbed by the sample to be reset at a fixed value whenever the RF frequency was changed. This was important as the coil had to be re-tuned and re-matched at each different frequency due its comparitively high Q-factor, and therefore narrow bandwidth.

Samples of 1,2-, 1,3- and 1,4-DCB and fully deuterated anthracene were obtained from Aldrich and used as supplied. The solutions comprised 10^{-4} mol dm^{-3} anthracene-d_{10} and (1-20) x 10^{-2} mol dm^{-3} DCB in mixtures of acetonitrile and cyclohexanol. All experiments were conducted at room temperature.

9.4.5 Theoretical work

The experimental work described here was carried out in tandem with theoretical investigations by Timmel and Hore, whose previous calculations [8] led to continued interest in the observation of OMFEs. Using the techniques described in [ref as above], calculations were performed on the anthracene-d_{10} / DCB systems (all three DCB isomers). The aim of these calculations was not to reproduce experimental spectra quantitatively, but to provide a guide to the magnitude and frequencies of the expected OMFEs in the systems involving the three different isomers. To this end, radical diffusion is not considered specifically, but the 'exponential model' described in chapter 3 is employed. The calculations illustrate the expected variation in singlet yield (measured by the extent of exciplex fluorescence) with RF frequency. They are illustrated in figure 9.4.5.

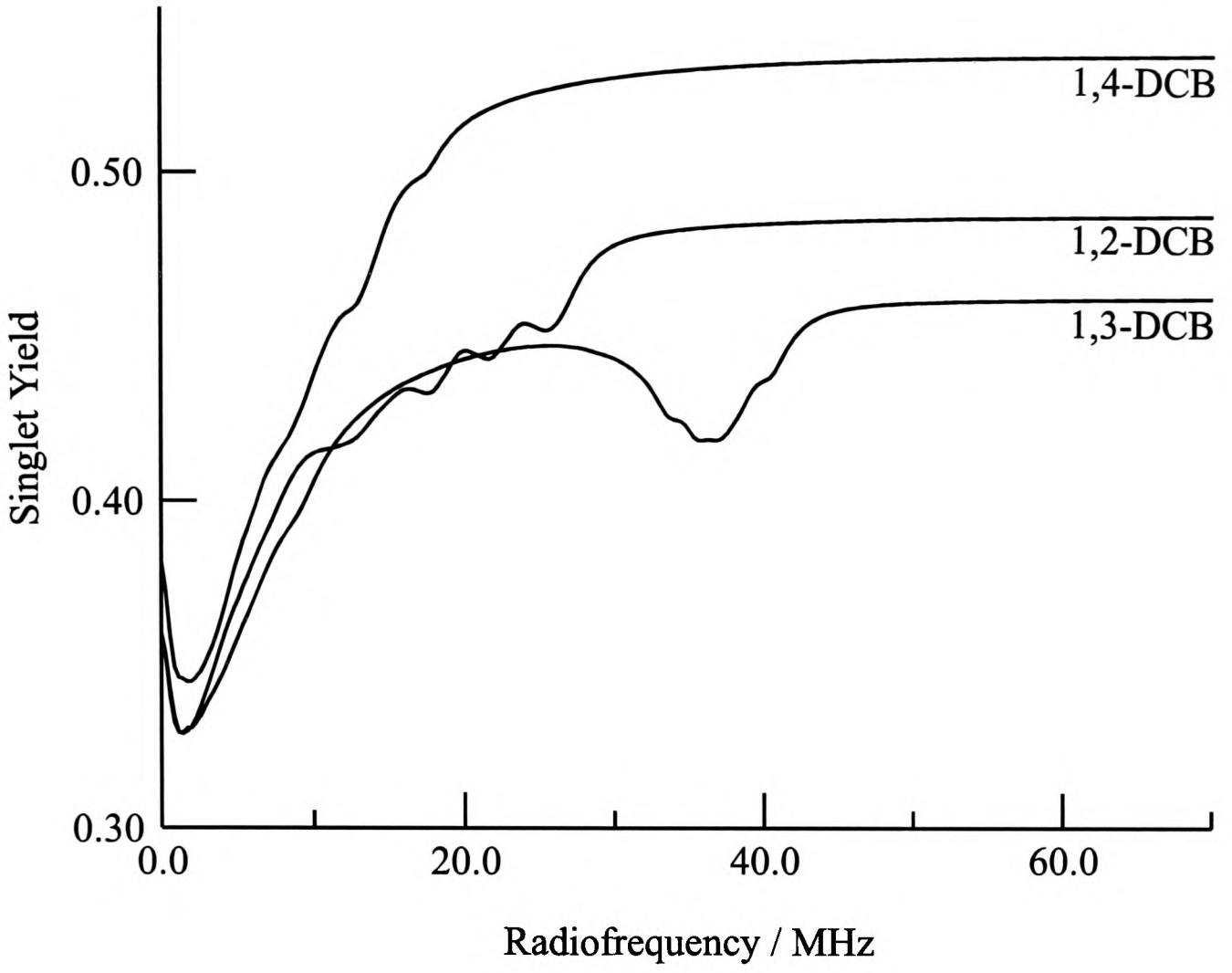

Figure 9.4.5. Calculated OMFEs for 1,2-, 1,3- and 1,4-DCB with anthracene-d_{10}. Singlet and triplet radical pairs were assumed to recombine at equal rates ($k=2.8 \times 10^6\ s^{-1}$) and the small ^2H hyperfined interactions in the anthracene-d_{10} radical cation were ignored. The (circularly polarised) radiofrequency field strength was 0.1mT. The hyperfine coupling constants for the DCB radical anions are given in appendix 2. Electron exchange and dipolar interactions were ignored. No static field was included: similar, but somewhat smaller field effects in the frequency range 20-60MHz are predicted in the presence of a 0.05mT static field.

It is clear from these calculations, that only the system containing 1,3-DCB is expected to show a pronounced resonance, centred at ~36MHz. A radical pair with just two equivalent protons on the same radical, with hyperfine couplings of 23.2MHz (by far the largest of the couplings in 1,3-DCB) would show a resonance at 1.5 x this frequency [8], i.e. 34.8MHz. The value of 36MHz shown in the figure arises due to contributions from the other, smaller hyperfine interactions in the anion. Using a rate constant of $2.8 \times 10^6\ s^{-1}$, the 36MHz resonance represents approximately a 10% reduction in the singlet yield. The

1,2- and 1,4- isomers have much weaker and largely unresolved 'bumps' at lower frequencies due to their smaller hyperfine couplings.

The theoretical origin of the OMFE [8] is similar in origin to that of the LFE [13], in that application of either a static or oscillating field lifts the degeneracy of some of the coherent superpositions of the spin eigenstates of the pair, allowing the coherences to oscillate which causes additional S $\leftrightarrow$ T interconversion. The mixing frequencies are simply the energy level splittings produced by the field and so significant effects are only expected when the radical pair lifetime is at least comparable with the reciprocal of the Larmor precession frequency of the applied field.

Besides the OMFE, figure 9.4.5 also illustrates the low field effects. At frequencies higher than any resonance with the oscillating field, the radical pair sees the oscillating field averaged to zero and so this region represents the singlet yield in the *absence* of an applied field. Conversely, the yield at zero frequency, is that under a weak static field, in this case 0.1mT. This information illustrates then, that the OMFE is approximately 40% the magnitude of the LFE for 1,3-DCB. Both the LFE and OMFE are attenuated if the lifetime of the radical pair is reduced. The origin of minimum in each of the signals at around 2MHz, is currently unclear.

9.4.6 Results

The theory discussed above reveals the importance of static magnetic field effects in relation to the observation of OMFEs. Thus static magnetic field effects were recorded using the modulated MFE experiment [12] for each of the DCB isomers with anthracene-d_{10}. The detected signal is the derivative (with respect to B_0) of the actual MFE [11], producing inversion symmetry about B_0=0.

The results are shown in figure 9.4.6 and are highly similar in nature to the plots obtained for the DCB isomers with pyrene [12].

These results establish a number of points.

1. It is clear that the radical pair is involved in the generation of the exciplex and its fluorescence.

2. The inset illustrates a small but definite LFE for the 1,3-DCB system. This is the first time such a feature has been recorded in this system.

3. No LFEs could be observed for the 1,2- and 1,4- isomers due to the low signal-to-noise ratio in these systems. Figure 9.4.5 predicts larger LFEs for these isomers than for 1,3-DCB and so it is likely that they are present, but unobservable due to experimental limitation.

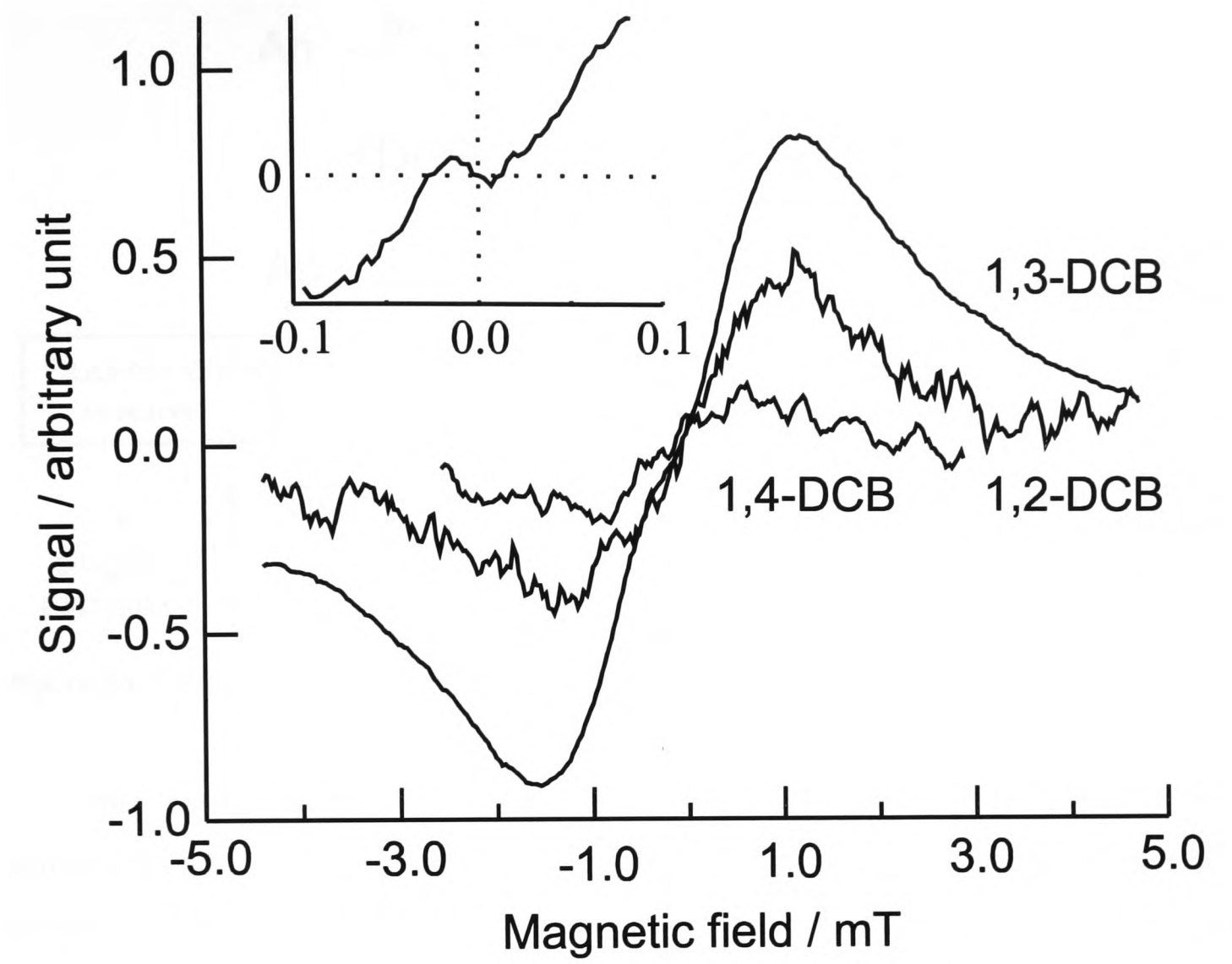

Figure 9.4.6 Static magnetic field effects for the three isomers of DCB with anthracene-d_{10}. The three curves have been scaled arbitrarily relative to one another. The inset shows an expanded region of the 1,3-DCB curve recorded with a smaller modulation field depth and increased averaging. The reaction conditions are [anthracene-d_{10}] = 10^{-4} mol dm^{-3}, [1,3-DCB] = 10^{-2} mol dm^{-3}, [1,2-, 1,4-DCB]=0.2 mol dm^{-3}. The ratio of cyclohexanol : acetonitrile in the solvent mixture was 9 : 1 for 1,3-DCB and 4 : 1 for the other two isomers.

It is assumed that the reaction scheme for the An / DCB system is similar to the Py / DCB one with the essential processes indicated in figure 9.4.7. Anthracene has a much shorter singlet lifetime than pyrene, undergoing much more rapid intersystem crossing to the singlet state. The triplet state of anthracene is much lower in energy than the singlet state and it is unlikely that exciplex formation can occur via this route. This means that the likely quantum yield of exciplex formation is much lower than in the pyrene system but still occurs to a sufficient extent for experimental observation. The significant chemical processes are indicated in figure 9.4.7.

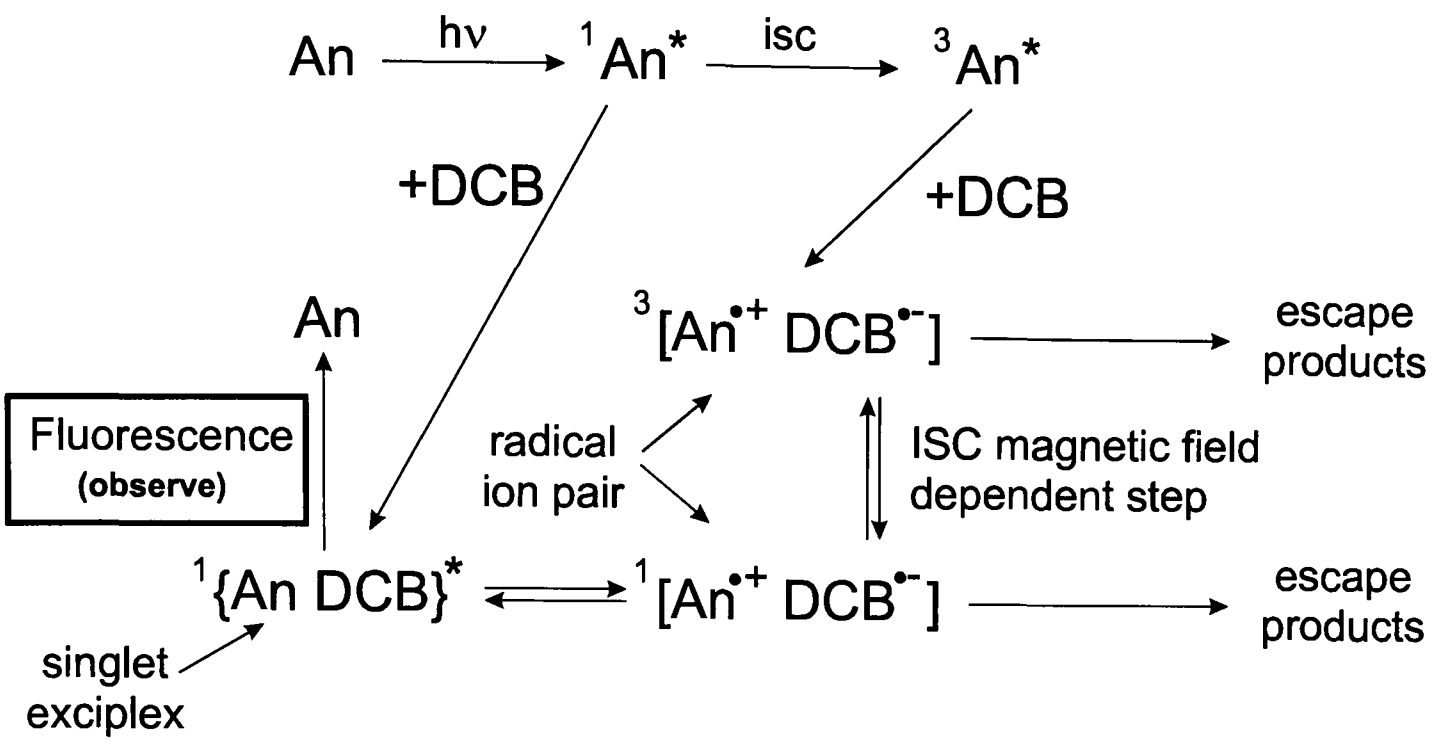

Figure 9.4.7. Reaction scheme for the anthracene / DCB system.

RF experiments were performed many times on systems containing anthracene-d_{10} and each of the DCB isomers. The signals observed from each solution as a function of RF frequency are given in figure 9.4.8. As predicted by the theoretical calculations, a resonance only appears for solutions containing the 1,3 isomer and is centred at a frequency of approximately 34MHz, which is very close to the predicted frequency of 36MHz. The lack of a signal in the 1,2- and 1,4-DCB containing solutions is of great significance. It rules out the possibility that the signal in the 1,3 isomer (obtained under identical experimental conditions) is due to direct pick-up of modulated RF power by the detection system, or that the fluorescence due to anthracene itself is, by some unknown mechanism, being modulated. There is then no reason to believe that the resonant effect of radiofrequency radiation centred around 34MHz on the An-d_{10} / DCB system is not genuine. This is the first observation of an effect of this kind.

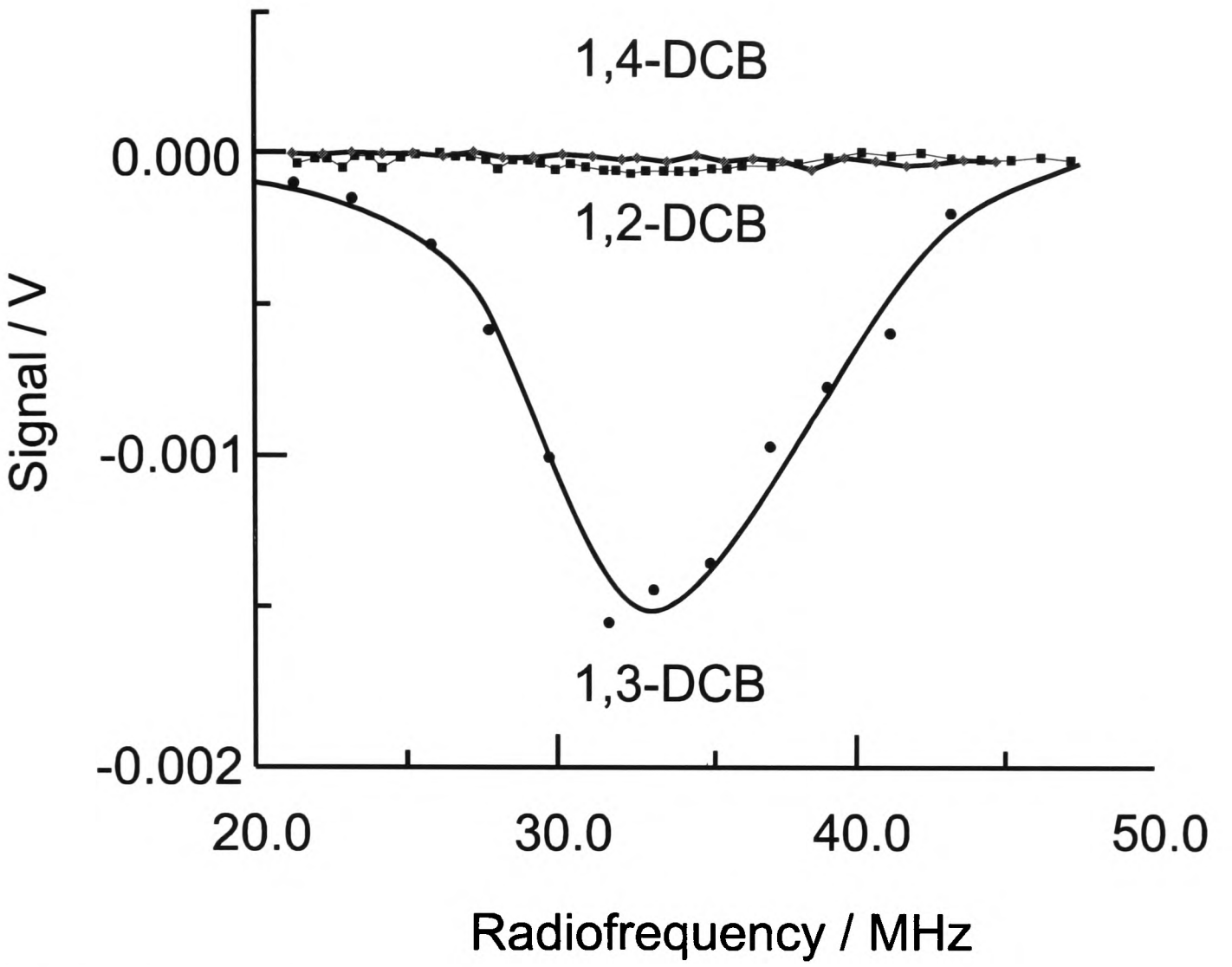

Figure 9.4.8. Intensity of the de-modulated fluorescence of solutions of anthracene-d_{10} with 1,2-, 1,3- and 1,4-DCB as a function of RF frequency. The smooth curves are drawn only as a guide to the eye and have no physical significance. For consistency with figure 9.4.5, the signals are plotted as negative voltages.

The absence of an OMFE from 1,2- and 1,4-DCB is presumably due to the size of the hyperfine couplings as discussed in section 9.4.5. However, the possibility that a small effect is present but is too weak to be detected (like the LFE) cannot be ruled out completely.

Figure 9.4.9 shows the de-modulated fluorescence intensity as a function of frequency for various applied RF powers in the 1,3-DCB system. The effect of an increase in power is to cause the resonance to become stronger and broader. There also appears to be a shift to higher frequency. The actual frequency of the RF incident on the sample was determined immediately after

each fluorescence measurement using a Tektronix TDS520 digital oscilloscope with a frequency read-out. Thus it would appear that this frequency shift is genuine, although its origin is currently unclear.

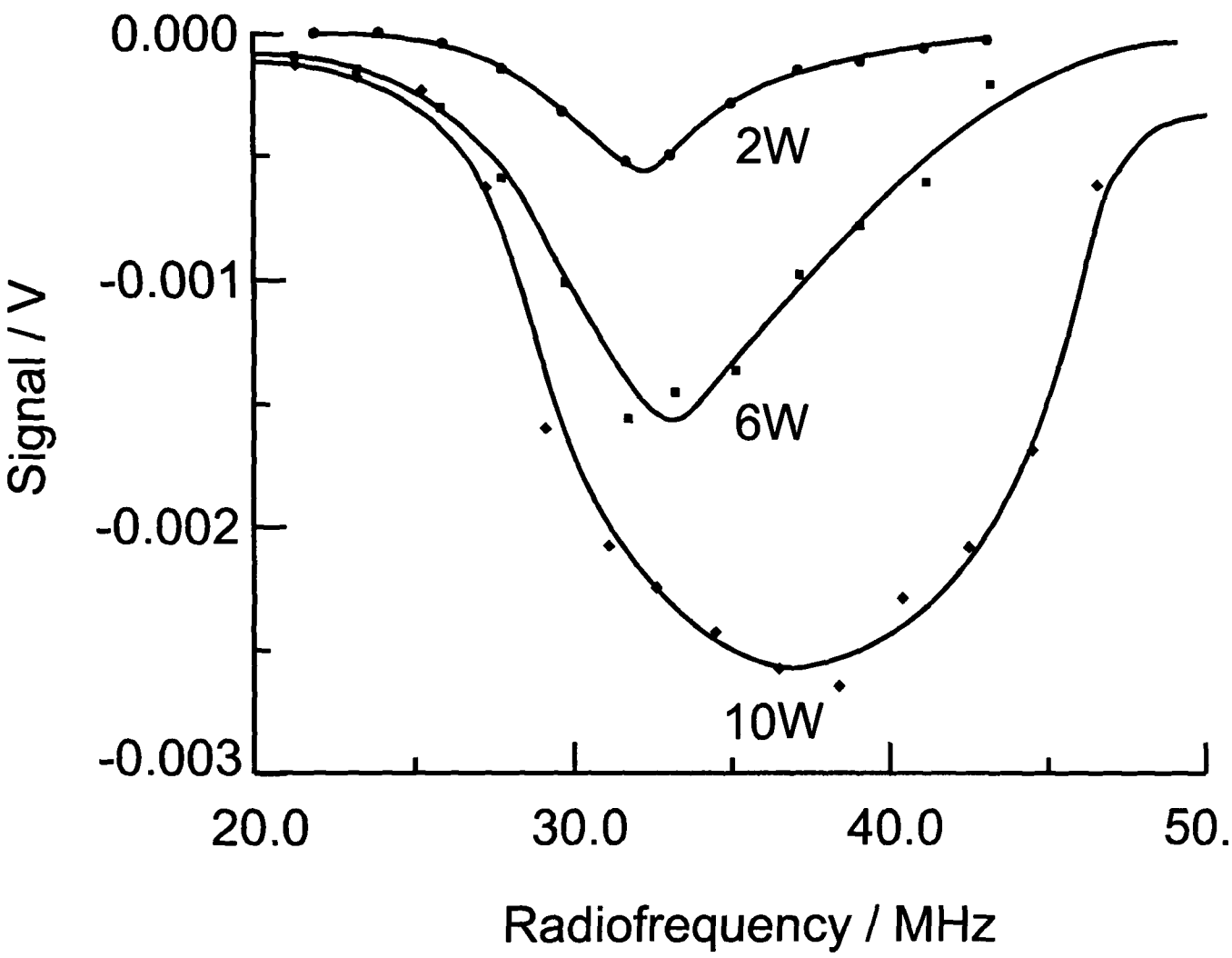

Figure 9.4.9. De-modulated fluorescence intensities for 1,3-DCB at three different power levels. The resonance is strengthened, broadened and frequency-shifted at increased RF power. Once again the signal is plotted as a negative voltage for ease of comparison with figure 9.4.5.

Comparison of the theoretical and experimental results allows rough estimates for the average radical pair lifetime and the amplitude of the RF field B_1 to be made, by observing that the width of the resonance is approximately linear in B_1 (proportional to the square root of the RF power). Interpreting the extrapolated width at zero power as the usual lifetime broadening $(\pi\langle\tau\rangle)^{-1}$ Hz, the lifetime of the pair is given as $\langle\tau\rangle \approx 100$ns. This is similar to that reported in the Py / DCB system [6]. Comparison of the simulations for a variety of B_1

values with the experimental data gives a value of $B_1 \approx 0.1$mT at 2W RF power. Both values are approximate, but appear physically reasonable. The lifetime is likely to be a weighted average, with a proportionally larger contribution from the longer-lived radical pairs due to the stronger OMFEs they should exhibit [8].

In an ideal situation, calculation of the B_1 power from the RF power and the known dimensions of the Helmholtz coil should be possible. Such a calculation, however, is not straightforward and requires measurement of, and correction for, the inductance and capacitance of the Helmholtz assembly at the frequencies used. For the apparatus used, such a calculation is sufficiently inaccurate to be unwarranted. The experiment was only designed to investigate the existence and basic properties of an OMFE. In future experiments, the coil can be replaced with a tightly-wound solenoid for which the field can be calculated from the easily-measured RF current, without the need for correction. It is hoped that spectra can be recorded under more controlled conditions so that quantitative analysis can be undertaken.

9.4.7 Concluding remarks

The experimental system demonstrates a resonant effect of radiofrequency radiation on the yield of a radical recombination reaction in the absence of any static magnetic field. It is believed that this is the first time such an observation has been made. The result is in agreement with theoretical calculations and implies that an RF resonance will be more pronounced in which one nucleus, or set of equivalent nuclei in the system, has a significantly larger hyperfine coupling than all other nuclei.

The potential for experiment based on this result is great indeed. As described above, the next logical step involves tightening of the experimental parameters to allow quantitative observations to be made. Although of greater

experimental difficulty, design of a system that allows observation over a wider range of RF frequencies is desirable. A logical approach is, perhaps, to use an untuned RF circuit with the application of RF at greater power levels. The magnitude of the signal in the An / 1,3-DCB system indicates that effects may be detectable in a pulsed experiment without the use of modulation. This would provide greater information on the system's kinetics by allowing time-resolved observation of the RF resonance. It is hoped that future work will be conducted in these directions.

References

[1] **Batchelor, S.N.**
Part II thesis, Oxford University 1990

[2] **Weller, A.**
Z. Phys. ChemNF. **133** (1982) 93

[3] **Orbach, N. & Ottenlenghi, M.**
Chem. Phys. Lett. **35** (1975) 175

[4] **Ottenlenghi, M.**
Acc. Chem. Res. **6** (1973) 153

[5] **Rieger, P.H. & Fraenkel, G.K.**
J. Chem. Phys. **37** (1962) 2795

[6] **Batchelor, S.N., McLauchlan, K.A. & Shkrob, I.A.**
Mol. Phys. **75** (1992) 501

[7] **Batchelor, S.N., Kay, C.W.M., McLauchlan, K.A. & Shkrob, I.A.**
J. Phys. Chem. **97** (1993) 1325.

[8] **Timmel, C.R., & Hore, P.J.**
Chem. Phys. Lett. **257** (1996) 401

[9] **Kay, C.W.M.**
DPhil thesis, Oxford University 1993

[10] **Poole, C.P. 'Electron Spin Resonance'.**
2nd edition, John Wiley & Sons, Inc. 1983

[11] **Philips, L.F.**
Prog. React. Kinet. **7** (1975) 83

[12] **Hamilton, C.A., Hewitt, J.P., McLauchlan, K.A. & Steiner, U.E.**
Molec. Phys. **65** (1988) 423

[13] **Brocklehurst, B. & McLauchlan, K.A.**
Int. J. Radiat. Biol. **69** (1996) 3

Appendix A

Physical constants and conversions

Physical constants of significance to this thesis are listed below

Boltzmann constant	$k = 1.38066 \times 10^{-23}\ JK^{-1}$
g-value of nucleus	g_N (nucleus dependent)
g-value of free electron	$g_e = 2.0023$
Planck's constant	$h = 6.62618 \times 10^{-34}\ Js$ $\hbar = \frac{h}{2\pi} = 1.05459 \times 10^{-34}\ Js$
Bohr Magneton	$\mu_B = 9.27408 \times 10^{-24}\ JT^{-1}$
Nuclear Magneton	$\mu_N = 5.05082 \times 10^{-27}\ JT^{-1}$
speed of electromagnetic radiation in a vacuum	$c = 2.997925 \times 10^{8}\ ms^{-1}$
charge on an electron	$e = 1.60219 \times 10^{-19}\ C$
mass of an electron	$m_e = 9.10953 \times 10^{-31} kg$
Pi	$\pi = 3.14159265359$

Interconversion between magnetic field units and radiofrequencies can be achieved by considering the energy of an electron in a 1mT field.

$$1\ mT = 10^{-3}\ T = 10\ G = 28.0\ MHz$$

Appendix B

Structures of molecules used

acetonitrile	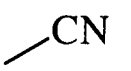
anthracene	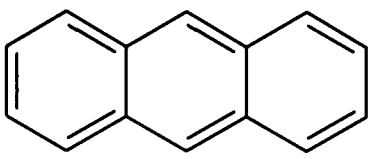
benzophenone	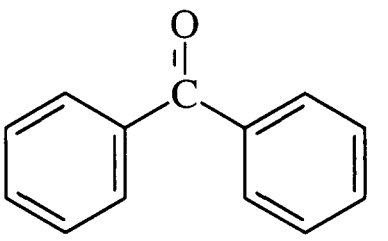
cyclohexanol	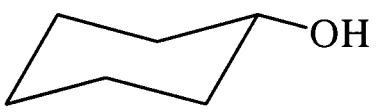
1,2-dicyanobenzene	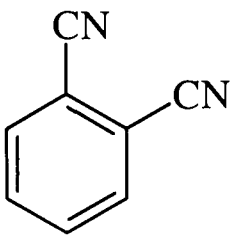
1,3-dicyanobenzene	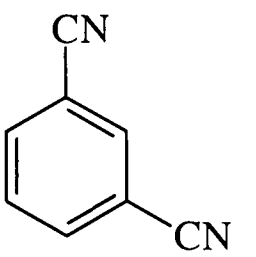
1,4-dicyanobenzene	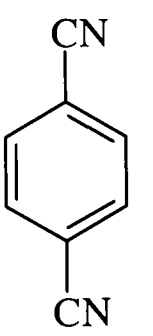
1,3-dihydroxyacetone	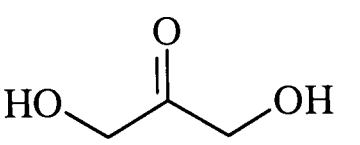

Appendix C

Hyperfine coupling constants for chemical systems studied

Radical	g-value	hyperfine coupling / mT	References
$\cdot CH_2OH$	2.0033	2H(α) = 1.742 H(β) = 12.8	Hefter, H. & Fischer, H. Ber. Bunsenges Phys. Chem. **73** (1969) 633 Photolysis of hydoxyacetone in methanol at 273K
	2.00333	2H(α) = 1.726 H(β) = 0.10	Livingstone, R. & Zeldes, H. J. Chem. Phys **44** (1966) 1245 Reaction of OH· with methanol at 314K
$CH_2OHCO\cdot$	2.0011	2H(β) = 0.15	Vollenweider, J. & Paul, H. Int. J. Chem. Kinet. **18** (1986) 791
$(C_6H_5)_2C(OH)\cdot$	2.00300	4H(2,6) = 0.321 4H(3,5) = 0.123 2H (4) = 0.364 H(OH) = 0.291	Wilson, R. J. Chem. Soc. B (1968) 84 Photoreduction of benzophenone in methanol at 298K
$C_6H_5C\cdot(OH)C_6H_4OH$		2H(2,6) = 0.362 2H(3,5) = 0.131 H(4) = 0.409 H(8,12) = 0.303 H(9.11) = 0.113 H(14,OH) = 0.314	Wilson, R. J. Chem. Soc. B (1968) 1581 Photoreduction of 4-hydroxybenzophenone in THF at 298K.
$Pyrene^+$		4H(1,3,6,8) = 0.538 4H(4,5,9,10) = 0.212 2H(2,7) = 0.118	Lewis, I.C. & Singer, L.S. J.Chem. Phys. **43** (1965) 2712 Solution in $SbCl_5$ / CH_2Cl_2 at 183K
$Anthracene^+$		4H(1,4,5,8) = 0.308 4H(2,3,6,7) = 0.138 2H(9,10) = 0.647	Lewis, I.C. & Singer, L.S. J.Chem. Phys. **43** (1965) 2712 Reymond, A. & Fraenkel, G.K. J. Phys. Chem. **71** (1967) 4570 Solution in $SbCl_5$ / CH_2Cl_2 at 183K
1,2-dicyanobenzene$^-$		2H(3,6) = 0.042 2N(1,2) = 0.175 2H(4,5) = 0.413	Reiger, P.H. and Fraenkel, GK. J. Chem. Phys. **37** (1962) 2795 Electrochemical reduction in DMF
1,3-dicyanobenzene$^-$		H(2) = 0.144 H(5) = 0.008 2H(4,6) = 0.829 2N(1,3) = 0.102	Reiger, P.H. and Fraenkel, GK. J. Chem. Phys. **37** (1962) 2795 Electrochemical reduction in DMF
1,4-dicyanobenzene$^-$		4H(2,3,5,6) = 0.159 2N(1,4) = 0.118	Reiger, P.H. and Fraenkel, GK. J. Chem. Phys. **37** (1962) 2795 Electrochemical reduction in DMF

Appendix D

Composition of buffer solutions

Yeast experiments

YEPD medium

10g/l Yeast Extract (Difco)
10g/l Bacto Peptone (Difco)
20g/l D-glucose

DNA plasmid experiments

LB (Luria Bertani) medium

10g/l Bactotryptone (Difco)
5g/l Bacto Yeast Extract (Difco)
10g/l sodium chloride

Cell resuspension solution

50mM Tris-HCl, pH7.5
10mM EDTA
100μg/ml Rnase A

Cell lysis solution

0.2M NaOH
1% SDS

TE Buffer

10mM Tris-HCL, pH7.5
1mM EDTA

Column Wash Solution

200mM NaCl

20mM Tris-HCl, pH7.5

5mM EDTA

Dilute with 95% ethanol, final ethanol concentration = 55%

Neutralisation solution

1.32M Potassium acetate, pH4.8

TBE buffer

10.8g/l Tris

5.5g/l Boric acid

0.93g/l EDTA

Single cell microgel experiments

Cell growth medium

Minimal Essential Mdeia (MEM, Life Technologies) plus Earles salts

10% Foetal bovine serum

100 U/ml Penicillin

100 μg/ml Streptomycin

PBS (Phosphate Buffered Saline)

0.1M sodium phosphate

0.1M sodium dihydrogen phosphate

2.7mM potassium chloride

0.137M sodium chloride

Appendix E

Supplementary data from yeast experiments

		Irradiation time / min							
	Sample Contents	**0**	**2**	**4**	**7**	**11**	**15**	**20**	**30**
Expt 1	No benzophenone, no magnetic field	100	89.17	102.5	98	111.67	92.67	108	99.13
	No benzophenone, magnetic field	100	113	96.67	88.83	103	94.67	92.5	101.33
	Benzophenone, no magnetic field	100	96.33	102.17	108	42.5	4.33	0.67	0
	Benzophenone, magnetic field	100	111.67	108.3.	92.17	56.17	3.5	0	0
Expt 2	No benzophenone, no magnetic field	100	96.17	111	106.33	92.83	91	99.33	107.17
	No benzophenone, magnetic field	100	105.33	101	91.67	90	98.33	104.17	92
	Benzophenone, no magnetic field	100	92	93.33	100.67	72.66	11.83	1.33	0
	Benzophenone, magnetic field	100	98.33	106	91.83	64.5	9	1.67	0
Expt 3	No benzophenone, no magnetic field	100	101	106	92.67	97.33	89.83	94	104.13
	No benzophenone, magnetic field	100	95.33	107.63	86.83	92.5	93	105.13	99.5
	Benzophenone, no magnetic field	100	98.5	109.83	82.33	26.5	1.67	0	0
	Benzophenone, magnetic field	100	113.83	95	86.66	33.33	2	0	0

Appendix F

Publications to which this work has contributed

"Resonant radiofrequency effects in spin chemistry",

Jackson, R.J., McLauchlan, K.A. & Woodward, J.R.

Chemical Physics Letters **236** (1995) 395-401

"Resonant radiofrequency magnetic field effects on a chemical reaction"

Woodward, J.R., Jackson, R.J., Timmel, C.R., Hore, P.J. & McLauchlan, K.A.

Chemical Physics Letters **272** (1997) 376-382